7 January 2025, Preprint v1 · CC-BY 4.0 Qeios PREPRINT

Review Article

Comprehensive Review of MAX Phase and MXene Materials: Synthesis, Properties and Applications

C. B. Subba[1], Dibya Prakash Rai[1], Mukhriddin E. Tursunov[2], Avazbek T. Dekhkonov[2], Z. Pachuau[1]

1. Department of Physics, Mizoram University, Aizawl, India; 2. National University of Uzbekistan named after Mirzo Ulugbek, Uzbekistan

In this paper, we present a detailed and comprehensive review of the MAX phase (bulk) and their 2D derivative MXenes on the basis of their synthesis, properties, and applications. MAX/Mexene have emerged as a class of materials with tremendous potential for various applications in numerous emerging technologies. We thoroughly surveyed almost all of the relevant literature on MAX/Mexene. We provide a comprehensive report on the synthesis methods of MAX phases, including traditional and innovative approaches such as solid-state synthesis and spark plasma sintering, highlighting their structural and compositional diversity. The unique physical, chemical, and mechanical properties of MAX phases, such as high thermal stability, electronic, magnetic, electrical conductivity, and flexibility, are explored along with the underlying mechanism. Furthermore, the review highlights the current research trend in MAX phase and MXene and their advancement in energy harvesting applications such as H_2 production, solar cells, energy storage, catalysis, spintronics, electronic devices and environmental remediation. Their added features are damage tolerance, radiation tolerance, heat tolerance, crack-healing, heat exchangers, etc. In addition, this review provides information on future research directions that utilize current knowledge and identify gaps. The purpose of this review is to facilitate advancements in the understanding and application of MAX phases and MXenes, positioning them as pivotal materials in next-generation technologies.

Corresponding authors: C. B. Subba, mzu240006111@mzu.edu.com; D. P. Rai, dibyaprakashrai@gmail.com; Z. Pachuau, zaiapach14@gmail.com

doi.org/10.32388/A3QP41

I. Introduction

MAX phase has drawn the attention of the science and research community due to the high demands of the 2D materials, and the exfoliation of MXene from it, which gives promising applications[1][2][3][4][5][6][7][8][9][10][11][12][13][14][15][16] in various fields due to its large group of structural and combination variances of the materials. The metal-nonmetal elemental combination variances in MAX phase ($M_{n+1}AX_n$), where metal (M) element having high temperature stability while the nonmetallic A element forms the layered structure, as a result deliver a unique ceramic-like mechanical properties, high electrical, high thermal conductivity, excellent machinability, and good corrosion resistance. However, for device fabrication to integrate these unique properties for practical application, the exfoliation of MAX into the 2D layer (MXene) is crucial. MXene is a 2D sheet having few nanometer thicknesses with a large surface-to-volume ratio that offers high interaction ability with various ions, enabling rapid charge-and-discharge processes in energy storage applications. Moreover, the properties of MXene can easily be manipulated to obtain desired functionalities through various methods such as strain engineering, applied electric field, surface functionalization (-OH, -F, or -O groups), etc. Since then, the research interest have been mounting on the production of MXenes from various methods such as solid state reaction[17][18], hot pressing[19][20], spark plasma sintering(SPS)[21][22], self-propagating high-temperature synthesis (SHS)[23][24][25][26], microwave-assisted heating[27][28], molten salt-assisted synthesis[29], physical vapor deposition[30][31][32][33], chemical vapor deposition[34][35], and thermal spraying[36][37] to synthesize and find its correlation with distinct properties has been explored. It has excellent properties such as corrosion resistance[38][39][40][41], crack healing properties[42][43][44][45][46][47], oxidation resistance[43][48][49][50][51][52][53][54] and radiation resistance[55][56][57][58][59][60]. It has shown wide promising applications as catalysis[61][62][63], biomedicine[64][65][66], energy storage[67][68], sensors[69], and nanocomposites[26][67][70][71][72]. The history of MAX phases dates back to the 1960s; the pioneer work done by Hans Nowotny and his coworkers[73], made their remarkable efforts resulted in the discovery of more than 100 new carbides and nitrides within that decade. In those decades more than 30 s were called H or Hagg phases having chemistry M_2AX, where M is an early transition metal, A is an element of group A (mainly III A and IVA) and X is C or N. Few years later in 1967 they discovered M_3AX type phases that are hexagonal layered interleaved with layers of pure A forming a structure similar to H-Phase. With time and research, more discovery[16][74][75][76][77][77][78][79][80][81][82][83][84][85][86][87][88][89][90][91][92][93][94] of different such phases finally leads to the realization of the general formulation M_{n+1}

AX_n, which is known as the MAX phase (where $n = 1 - 3$, M is an early transition metal, A is an element from group $13 - 16$ and X is C or N. Later, also discovered the hybrid structure of the MAX phase $n > 3$ [33]).

The MAX phase parent compound of MXenes in its own has tremendous potential and promising applications[71][95][96][97][98][99][100][101][102][103][104][105] due to the diverse class of nanolaminate materials showing dual metallic-ceramic properties. To date, there are 342 MAX phases that span 28 M elements, 28 A elements, and 6 X elements, including alloys[106]. There is an emerging more stable combination called the in-plane and out-of-ordered plane (i / o-MAX)[107][108], and a solid solution[109] adds more numbers to the present figure, but lacks a standardized formulation due to complex structures[93][110][111], synthesis complexity[112], mechanical properties[113] and lacks corrosion resistance above a certain temperature[112].

Since the discovery of MXene in 2011[114], which forms the hexagonal layered exfoliate of the MAX phase, researchers and engineers have devoted much of their time to studying its promising applications. It has shown excellent properties including nanocomposite capabilities[15][15][115][116][117], high electrical conductivity[118][119][120][121], outstanding mechanical strength[122][123][124], hydrophilic (water-attracting) surfaces[125][126], high tunability[127][128], excellent flexibility[129], good capacitance[15][119][130][131][132], and suitability for energy storage[119][133][133][134][135][136][137].

Furthermore, MXene is effective in applications such as nanofluids[138], thermal conductivity[139], and devices such as sensors and actuators[140][141]. It also shows interesting electronic[142][143][144], magnetic[145][146], optical[144][147], and thermoelectric behaviors, opening up a wide range of applications. These applications include catalysis[148][149][150][151], electromagnetic interference shielding[12], environmental management[152][153], lubrication[154][155], and antibacterial functions[156][157]. It will soon surpass graphene and other 2D materials[158] which is studied exhaustively thus far.

Currently, MAX phases and MXenes have attracted considerable attention due to their exceptional properties, enabling their effective use in photocatalysis[159][160], environmental remediation[161][162][163], and capture CO_2[164][165][166][167]. Their functionality in these areas is rooted in their remarkable electronic, structural and chemical adaptability.

This review paper discusses its synthesis, properties, and applications in detail.

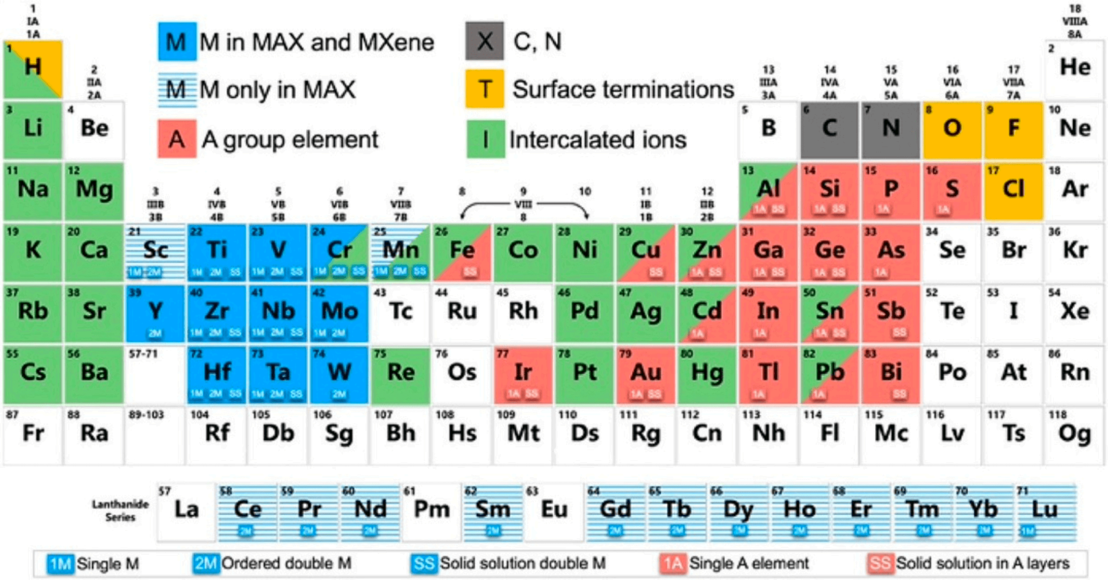

Figure 1. Elements involved in MAX phases, MXenes, and their intercalated ions. Blue-striped elements are found only in MAX phases, and their MXenes have not yet been synthesized. Red-background elements are the A elements in MAX phases that can be etched to form MXenes. Green-background cations have been intercalated into MXenes. Adapted with permission from Ref.[168], © Copyright (2019) American Chemical Society.

MAX/MXene	**Methods/Properties**	**Application**	**Ref**
Ti_2AlC, Ti_3AlC_2, Cr_2AlC, Al_2O_3	Atmospheric Plasma Spray (APS) method, Mechanical properties, high thermal stability	High-temperature structures, thermal barrier coatings for gas-turbine engines, heating elements	[169] [170] [171] [172] [173]
Ti_2AlN, Ti_3AlC_2, Ti_3C_2	Reactive sintering method, Filtration membranes	Water purification, gas separation, industrial processes	[174] [175] [176]
Ti_3SiC_2 , Ti_3AlC_2, Cr_2AlC, PLA-MoAlB	Fused deposition modeling (FDM) method, Tunable electromagnetism	Electromagnetic interference shielding	[177] [178] [179]
Cu/Ti_3SiC_2	Electrofriction properties	Electrofriction material, lubrication	[180] [181]
Cr_2AlC, Ti_2AlC	SPS + Powder Milling,	Crack healing	[182] [183]
Cu-MAX phase, Ti_2AlC	Electrodeposition, Evaporation, High electrical conductivity	Composite coating	[184] [185]
TiC_x-TiB_2	Combustion synthesis and hot press Method, compression properties, abrasive wear behavior and thermo-physics properties	Heat Sink	[186]
$Ti_3C_2T_x$,Ti_3AlC_2	Selective etching Method,lubrication	Biomedical	[66] [187] [188] [189] [190]
$Ti_3C_2T_x$	ball milling $+$ Selective etching method, electrolyte/cation interfacial charge transports properties	Supercapacitors	[191]

MAX/MXene	Methods/Properties	Application	Ref
Fe_2AlB_2,Al_2O_3-C	Hot pressing Method, Damage tolerance, electrical conductivity, and machinability	Thermal shock resistance	[192] [193]
$Hf_3C_2T_x$,Mo_2CT_x	selective etching method, chemical properties	Batteries	[68] [194] [195]
Cr_2AlC	Pressure-less sintering method, physico-chemical properties	Photocatalysis	[160]
M_2N (M = Ti, Zr, Hf, V, Nb, Ta, Cr, Mo, and W)	Theoretical simulations, Perdew–Burke–Ernzerhof (PBE-D3)	CO_2 capture	[166] [167]
V_2XT_2 (X: C, N; T: O, F)	Full potential linearized augmented plane-wave (FP-LAPW)	Spintronics	[196]

Table I. Methods/properties and applications of different MAX and MXene materials

II. Structure of MAX phase and MXene

A. Structure of the MAX phase

The MAX phase is a nanolayered ternary group compound with hexagonal lattice structure and forms a $P6_3/mmc$ space group with atomic planes of A atoms interleaving rock salt-structured [M_6C]-octahedra[197][198] shown in Fig.2. In Fig.2(a-c) the 211 MAX phase represents a class of materials with the stoichiometry M_2AX, consisting of two layers of transition metal (M), one layer of an element of the A group (A), and a single layer of carbon or nitrogen (X) arranged in an alternating structure.

The 312 MAX phase features a stoichiometry of M_3AX_2, where three layers of transition metal alternate with a single layer of the A group element and two layers of carbon or nitrogen. The 413 MAX phase is characterized by a composition of M_4AX_3, containing four layers of transition metal interleaved with one layer of an A-group element and three layers of carbon or nitrogen.

Similarly, there are higher n values such as the 514 MAX phase, which follows the formula M_5AX_4, with five layers of transition metal, a single layer of the A-group element, and four layers of carbon or nitrogen, and the 615 MAX phase, which exhibits a stoichiometry of M_6AX_5, involving six layers of transition metal, one layer of the A-group element, and five layers of carbon or nitrogen in a repeating pattern.

Some of different type of MAX phase materials are as follows:

- 2:1:1 → Ti_2ZnN[199] V_2ZnC[200] Nb_2CuC[201] Mn_2GaC[202] Mo_2AuC[203] Ti_2AuN[204] $(Ti_{1-x}Cr_x)_2AlC$ (x $= 0.25$, x$= 0.75$)[205][206], $V_2(Sn_{0.67}Fe_{0.33})C$[207] etc.
- 3:1:2 → V_3AlC_2[208] Ti_3SiC_2[23] Ta_3AlC_2[209] Ti_3ZnC_2[210] Zr_3AlC_2[19] $(Ti_{0.5}V_{0.5})_3AlC_2$[211] $(V_{0.5}Cr_{0.5})_3AlC_2$[212] etc.
- 4:1:3 → Ti_4AlN_3[213] V_4AlC_3[214] Nb_4AlC_3[215] Ta_4AlC_3[216] $(Mo,V)_4AlC_3$[217]$(Ti_{3/8}Cr_{5/8})_4AlC_3$[107] etc.
- 5:1:4 → Mo_4VAlC_4[218], $(Ti_{0.5}Nb_{0.5})_5AlC_4$[219], etc.

Some of different type of MXene materials are as follows:

- Single transition metal MXene (2:1): Mo_2N[220], $(Ti_{2-y}Nb_y)C$[221], V_2C[222], Nb_2C[222], Mo_2C[223], $Mo_{1.33}C$[224], Ti_2N[225], $(V_{2-y}Nb_y)C$[221], $(Ti_{2-y}V_y)C$[221], Ti_2C[226], $W_{1.33}C$[227], $Nb_{1.33}C$[228], $Mo_{1.33}Y_{0.67}C$[224]
- Single transition metal MXene (3:2): Hf_3C_2[194] Ti_3C_2[116], Zr_3C_2[229] and Ti_3CN[226]
- Single transition metal MXene (4:3):Ta_4C_3[226], Nb_4C_3[142], V_4C_3[230], Ti_4N_3[231]$(Mo,V)_4C_3$[232]
- Single transition metal MXene (5:4): Mo_4VC_4[218]
- Double transition metal MXene (2:1:2) MXenes: Mo_2TiC_2[233], Mo_2ScC_2[234] Cr_2TiC_2[233]
- Double transition metal MXene (2:2:3) MXenes: $Mo_2Ti_2C_3$[233]

In this way, the MAX phase forms a regular arrangement of atoms that form $M_{n+1}X_n$ layers, where X atoms sandwiched between M layers and the layer of A atoms stack again alternatively with the $M_{n+1}X_n$ layer along the c-axis direction[235].

Fig.1 illustrates the elements present in the MAX phases, MXenes, and their intercalated ions. The elements marked with blue stripes are exclusive to MAX phases, and their corresponding MXenes have not been synthesized yet. Elements with a red background represent the A elements in MAX phases that can be etched to produce MXenes. Cations with a green background have been successfully intercalated into MXenes.

There are more than one type of M elements, unlike the traditional trinary MAX phase that has the same M elements. Such MAX phase is the so-called solid solution in which two or more different metals are randomly distributed within and between the metal layers such as $(\mathrm{Ti}_{1-x}\mathrm{V}_x)_2\mathrm{AlC}$ and $(\mathrm{V}_{1-x}\mathrm{Cr}_x)_2\mathrm{AlC}$[236]. Similarly, in the same spirit, when more than two M metals are present, it is called the high entropy MAX phase that has also been synthesized[237][238][238][239][240][241][242][243][244][245][246][247][248][249].

There are two other types of structure called the out-of-plane ordered[107][234][245][250][251] (o-MAX) quaternary MAX phase $(\mathrm{M}',\mathrm{M}'')_3\mathrm{AX}_2$ or $(\mathrm{M}',\mathrm{M}'')_4\mathrm{AX}_3$ and the in-plane ordered (i-MAX) phases $(\mathrm{Mo}_{2/3},\mathrm{Sc}_{1/3})_2\mathrm{AlC}$, $(\mathrm{V}_{2/3},\mathrm{Zr}_{1/3})_2\mathrm{AlC}$, $(\mathrm{Mo}_{2/3},\mathrm{Y}_{1/3})_2\mathrm{AlC}$, $(\mathrm{Cr}_{2/3},\mathrm{Zr}_{1/3})_2\mathrm{AlC}$ and $(\mathrm{Cr}_{2/3},\mathrm{Zr}_{1/3})_2\mathrm{AlC}$ [108][252].

In i-MAX featuring a 211 stoichiometry, the M elements is in an in-plane arrangement. Theoretical and empirical knowledge have allowed the formulation of rules governing i-MAX formation, involving certain criteria such as a ratio of 2: 1 for M1: M2, the two metals differ significantly in size, with M2 being larger than M1. Furthermore, electrons tend to occupy bonding orbitals, strengthening the connections between atoms and the small A element, which influences how it fits within metal layers[110][253]. whereas o-MAX phase materials follow a general formula of $(\mathrm{M}_1,\mathrm{M}_2)_{n+1}\mathrm{AlC}_n$, with n being either 2 or 3. In these structures, two M_1 layers surround one or two M_2 layers within each M layer, creating a distinctive arrangement. The first o-MAX phase, $(\mathrm{Cr}_{2/3}\mathrm{Ti}_{1/3})_3\mathrm{AlC}_2$, was discovered by a solid-state reaction between $\mathrm{Cr}_2\mathrm{AlC}$ and TiC[18].

MAX phases can undergo phase transitions when exposed to extreme conditions, such as high temperature or pressure[254]. These changes usually involve modifications to the layer stacking sequence or a shift from a hexagonal structure to a more compact form. For example, at elevated temperatures, MAX phases can transform from a hexagonal to a more organized or distorted configuration. Similarly, when they are subjected to mechanical stress, these phases may experience delamination or exfoliation, leading to the creation of MXenes. MAX phases, including $\mathrm{Ti}_3\mathrm{SiC}_2$ and $\mathrm{Ti}_2\mathrm{AlC}$, undergo phase transitions under extreme conditions such as temperature and mechanical stress. At high temperatures, they can change from a hexagonal structure to a more ordered or distorted structure[101][255][256].

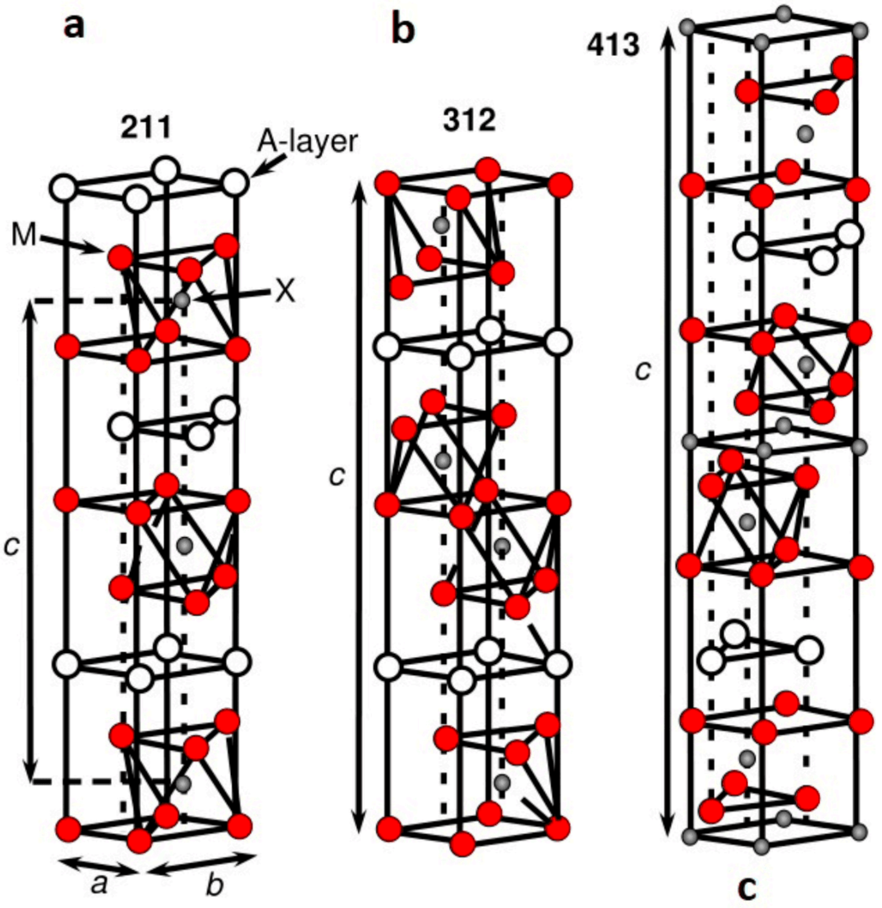

Figure 2. MAX phase unit cells: (a) 211, (b) 312, and (c) 413 phases. Reprinted with permission from Ref.[257]. © Copyright (2017) Elsevier.

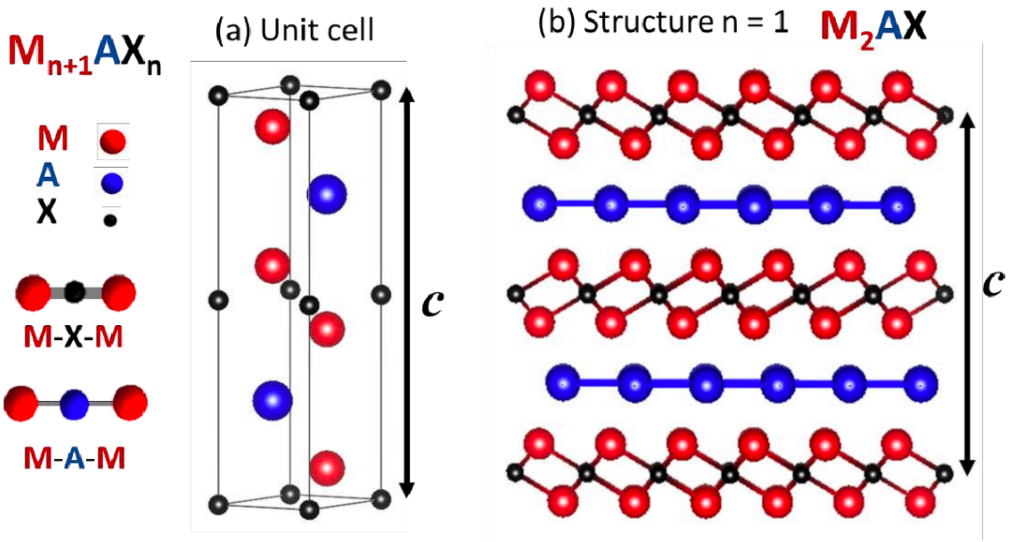

Figure 3. (a) Mn+1AXn phase unit cell with the c-axis nor- mal to the basal plane. (b) Nanolaminated Mn+1AXn phase structure with n = 1, where the monolayer of the A element is interleaved by M-X-M slabs. Redrawn from Ref.[258].

Figure 4. MAX phases and $\mathrm{M}_{n+1}\mathrm{AX}_n$ phase structures

B. Structure of MXene

The structure of MXene retains the symmetry of its precursor MAX phase with P6$_3$/mmc space group, which has a hexagonal crystal structure and the general formula $\mathrm{M}_{n+1}\mathrm{X}_n$, where M and X represent the early transition metal and (C or N) respectively & $n = 1, 2, 3$. However, during the etching process used to separate MXene from the MAX phase, termination groups such as -F, -OH, or =O are added. This results in a more general formula: $\mathrm{M}_{n+1}\mathrm{X}_n\mathrm{T}_z$, where $n = 1, 2, 3$ and T represent the termination groups[259].

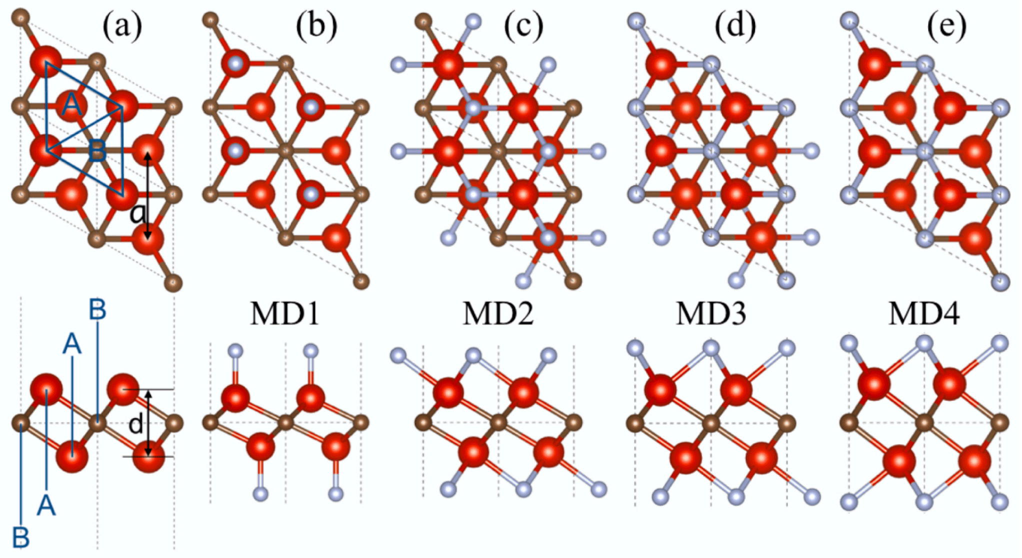

Figure 5. Atomic structure of (a) pristine M_2X with the two types of hollow sites A and B, and terminated M_2XT_2 in the four configurations: (b) MD1, (c) MD2, (d) MD3, and (e) MD4. M, X, and T elements are respectively in red, brown, and blue. Reprinted (abstract/excerpt/figure) with permission from Ref.[260] © Copyright (2018) by the American Physical Society.

Similarly, out-of-plane o-MXene has hexagonal symmetry with a general formula of $M'_2M''X_2$ or $M'_2M''_2X_3$, while in-plane i-MXene has the formula $(M'_{2/3}M''_{1/3})_2X$. Upon functionalization and the addition of termination groups, the stability of MXenes is further improved thermodynamically[261].

MXenes can also experience phase transitions when exposed to harsh conditions such as high temperatures or mechanical stress. Such transformations play a crucial role in the properties of MXenes, particularly in their use in energy storage and catalytic applications. These transitions typically involve changes in the structural arrangement of the layers, such as a shift from a hexagonal structure to a more compacted form. Specifically, $Ti_3C_2T_x$ MXene undergoes two main phases: (1) a low temperature phase transition (700–1000 $^\circ$ C), forming a mixture of Ti_2C and TiC_y, and (2) a high temperature transition above 1000 $^\circ$ C, resulting in a pure TiC_y phase[262]. Mechanical stress, such as delamination of the MAX phases, can also lead to MXenes forming as two-dimensional materials, altering their atomic configurations and properties. These transitions are essential for the development of MXenes in applications such as energy storage and catalysis.

III. Synthesis

A. Synthesis of MAX phase

In general, there are two approaches for MAX phase synthesis: top-down and bottom-up approaches. Most traditional ternary MAX phases have been synthesized using the bottom-up approach. These approaches involve powder metallurgy (powder synthesis) and thin film deposition[71][107][237][249][263][264][265]. These methods open the doors to substituting the A-site with different possible chemical compositions, exploiting a wider range of material properties.

The top-down approach allows for modification of post-synthesis layer A, and we can expand the elements of group A beyond group 12 to 16[201][266][267][268][269].

1. Bottom-up approach

The main characteristic of the bottom-up approach is the direct synthesis method, such as solid-state reaction, hot pressing[19][20], spark plasma sintering(SPS)[270][271][272][273][274], self-propagating high-temperature synthesis (SHS)[23][24][25][26], microwave-assisted heating[27][28], physical vapor deposition[30][31][32][33], chemical vapor deposition[34][35], and thermal spraying[36][37].

2. Top-down approach

The top-down approach is characterized by the way the A-group layer is modified. These phases are typically obtained from a bottom-up method, where the layers A are partially or completely modified after synthesis using techniques such as molten salt-assisted synthesis[29], sputter deposition, laser processing, ball milling, and reactive sintering[265], among others.

Fig.6 illustrates the different methods for synthesizing MAX phases, and Table II summarizes some of the well-known synthesized MAX phases, properties and methods.

The following are some of the standard synthesis methods of MAX phase.

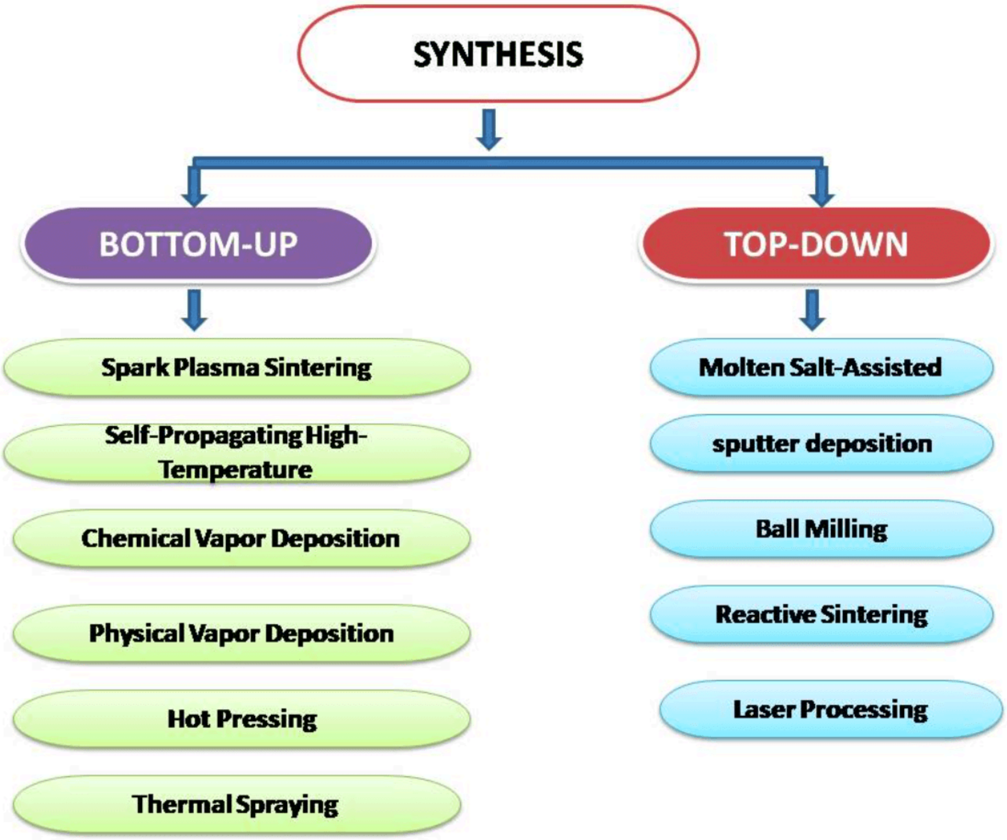

Figure 6. Illustration of MAX Phase Synthesis methods

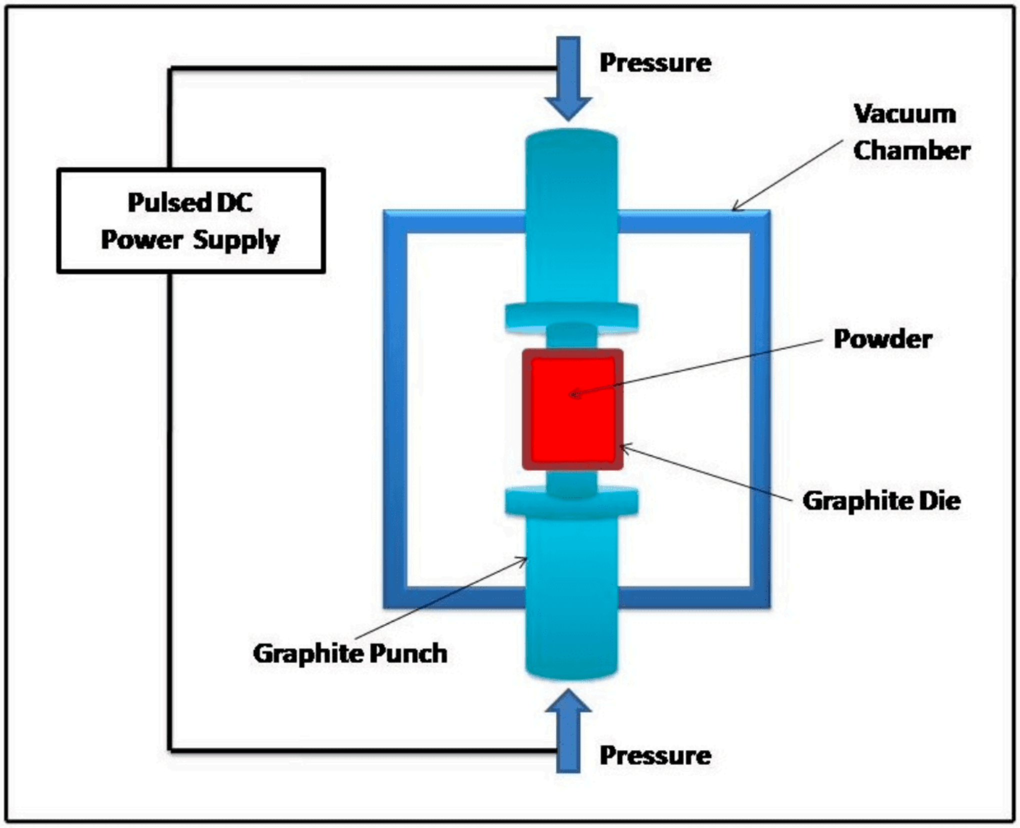

Figure 7. Diagram of spark plasma sintering (SPS) setup

A1. Spark Plasma Sintering(SPS)

The synthesis of MAX phases by Spark Plasma Sintering (SPS) as shown in Fig.7 is a precise and efficient technique that integrates high temperatures, uniaxial pressure, and pulsed electric currents[275][275][276]. The process begins with mixing stoichiometric amounts of fine powders, such as Maxthal powder, consisting of a transition metal (e.g., Ti), an A-group element (e.g., Al), and a carbon or nitrogen source, to achieve uniformity. The blended powder is then placed into a graphite die, with graphite foil used as a protective layer to prevent sticking between the powder and the die components.

During sintering, the SPS system applies rapid heating rates, typically ranging from 50-100 °C/min, to reach the target temperature, which is generally between 1000° C and 1500° C, depending on the specific MAX phase. At the same time, two different uniaxial pressures of 20 to 50 MPa are applied through two axes to help the material become denser. This pressure helps to reduce air gaps between the particles, encourages the particles to fit together more tightly, and improves the bonding between them, leading to a stronger and more solid structure. Pulsed direct current passes through the graphite die, producing localized heating and plasma, which accelerates diffusion and the chemical reactions necessary for phase formation. The temperature is maintained for 5 to 30 minutes to allow complete development of the MAX phase structure. Controlled cooling follows to prevent structural defects, such as cracks or unintended phase changes. The sintered material is then characterized using methods like X-ray diffraction (XRD) for phase verification and scanning electron microscopy (SEM) for microstructural analysis. This method yields high-purity MAX phases with customizable properties that can be subsequently converted into MXenes by selectively etching out the A-group element. In this process, several factors contribute to the final properties of the material. The choice of solvent can affect precursor dispersion and reactivity. Temperature plays a critical role in driving the sintering process and ensuring proper phase formation. The environment, such as a controlled atmosphere, prevents oxidation and preserves phase stability. Pressure aids in densifying the material and improving crystallinity. Finally, the cost of preparation is influenced by the energy-intensive nature of SPS, which requires specialized equipment to precisely control these conditions.

A2. Self-Propagating High-Temperature Synthesis (SHS)

Synthesis of MAX phases using Self-Propagating High-Temperature Synthesis (SHS) involves an efficient exothermic reaction that begins with the application of a small external energy input and then propagates autonomously[277][278][279][280][281]. The process begins by preparing a mixture of stoichiometric powders, typically comprising a transition metal (such as titanium), an element of group A (such as aluminum), and a carbon or nitrogen source in appropriate ratios. These reactants are carefully blended to ensure uniformity.

Once the powders are mixed, the reaction is initiated by applying heat, which triggers the exothermic reaction between the fuel and the oxidizer. The heat generated during this reaction is sufficient to sustain the process without the need for continuous external energy input, rapidly raising the temperature of the reactants to more than 1000 ° C. This high temperature facilitates the formation of the MAX phase, a metal carbide or nitride with a unique layered structure.

The SHS reaction is typically conducted in an inert atmosphere or vacuum to prevent unwanted oxidation and ensure the desired reaction. The synthesis can be performed in different forms, such as powder compaction or thin-layer deposition, to control the morphology and size of the final product. After the reaction, the material was allowed to cool, usually rapidly, to preserve its microstructure and phase purity.

The resulting MAX phase was then characterized by various techniques, such as XRD and scanning electron microscopy (SEM), to confirm the phase structure and examine its microstructure. SHS offers a highly energy-efficient and cost-effective method for synthesizing MAX phases, producing high-purity materials suitable for a range of advanced applications.

Maintaining temperature is vital in this process as it initiates and sustains the exothermic reaction driving the synthesis and also controlling environmental factors, such as the atmosphere, is essential to prevent oxidation and pressure plays a role in the reaction kinetics and the evolution of phases, while SHS's energy-efficient nature keeps preparation costs low by minimizing the need for external heating compared to other methods.

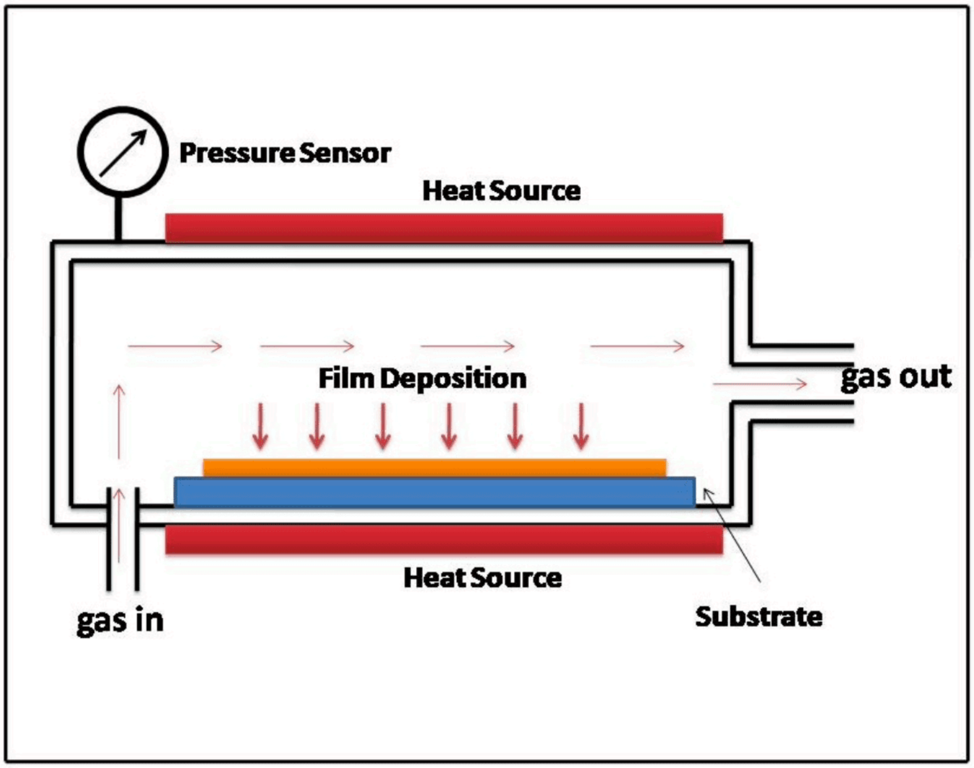

Figure 8. Schematic diagram of CVD

A3. Chemical Vapor Deposition(CVD)

This method is usually used to obtain thin film MAX phases. Fig.5 represents the schematic representation of CVD setup. It involves a sequence of steps where metal(M), aluminum(A), and carbon/nitrogen-based precursor gases are introduced into a reaction chamber and undergo chemical reactions on a heated substrate, ultimately forming the desired MAX phase structure. Initially, gaseous precursors, such as metal halides (e.g. titanium chloride, vanadium chloride), aluminum compounds (e.g. aluminum chloride, aluminum alkyls), and carbon sources (e.g., methane, acetylene, or carbon monoxide), are introduced into the chamber. This reaction chamber is heated to temperatures ranging from 800°C to 1100 ° C, depending on the specific MAX phase that is being synthesized.

When the gaseous precursors come into contact with the heated substrate, typically a ceramic or metal surface, they react chemically to form the MAX phase material. For example, to synthesize Ti_3AlC_2, titanium and aluminum precursors are introduced into the chamber, together with a carbon source. These react at high temperatures to produce Ti_3AlC_2, with byproducts such as hydrochloric acid or other gases being vented. The key to a successful CVD process lies in maintaining precise control over the temperature, pressure, and precursor flow rates, ensuring the correct stoichiometry and crystalline structure of the MAX phase. CVD can be performed at atmospheric pressure (APCVD) or low pressure (LPCVD), depending on the requirements of the application. To achieve the desired MAX phase, careful control over the chemical composition of the precursors is necessary. For example, the carbon source must be accurately regulated to prevent excess carbon, which could lead to the formation of undesired carbide phases instead of the intended MAX phase. Once the deposition is complete, additional post-deposition treatments, such as sintering or annealing, may be applied to refine the microstructure and enhance the crystalline quality of the MAX phase. This method allows for the production of dense, uniform films that adhere well to the substrate, making it an effective approach for the fabrication of MAX phases for various applications, including protective coatings, electronic devices, and energy storage systems.

A4. Physical Vapor Deposition(PVD)

MAX phases through the Physical Vapor Deposition (PVD) process involve the deposition of metal (M), aluminum (A), and carbon or nitrogen (X) atoms from a vapor phase onto a substrate, where they react under controlled conditions to form the desired structure of the MAX phase[282][283]. The process begins by introducing solid precursor materials, such as titanium, vanadium, or aluminum, into a vacuum chamber where they are heated or evaporated. In some cases, carbon sources (such as graphite or methane) are also introduced to ensure the carbon content necessary for MAX phase formation. The chamber is typically maintained at low pressure, and the evaporated precursors are directed onto the substrate surface, where they condense and react to form a thin film of the MAX phase. In PVD, the metal and carbozn precursors undergo physical vaporization processes such as thermal evaporation, sputtering, or laser ablation. Upon reaching the heated substrate, these atoms or ions condense to form the MAX phase material. For example, to produce Ti_3AlC_2, titanium and aluminum are vaporized and deposited on a substrate, where they react with carbon atoms, leading to the formation of the Ti_3AlC_2 structure. The main challenge in PVD for MAX phases is to achieve proper stoichiometry by controlling the flux and energy of the arriving species, ensuring the correct atomic ratio between the metal, aluminum, and carbon.

The PVD process can be performed using various techniques, such as thermal evaporation, sputtering, or pulsed laser deposition (PLD), with each technique offering distinct advantages depending on the specific requirements of the MAX phase. The process can be conducted under vacuum or low pressure conditions, and the temperature of the substrate is typically controlled to ensure proper deposition and phase formation. Once the MAX phase is deposited, post-deposition treatments such as annealing or additional sintering steps may be required to refine the crystal structure and improve the phase purity of the final product. The PVD process enables the formation of dense, high-quality MAX phase films that adhere well to substrates, making it a promising technique for producing MAX phases for applications such as protective coatings, electronic devices, and energy storage materials.

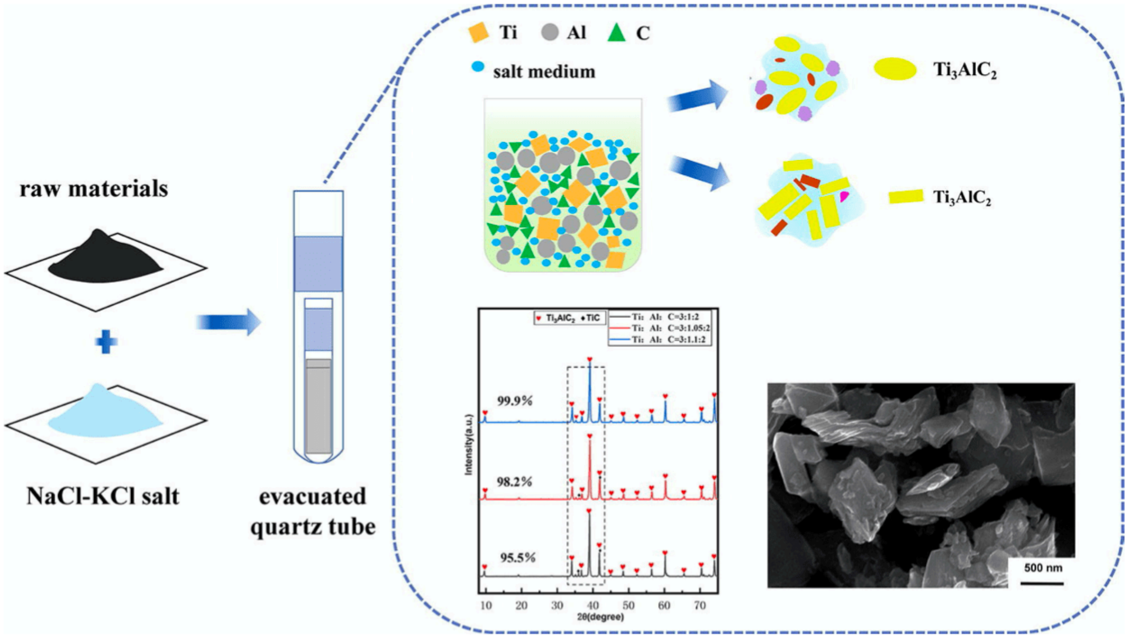

Figure 9. Diagram of Molten Salt-Assisted synthesis. Reproduced with permission from Ref[284] Copyright (2020) Elsevier

A5. Molten Salt-Assisted synthesis

This approach uses molten salts to accelerate reaction rates and allow the formation of MAX phases at temperatures lower than those of conventional methods. The process starts with the selection of precursors, including metal powders, salts (both metal and non-metal), carbon sources, and molten salts such as NaCl or KCl. These materials are mixed in stoichiometric proportions and ball-milled for uniformity. The mixture was then placed in a crucible, heated in a high-temperature furnace under an inert atmosphere, and molten salt was added to aid in the diffusion of the reactant. The molten salt functions as a flux, lowering the reaction temperature and helping to reduce the number of metal oxides by carbon, which promotes the formation of carbide or nitride phases. Once the reaction is complete, the system is cooled, and the solidified salts are separated from the product. The MAX phase is then washed to remove any remaining salts or impurities. The final product is characterized using methods like X-ray diffraction, scanning electron microscopy, and energy dispersive X-ray spectroscopy to verify its purity, structure, and morphology. This method offers benefits such as lower reaction temperatures, enhanced diffusion of reactants, and better phase control, although challenges such as maintaining exact stoichiometry and effectively removing molten salts persist. The technique has been successfully used to synthesize various MAX phases, such as Ti_3AlC_2, Ti_2AlC[284][285][286], Ti_3SiC_2, Ti_2AlN, Ti_2AlC, Ti_3AlC_2, V_2AlC, as well as MoAlB and Cr_2AlB_2[287][288].

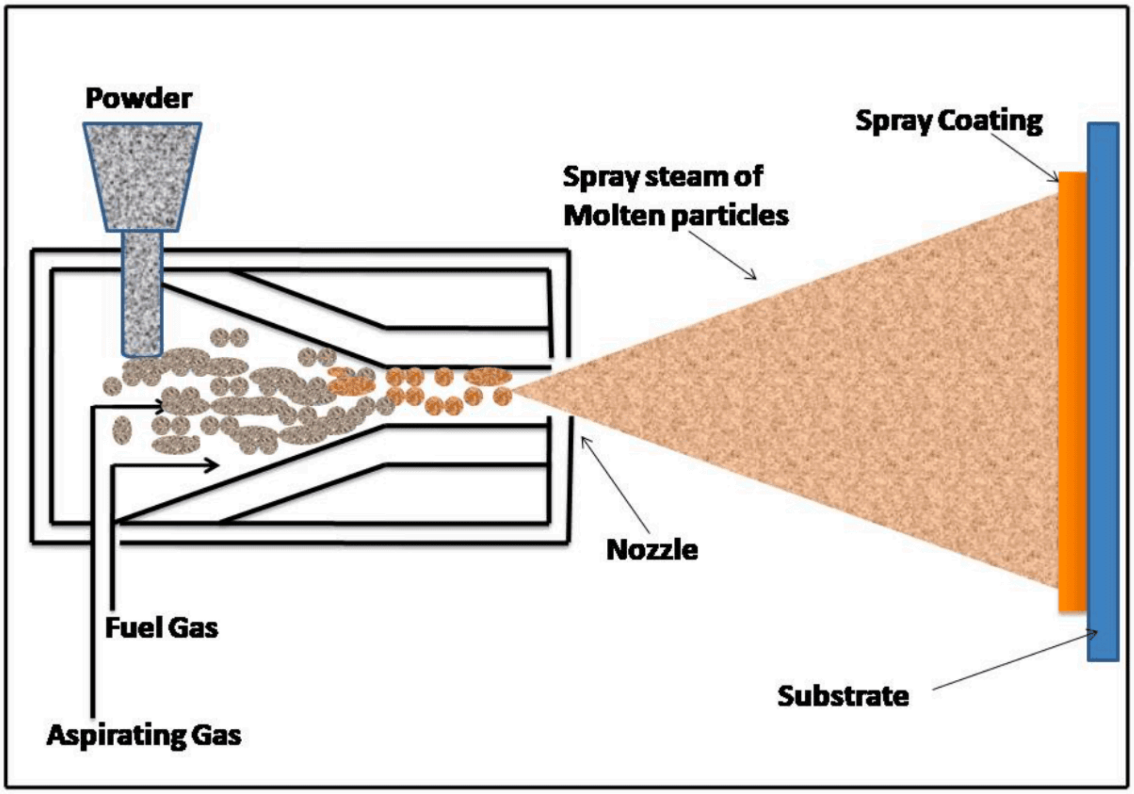

Figure 10. Schematic representation of Thermal Spray Method

A6. Thermal Spraying

Thermal spraying is another method used to synthesize MAX phases, such as Ti_3AlC_2, by coating substrates with powdered precursors that are heated and sprayed onto a surface. Fig.10 illustrates the schematic process of the thermal spray method. The process typically involves using a high-temperature flame or plasma to melt the precursor powders and propel them onto a substrate, where they rapidly cool and form a solid coating. In the case of MAX phases, the powders generally consist of elemental titanium (Ti), aluminum (Al), and carbon (C) or a mixture of these components in the desired stoichiometric ratios. The thermal spraying method allows for the deposition of these materials in a controlled manner, enabling the formation of a dense MAX phase coating. One key advantage of this method is that it can be performed at relatively low temperatures compared to traditional sintering techniques, preventing undesirable reactions or decomposition. In addition, the rapid cooling process helps to achieve finer microstructures. Various types of thermal spraying techniques, such as plasma spray, flame spray, or high-velocity oxygen fuel (HVOF) spraying, can be employed depending on the desired coating characteristics and the substrate material. After the spraying process, the MAX phase coating is often subjected to post-deposition treatments, such as heat treatment or annealing, to further enhance the quality and phase purity of the MAX phase. The method offers flexibility in producing thin, uniform coatings and is particularly useful in applications where high-performance coatings with specific mechanical properties, such as wear resistance and thermal stability, are required.

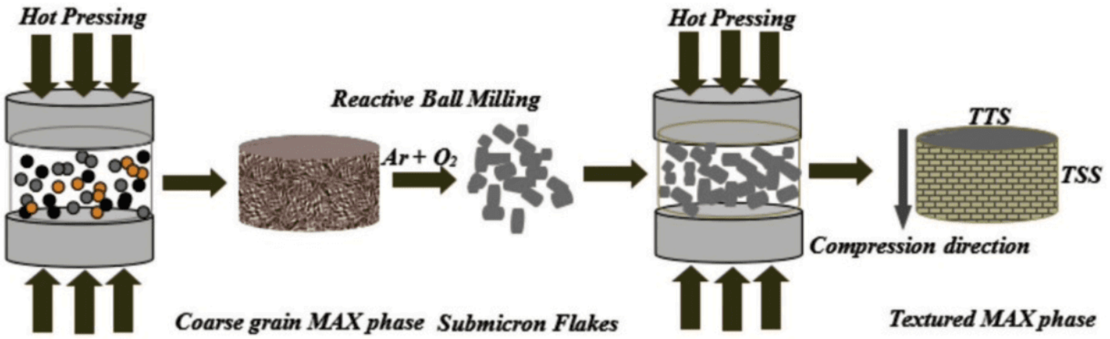

Figure 11. Schematic representation of Hot Pressing Method. Reproduced with permission from Ref[289] Copyright (2020) Elsevier

A6. Hot Pressing

It is a popular method for making MAX phases by applying high temperature and pressure to compact and form the material from powdered precursors. Fig.11 represents a schematic diagram of Hot Pressing method. In this process, a mixture of elemental powders such as M, A, and X is placed in a mold. The powders are then heated and compressed in a controlled environment, typically under an inert atmosphere, to create the desired MAX phase.

The temperature during hot pressing is usually set between 1200 ^{o} C and 1600 ^{o} C[24], depending on the specific MAX phase being performed. The pressure applied can range from a few MPa to several hundred MPa, helping to make the material more compact, reduce air pockets, and ensure a uniform product. This combination of heat and pressure speeds up the diffusion of atoms and encourages the formation of the desired phase, resulting in a high-quality, dense MAX phase.

One of the main advantages of hot pressing is its ability to produce dense materials with minimal pores, which is important to achieve strong and hard MAX phases. The process also allows for better control over the grain structure, as the applied pressure and heat help align the grains in the final product. Hot pressing is suitable for both small-scale laboratory production and large-scale industrial manufacturing of MAX phases. However, there are challenges with hot pressing, such as ensuring an even temperature and pressure throughout the sample, which can affect the quality of the final material. The method also requires specialized equipment and careful optimization of conditions to achieve the desired properties and phase purity[23][290]. Despite these challenges, hot pressing remains an effective and versatile technique for making MAX phases with excellent mechanical properties.

Ceramics Composition	Applied Method	Properties	References
Ti_3AlC_2	SHS	TMD = 99.29%; HV = 4.22±0.96 GPa; K_{iC} = 8.52±1.86 $MPa^{1/2}$	[291]
Ti_2AlC	SHS	TMD = 74.56%; HV = 0.62±0.27 GPa; K_{iC} = 7.88±0.57 $MPa^{1/2}$	[291]
Ti_2AlC	SPS	TMD = 94.42%; capacitance = 73 mF/g	[22]
V_4AlC_3	SPS	TMD = 99%; HV = 6.74 ± 0.12 GPa; BS = 389 ± 19 MPa	[21]
Ti_3AlC_2	Molten Salt-Assisted	TMD $>$ 99.0%;	[284]
Nb_4AlC_3	Reactive Hot Pressing	$\alpha = 7.10 \times 10^{-6}$ °C^{-1}; E = 350 GPa; K_{iC} = 6.0 $MPa^{1/2}$	[20]
Ti_2AlC	Ball Milling + SPS	TMD = 95.0%; HV = 8.7 GPa; k_{fr} = 0.35	[292]
Zr_3AlC_2C	Reactive Hot Pressing	HV = 4.4 ± 0.4 GPa	[19]
Ti_3SiC_2	Molten Salt Shielded Synthesis	TMD = 95.3%	[288]
Ti_3AlC_2	Microwave-assisted Heating	TMD = 98.5%	[286]

Table II. Table illustrates some common MAX Phases fabricated by different methods and their Theoretical Maximum Density (TMD), Vickers Hardness (HV), Bending Strength (BS), Fracture Toughness (K_{Ic}), Young Modulus (E), Coefficient of Thermal Expansion (α), Friction coefficient (k_{fr}) values.

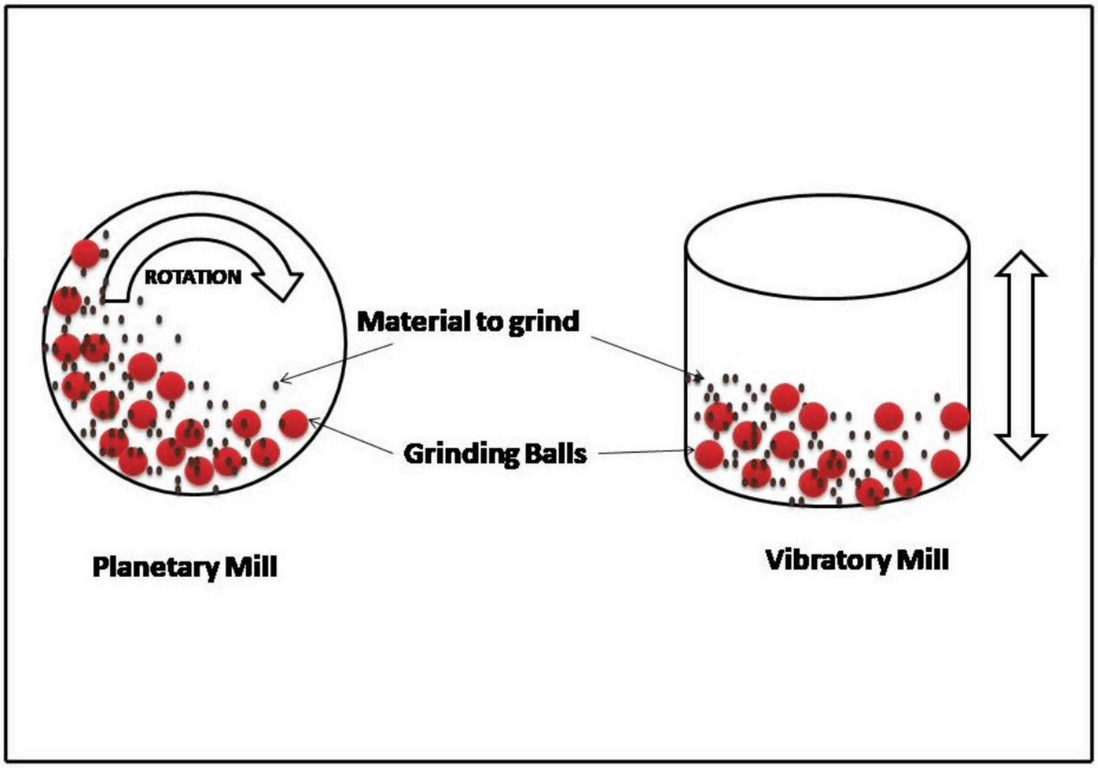

Figure 12. Schematic diagram of Ball Milling Method

A7. Ball Milling

The synthesis of MAX phases through ball milling follows a structured process that integrates mechanical alloying with subsequent thermal treatment to create the desired nanolaminate structures. Fig.12 represents schematic diagram of the process. Initially, the precursor materials required, which are typically high-purity elemental powders of M (transition metal), A (IIIA group IIIA or IVA element), and X (carbon or nitrogen), were accurately weighed in stoichiometric proportions. These powders are then placed in a high-energy ball mill, such as a planetary or shaker mill, alongside milling media such as hardened steel or tungsten carbide balls. To achieve optimal results, the ball-to-powder weight ratio (BPR) is adjusted, usually within the range of 5:1 to 15:1, depending on the specific materials and the milling setup. Milling is conducted under an inert atmosphere, such as an argon atmosphere, or in a vacuum to prevent oxidation and contamination. During the milling process, repeated impact and friction between balls and powder particles facilitate mechanical alloying. This process induces plastic deformation, particle fracture, and cold welding, leading to a uniform powder mixture and a significant reduction in particle size to the nanometer scale. The duration of milling, which can range from a few hours to several tens of hours, is crucial to obtaining a fine and homogeneous powder mixture. Extended milling ensures thorough mixing and activates the powders, enhancing their reactivity in the subsequent stages. The milled powder is then subjected to thermal treatment, typically in a tube or box furnace, to promote the formation of the MAX phase. The powder is either compacted into pellets or placed in a crucible before being heated to temperatures ranging from 1000°C to 1500°C, depending on the target MAX phase. This heating process is carried out under an inert or reducing atmosphere, such as an argon or argon-hydrogen mixture, to prevent oxidation. The temperature is maintained for an optimized dwell time, often lasting several hours, to ensure a complete phase transformation. After synthesis, the sample was cooled to room temperature and analyzed using techniques such as X-ray diffraction (XRD) to verify the formation of the MAX phase. If secondary phases are identified, adjustments to parameters such as milling duration, temperature, or stoichiometric ratios may be necessary. Finally, the resulting MAX phase is examined using microstructural characterization methods, such as scanning or transmission electron microscopy, to assess its laminar structure and purity. This approach is popular because of its simplicity, cost-effectiveness, and ability to produce fine reactive powders.

doi.org/10.32388/A3QP41

Category	Synthesized
Single-Metal MAX Phases	- Al: Ta_2AlC[81], Ti_2AlN[293], Ti_3AlC_2[93], Zr_3AlC_2[19], Ta_3AlC_2[294], Ti_2AlC[81], V_2AlC[81], Cr_2AlC[81], Zr_2AlC[19], Nb_2AlC[81], Hf_2AlC[19], Hf_3AlC_2[19], V_4AlC_3[295], Nb_4AlC_3[215], Ta_4AlC_3[296], Ti_4AlN_3[16], Ta_6AlC_5[294], $Ti_5Al_2C_3$[297]. - Si: Ti_3SiC_2[75], Ti_4SiC_3[33], $Ti_5Si_2C_3$[33], $Ti_7Si_2C_5$[33]. - P: V_2PC[298], Nb_2PC[299]. - S: Ti_2SC[300], Zr_2SC[300], Nb_2SC[299], Hf_2SC[92], Zr_2SB[301], Nb_2SB[302], Hf_2SB[301]. - Fe: Ta_2FeC[303], Nb_2FeC[303], Ti_2FeN[303]. - Co: Nb_2CoC[267], Ta_2CoC[267]. - Ni: Nb_2NiC[267], Ta_2NiC[267]. - Cu: Nb_2CuC[201], Ti_4CuN_3[304]. - Zn: Ti_2ZnC[199], V_2ZnC[199], Ti_3ZnC_2[199], Nb_2ZnC[199], Ti_2ZnN[199]. - Ga: Ti_2GaC[83], V_2GaC[81], Cr_2GaC[79], Mn_2GaC[305], Nb_2GaC[83], Mo_2GaC[81], Ta_2GaC[83], Ti_2GaN[83], V_2GaN[92], Cr_2GaN[306], Ti_3GaC_2[307], Ti_4GaC_3[307], Mo_2Ga_2C[308][309]. - Ge: Ti_2GeC[82], V_2GeC[79], Cr_2GeC[79], Nb_2GeC[30], Zr_2GeC[310], Ti_3GeC_2[77], Ti_4GeC_3[311], $Ti_5Ge_2C_3$[311], Ti_7Ge_2C[311]. - As: V_2AsC[312], Nb_2AsC[92]. - Se: Zr_2SeC[313], Hf_2SeC[314], Zr_2SeB[315], Hf_2SeB[315]. - Cd: Ti_2CdC[83], $Ti_3Cd_2C_2$[316]. - In: Ti_2InC[82], Zr_2InC[82], Hf_2InC[82], Nb_2InC[83], Ti_2InN[83], Zr_2InN[83], Ti_3InC_2[307], Zr_3InC_2[25], Hf_3InC_2[25], Hf_2InN[84]. - Sn: Sc_2SnC[317], Ti_2SnC[81], V_2SnC[318], Zr_2SnC[81], Nb_2SnC[83], Hf_2SnC[81], Lu_2SnC[319], Hf_2SnN[320], Nb_2SnB[310], Ti_3SnC_2[321], Zr_3SnC_2[25], Hf_3SnC_2[25], Ti_7SnC[322]. - Sb: Ti_2SbP[323], Zr_2SbP[323], Hf_2SbP[323], Nb_2SbC[316], Ti_3SbC_2[316]. - Te: Hf_2TeB[324]. - Ir: Ti_3IrC[97]. - Pt: Nb_2PtC[316]. - Au: Ti_3AuC_2[97], $Ti_3Au_2C_2$[97], Ti_2Au_2C[325], Mo_2AuC[203], Nb_2AuC[316], Cr_2AuC[326], Ti_2AuN[204]. - Ti: Ti_2TlC[83], Zr_2TlC[327], Hf_2TlC[327], Zr_2TlN[84]. - Pb: Sc_2PbC[41], Ti_2PbC[83], Zr_2PbC[327], Hf_2PbC[327], Zr_3PbC_2[41], Hf_3PbC[41]. - Bi: Nb_2Bi_2C[316].

Category	**Synthesized**
o-MAX	• Al: Mo_2VAlC_2[328]$Mo_2V_2AlC_3$[328] $(Mo_2Ti_2)Al_3$[251] $(Mo_2Ti)AlC_2$[250][251], Cr_2TiAlC_2[107], $(Cr_{0.75}V_{0.25})_2VAlC_2$[329], $(Cr_{2/3}V_{1/3})_3AlC_2$[329], $(Cr_{2/3}Ti_{1/3})_3AlC_2$[107], $(Mo_2Sc)AlC_2$[234], $(Cr_2V_2)AlC_3$[329], $(Mo_2Ti_2)AlC_3$[251], $Cr_{2+x}Ti_2-xAlC_3$ $(x = 0.5)$[107], $(Cr_{0.7}V_{0.3})_2(Cr_{0.2}V_{0.8})_2AlC_3$[329], $Mo_2Nb_2AlC_3$[330].
i-MAX	• Al: $W_{1/3}Mo_{1/3}R_{1/3\,2}AlC$ (R = Gd, Tb, Dy, Ho, Er, Y)[331], $Mo_{2/3}Sm_{1/3}AlC$[332] $Mo_{2/3}Dy_{1/3}AlC$[332] $W_{4/3}Y_{2/3}AlC$[227], $W_{4/3}Gd_{2/3}AlC$[333], $W_{4/3}Tb_{2/3}AlC$[333], $W_{4/3}Dy_{2/3}AlC$[333], $W_{4/3}Ho_{2/3}AlC$[333], $W_{4/3}Er_{2/3}AlC$[333], $(Mo_{2/3}Sm_{1/3})_2AlC$[332], $(Mo_{2/3}Nd_{1/3})_2AlC$[332], $(Mo_{2/3}Gd_{1/3})_2AlC$[332], $(Mo_{2/3}Tb_{1/3})_2AlC$[332], $(Mo_{2/3}Ho_{1/3})_2AlC$[332], $(Mo_{2/3}Dy_{1/3})_2AlC$[332], $(Mo_{2/3}Er_{1/3})_2AlC$[332], $(Mo_{2/3}Tm_{1/3})_2AlC$[332], $(Mo_{2/3}Ce_{1/3})_2AlC$[332], $(Mo_{2/3}Pr_{1/3})_2AlC$[332], $Mo_{4/3}Sc_{2/3}AlC$[334], $Mo_{4/3}Y_{2/3}AlC$[108], $W_{4/3}Tm_{2/3}AlC$[333], $W_{4/3}Lu_{2/3}AlC$[333] , $V_{4/3}Sc_{2/3}AlC$[252], $V_{4/3}Zr_{2/3}AlC$[335], $Cr_{4/3}Sc_{2/3}AlC$[18], $Cr_{4/3}Y_{2/3}AlC$[18], $Cr_{4/3}Zr_{2/3}AlC$[336], $(W_{2/3}Sc_{1/3})_2AlC$[227], $(Mo_{2/3}Y_{1/3})_2AlC$[108], $(V_{2/3}Zr_{1/3})_2AlC$[108], $(W_{2/3}Y_{1/3})_2AlC$[227], , $(Cr_{2/3}Sc_{1/3})_2AlC$[18] , $Cr_{4/3}Gd_{2/3}AlC$[337], $Cr_{4/3}Tb_{2/3}AlC$[337], $Cr_{4/3}Dy_{2/3}AlC$[337], $Cr_{4/3}Ho_{2/3}AlC$[337], $Cr_{4/3}Er_{2/3}AlC$[337], $Cr_{4/3}Tm_{2/3}AlC$[337], $Cr_{4/3}Lu_{2/3}AlC$[337], $W_{4/3}Sc_{2/3}AlC$[227] , $W_{2/3}Mo_{2/3}Gd_{2/3}AlC$[331], $(W_{0.5}Mo_{0.5})_{4/3}Tb_{2/3}AlC$[331], $(W_{0.5}Mo_{0.5})_{4/3}Dy_{2/3}AlC$[331], $(W_{0.5}Mo_{0.5})_{4/3}Ho_{2/3}AlC$[331], $(W_{0.5}Mo_{0.5})_{4/3}Er_{2/3}AlC$[331] , $(Mo_{2/3}Sc_{1/3})_2AlC$[234][334], $(Cr_{2/3}Y_{1/3})_2AlC$[24], $(Cr_{2/3}Zr_{1/3})AlC_2$[24], $Mo_{4/3}Ce_{2/3}AlC$[332], $Mo_{4/3}Pr_{2/3}AlC$[332], $Mo_{4/3}Nd_{2/3}AlC$[332], $Mo_{4/3}Sm_{2/3}AlC$[332], $Mo_{4/3}Dy_{2/3}AlC$[332], $Mo_{4/3}Ho_{2/3}AlC$[332], $Mo_{4/3}Er_{2/3}AlC$[332], $Mo_{4/3}Tm_{2/3}AlC$[332], $(W_{0.5}Mo_{0.5})_{4/3}Y_{2/3}AlC$[331], $Nb_2(Al_{0.2}Au_{0.8})C$[316], $Ti_3(AI_{1/3}Cu_{2/3})C_2$[338] • Ga: $(Mo_{2/3}Gd_{1/3})_2GaC$[111], $(Mo_{2/3}Lu_{1/3})_2AlC$[332], $(Mo_{2/3}Tb_{1/3})_2GaC$[111], $(Mo_{2/3}Dy_{1/3})_2GaC$[111], $(Mo_{2/3}Er_{1/3})_2GaC$[111], $(Mo_{2/3}Ho_{1/3})_2GaC$[111], $(Mo_{2/3}Tm_{1/3})_2GaC$[111], $(Mo_{2/3}Lu_{1/3})_2GaC$[111], $(Mo_{2/3}Yb_{1/3})_2GaC$[111], $(Mn_{2/3}Sc_{1/3})_2GaC$[111], $(Cr_{2/3}Sc_{1/3})_2GaC$[111], $Cr_{4/3}Sc_{2/3}GaC$[339] $Mo_{4/3}Sc_{2/3}GaC$[253], $(Mo_{2/3}Y_{2/3}GaC$[253], $Mo_{4/3}Gd_{2/3}GaC$[340], $Mo_{4/3}Tb_{2/3}GaC$[340], $Mo_{4/3}Dy_{2/3}GaC$[340], $Mo_{4/3}Ho_{2/3}GaC$[340], $Mo_{4/3}Er_{2/3}GaC$[340], $Mo_{4/3}Tm_{2/3}GaC$[340], $Mo_{4/3}Yb_{2/3}GaC$[340], $Mo_{4/3}Lu_{2/3}GaC$[340], $(Mo_{2/3}Y_{1/3})_2GaC$[336], $(Mo_{2/3}Sc_{1/3})_2GaC$[336], $Mn_{4/3}Sc_{2/3}GaC$[339] $Mo_2(Ga_{0.1}Au_{0.9})_2C$[203]
High-Entropy MAX Phase	• $Ti_2VNbTaZr_2AlC$ (M = Zr, Hf)[255], Ti_2NbVZr_2SC[341], $Ti_3VCrMoAlC_2$[342], $Ti_{1/3}V_{1/6}Zr_{1/6}Nb_{1/6}Ta_{1/6\,2}AlC_xN_{1-x}$[343], M_4AlC_3 (M = Ti, V, Mo, Nb, Ta)[344].

Table III. Synthesized MAX Phases by Category

**Note: Table III represents one of the well-known synthesized MAX phases as Single-Metal, o-MAX, i-MAX and high-entropy categories with examples. Added recent synthesized data and reproduced from Ref.*[345]*. © Wiley.*

However, precise control over milling and sintering conditions is essential to avoid contamination and ensure the successful formation of high-purity MAX phases.

A8. Liquid / solid state reaction

It is a commonly used technique to synthesize MAX phases, which involves the interaction between liquid and solid precursors to drive phase formation[346][347][348]. The process starts with the careful selection of precursors tailored to the specific ($M_{n+1}AX_n$) phase being synthesized. Typical precursors include transition metals such as titanium and vanadium, A-group elements such as aluminum and silicon, and carbon or nitrogen sources such as graphite or boron carbide. These materials are finely ground and uniformly mixed—often through ball milling—to achieve a homogeneous mixture with fine particle sizes, which enhances the reaction kinetics. The prepared powder mixture is then compacted into pellets to improve particle contact and suppress the development of unwanted phases. During the heating stage, the compacted mixture is subjected to elevated temperatures under controlled conditions, such as in an inert or vacuum atmosphere, to prevent oxidation. When the temperature exceeds the melting point of the A-group element, a liquid phase is formed, which reacts with the solid transition metal and carbon or nitrogen to yield the desired MAX phase. This liquid phase significantly accelerates diffusion, promoting efficient phase formation and uniformity in the resulting structure. The reaction conditions, typically within the range of 1000 to 1500 $^\circ$C, and the duration of heating are meticulously optimized to ensure high product yield and minimal impurity content. After the reaction concludes, the material is cooled, and optional post-synthesis treatments, such as annealing, can be applied to further improve purity and crystallinity.

B. Synthesis of MXene

Thanks to M-A metallic bond which is weaker than the ionic and / or covalent M-X bond, it was possible to exfoliate MXenes from precursor MAX phase[349][350][351][352][353].The MXenes are produced by selectively etching specific layers of their MAX phase precursors. Selective etching is the widely used top-down approach.

Etching is one of the common methods to obtain Mxene from the MAX phase, where the etched layers are mixed with termination groups such as hydroxyl (-OH), oxygen (-O), or fluorine (-F). Those etched layers are held together by weak forces such as hydrogen or van der Waals. The use of hydrofluoric acid poses a risk; a different path has been explored. Ghidiu et al. first introduced the main substance used in which the mixture of hydrochloric acid (HCl) and lithium fluoride salt was introduced in Ti_3AlC_2[354]. This provides a basis for the use of other fluoride salts such as (NaF, KF, and NH_4F)[355][355][356]. Several bottom-up synthesis techniques have also been established, such as chemical vapor deposition (CVD)[4][357][358][359][360][361], the template method[362][363][364], and plasma-enhanced pulsed laser deposition (PEPLD)[365][366]. Compared with the selective etching process, materials created through these bottom-up approaches, especially CVD, exhibit high crystalline quality.

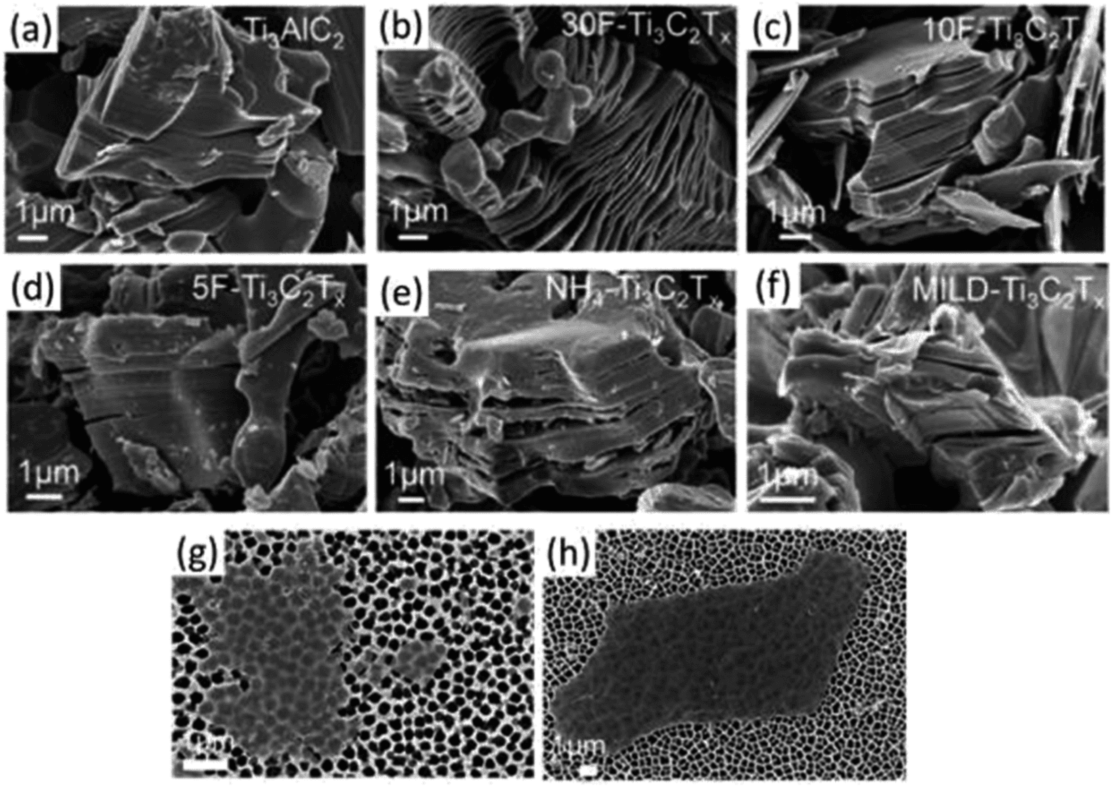

Figure 13. SEM images of MAX and MXene powders etched under various conditions.© Royal Society of Chemistry Ref.[367].

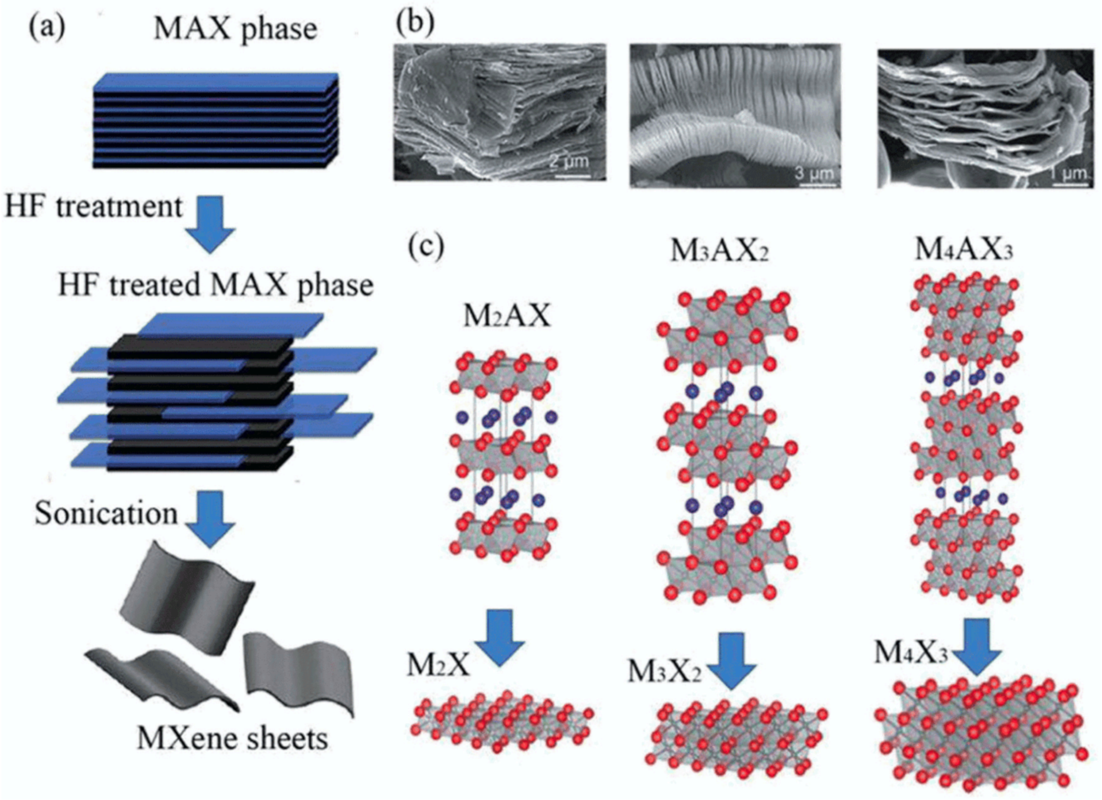

Figure 14. (a) Three main non-terminated MXene structures: M_2X, M_3X_2, and M_4X_3. (b) SEM images of Ti_2AlC, Ti_3AlC_2, and Ti_4AlC_3 (left to right) following HF treatment. (c) Schematic representation of MXene synthesis from MAX phases. © Royal Society of Chemistry Ref.[367].

The following are some common methods for synthesizing MXene.

B1. Selective etching methods

The selective etching method is a widely recognized and commonly used approach for the synthesizing of MXenes from their MAX phase precursors. As illustrated in Fig.14, this method involves the targeted removal of the "A" layer, typically composed of elements from group 13 or 14 of the periodic table such as aluminum (Al) or silicon (Si), followed by the exfoliation of MXene layers after treatment with hydrofluoric acid (HF). During the process, the MAX phase material is exposed to acidic solutions such as HF or other fluoride-based etchants, which selectively break the bonds connecting the "A" element to the surrounding layers. This reaction results in the formation of two-dimensional MXene sheets. Subsequent refinement steps, including washing and delamination, were performed to purify and separate the MXene layers, enabling their application in a variety of fields.

The first MXene synthesized using this method was $Ti_3C_2T_x$[116], obtained by immersing Ti_3AlC_2 powders in a 50 wt.% hydrofluoric acid (HF) solution. The differential reactivity of the M-A and M-X bonds toward HF facilitated the selective removal of Al layers. This process has since been used to produce various other MXenes[142][194][195][222][224][225][230][368][369].

Fig.13(a) shows the SEM images of $\mathrm{Ti_3AlC_2}$ (MAX) powder, showing its characteristic compact layered structure, (b-d) present multilayered powders $\mathrm{Ti_3C_2T}_x$ synthesized using HF solutions with concentrations of 30 wt.%, 10 wt.% and 5 wt.%, respectively. In particular, only the 30 wt.% HF treatment produces the distinctive accordion-like morphology. (e) illustrates $\mathrm{Ti_3C_2T}_x$ powder synthesized via ammonium ($\mathrm{NH_4}$)-assisted etching, while (f) highlights the MILD etching method using LiF in HCl. Both methods exhibit a limited opening of the MXene lamellae, similar to the results observed with 5 wt.% HF etching. Finally,(g) and (h) show individual MXene flakes etched using 5 wt% HF and the MILD technique, displayed on a porous alumina substrate.

B2. Chemical vapor depositions

Chemical Vapor Deposition (CVD) is a highly effective technique for the synthesis of MXenes, providing a controlled environment to produce high-quality thin films or flakes. In this method, precursor gases, which contain the elements necessary for the creation of MXene, are introduced into a heated reaction chamber. These gases, often composed of metals like titanium and other components such as carbon or nitrogen, react at elevated temperatures on a heated substrate to form a solid, thin layer of MXene. The process starts with the deposition of metal layers, commonly titanium, onto a substrate. These metal layers then react with carbon- or nitrogen-based gases to produce the desired MXene compound. For example, MXenes of titanium carbide (TiC) or titanium carbonitride (TiCN) can be synthesized by introducing carbon-rich gases such as methane (CH_4) or nitrogen-containing gases such as ammonia (NH_3). CVD offers precise control over growth parameters such as temperature, pressure, and gas composition, allowing manipulation of the morphology and structure of MXene. This leads to the formation of uniform, thin MXene layers that can be transferred onto various substrates for further processing. In 2015, Xu et al.[4] introduced the first successful method to grow high-quality ultrathin transition metal carbide (TMC) crystals by chemical vapor deposition (CVD). This approach utilized a bilayer metal foil, consisting of copper (Cu) and a transition metal, as the substrate for crystal growth. This method is especially advantageous for producing high-purity MXene films with controlled thickness and consistency, making it suitable for applications in sensors, energy storage, and flexible electronics.

B3. The hydrothermal method

It involves a reaction that occurs under high temperature and pressure within an aqueous environment[370][371]. This process is carried out in a sealed container known as an autoclave, which allows precise control over both temperature and pressure, thus facilitating the necessary chemical reactions to generate MXenes.[372][373][374][375] In this technique, the MAX phase precursor is combined with a suitable etching agent, typically a fluoride-based acid (such as hydrofluoric acid, HF). The mixture is then exposed to elevated temperatures, typically between 100 ° C and 250 ° C, and kept under high pressure for an extended period. These conditions promote selective etching of the "A" layer, commonly a metal such as aluminum (Al) or silicon (Si), from the MAX phase, resulting in the formation of MXene sheets. One of the main benefits of the hydrothermal method is that it allows for MXene synthesis under conditions more moderate than that obtained with alternative methods such as selective etching with HF. The controlled conditions within the autoclave lead to high purity and consistent quality of the resulting MXenes. Additionally, this approach can be tailored to produce MXenes with different surface functional groups, depending on the specific etching agents and reaction parameters used. Following hydrothermal treatment, the MXene sheets are typically separated, washed, and exfoliated to produce a few-layer high-quality MXenes suitable for a variety of applications, including energy storage[370][370], catalysis[376], capacitor[371] and detection[377].

B4. Ball Milling Method

It is a mechanical technique used to synthesize MXenes by applying high-energy collisions to the MAX phase precursor. In this process, the MAX phase powders are placed in a sealed container with hard milling balls and, occasionally, a liquid medium. The container is rotated at high speeds, causing the milling balls to collide with the MAX phase particles, imparting mechanical energy.[378][379][380]

This energy is sufficient to break the bonds between the "A" element (often aluminum or silicon) and the surrounding metal layers of the MAX phase, resulting in exfoliation and the formation of MXene sheets. The ball milling process is highly customizable and can be conducted under various conditions, such as dry or wet milling, in an inert atmosphere, or at different temperatures, depending on the desired properties of the MXenes. The physical and morphological properties of the resulting MXenes are influenced by several factors, including milling type (dry or wet), milling speed, ball-to-powder ratio, and milling duration. Huang et al.[179] synthesized a Pt/Nb_2C MXene composite-based catalyst through ball milling. They started by immersing 500 mg of Nb_2C MXene in 30 ml of 100% ethanol to prepare a homogeneous solution, assisted by ultrasonication. Chloroplatinic acid was added to the solution and the resulting sample was ball milled in a corundum tank at 150 rpm for 30 minutes to form the Pt/Nb_2C MXene composite. The final product was filtered using a vacuum filter and annealed at 600 ° C for 2 hours under inert conditions. This mechanochemical technique offers a novel, efficient and environmentally friendly method to produce noble electrocatalysts with Nb_2C MXene for energy storage and conversion applications. Ball milling provides a versatile and scalable method for synthesizing MXenes with controlled sizes, thicknesses, and surface characteristics, making it suitable for a wide range of applications, including energy storage, sensors, and catalysis. After milling, the MXene sheets are typically separated, washed, and exfoliated to obtain high-quality, few-layer MXenes, ready for further processing or immediate use.

B5. Electrophoretic deposition

Electrophoretic deposition (EPD) is a technique used to produce MXenes by applying an electric field to a suspension of MXene particles in a liquid medium, such as water or an organic solvent. In this process, the dispersed MXene flakes migrate to an electrode when exposed to the applied electric field[381][382]. The first step in the procedure involves the preparation of a stable suspension of MXene. This is achieved by dispersing exfoliated MXene sheets in a chosen solvent, with the addition of surfactants or stabilizers to prevent particle aggregation and ensure even dispersion. The concentration of MXene in the suspension is adjusted as a function of the desired film thickness and morphology. Once the suspension is ready, it is placed in a container between two electrodes-one acting as the anode and the other as the cathode. The electric field applied across the electrodes causes the charged MXene particles to move toward the electrode of opposite charge. The MXene flakes then deposit on the electrode surface, forming a thin film[383][384][385]. The deposition rate and film quality can be controlled by adjusting the applied voltage, deposition time, and concentration of MXene in the suspension. After deposition, the resulting MXene film is dried to remove any remaining solvent. Further processing, such as annealing or sintering, can be performed to improve the structural integrity, electrical conductivity, and other properties of the film. The electrophoretic deposition method enables the fabrication of uniform and controlled MXene films, making it ideal for applications in areas such as sensors, energy storage devices, and flexible electronics, where thin, precisely structured materials are required. The advantages of electrophoretic deposition include the ability to precisely control the thickness of MXene films, the potential for scalable production, and the flexibility to use different solvents and deposition parameters to customize the properties of the final film[386].

IV. Properties of MAX phase and MXene

1. Properties of MAX Phase

MAX phase is a class of ternary layered metal carbides and nitrides showing both metallic and ceramics properties[23][95][320][367][387][388] giving rise to variety in its applications. The strong metallic bond between M layers gives good electrical and thermal conductivities, and the covalent bond between M-X gives thermal stability. Its unique layered structure of the MAX phase is characterized by distinctive properties and also allows the creation of hybrid materials by mixing the MAX phase with other materials to reach desired applications.

Electronic Properties

The study of the electronic properties of MAX phases is crucial to understanding their various behaviors. The study of Ti-based carbides ($\mathrm{Ti_3SiC_2}$, $\mathrm{Ti_3AlC_2}$, and $\mathrm{Ti_2AlC}$) has been carried out in a comprehensive manner compared to other MAX phases. All MAX phases show high conductivity similar to that of metals, with refractivities ranging from 0.07 to 2 $\mu\Omega\mathrm{m}$[23][95][388]. Their resistivity increases linearly with temperature and they have very low Seebeck coefficients[387]. For example, the electronic resistivity of $\mathrm{Ti_2AlC}$ increases from 0.36×10^{-6} $\Omega\mathrm{m}$ at 300 K to approximately 1.0×10^{-6} $\Omega\mathrm{m}$ at 1200 K[389].

Fig.17(d) shows the electrical conductivity and resistivity of large-scale $\mathrm{Ti_2AlC}$ synthesized by the SHS/PHIP process from RT to 900° C, the resistivity increasing linearly, indicating the metallic conductivity. The electronic band structure of $\mathrm{Nb_2GaC}$, presented in Fig.15 and discussed in Ref.[390], demonstrates that the Fermi level (E_F) is represented by a horizontal dashed line, signifying the absence of a band gap due to the overlap of conduction and valence bands. This indicates that $\mathrm{Nb_2GaC}$ is a metallic solid. The energy dispersion along the Γ-A, H-K, and M-L pathways corresponds to the c-direction, while the A-H, K-Γ, Γ-M, and L-H pathways describe dispersion within the basal (ab) planes. A smaller dispersion is observed in the c-direction compared to the basal plane, suggesting that electronic conductivity is higher in the basal plane. The effective mass tensor is anticipated to be larger in the c-

direction, contributing to the reduced dispersion in that orientation. Consequently, the anisotropic nature of electronic conductivity, a hallmark of MAX phases, including Nb_2AlC, is observed in these materials[391].

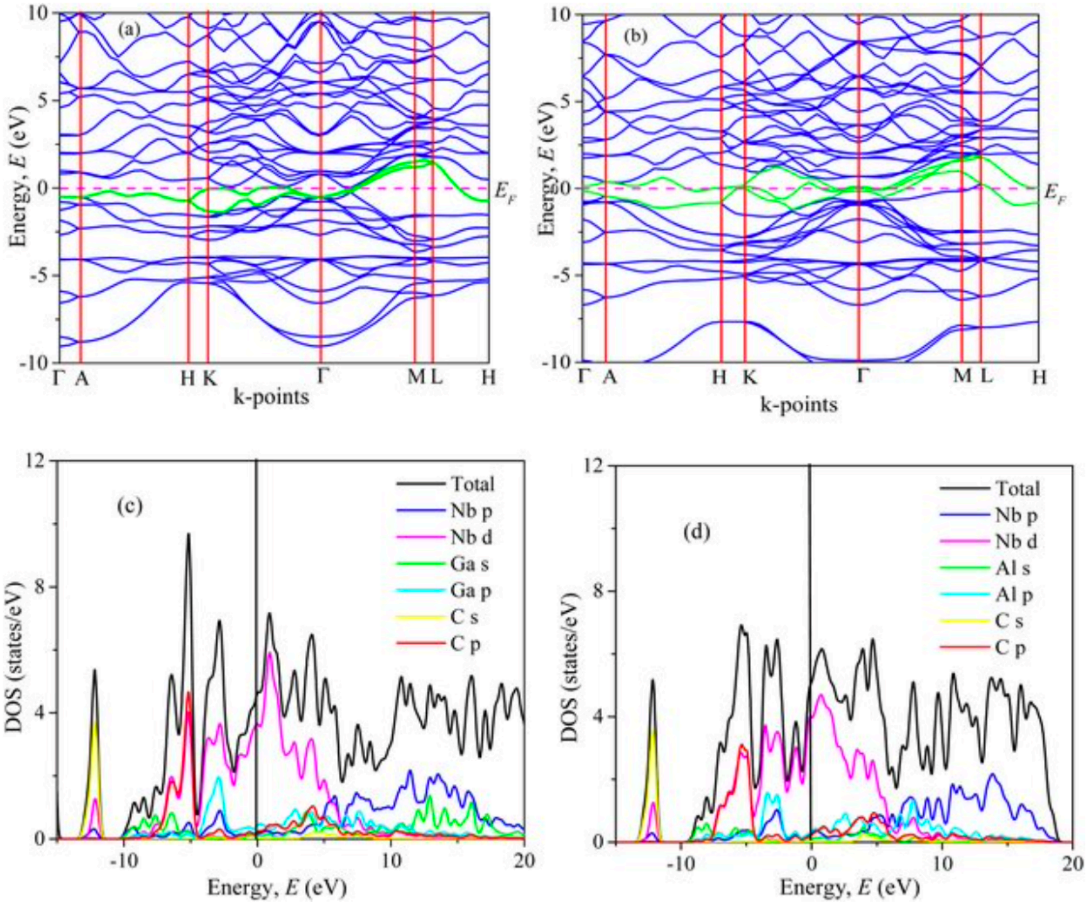

Figure 15. Band structures and the corresponding total and partial density of states (DOS) for (a, c) Nb_2GaC and (b, d) Nb_2AlC, obtained through GGA-PBEsol calculations. Reproduced with permission from Ref. [390] Copyright (2023) Royal Society of Chemistry

Thermal Properties

A thorough understanding of the thermal properties of MAX phases requires studying their thermal expansion coefficients, heat capacity, and conductivity at different temperatures. MAX phases are known for their distinctive thermal conductivity and typically have thermal expansion coefficients in the range of 7--$10 \times 10^{-6}\ \mathrm{K}^{-1}$. For example, Ta_4AlC_3 exhibits a relatively high thermal expansion coefficient. The thermal conductivity of these materials generally increases linearly with temperature, paralleling the behavior of electronic resistivity. Additionally, the contributions of electrons and phonons to the overall thermal conductivity change with temperature; electrons primarily dominate at room temperature, while phonons play a more significant role in Al-containing MAX phases. This increased phonon contribution in aluminum-rich compositions is attributed to the strong binding of aluminum atoms, which supports coherent vibrations with adjacent atoms[290][392][393][394][395].

Fig17 (f) shows the thermal conductivity, molar heat capacity, and thermal diffusivity of large-scale Ti_2AlC synthesized by the SHS/PHIP process over 200–1200° C. Fig17 (c) compares the temperature-dependent thermal conductivity of the large-scale sample with that of the small-scale sample and other typical MAX phases[389], (d) shows the variation of the electron, phonon, and total thermal conductivities with temperature.

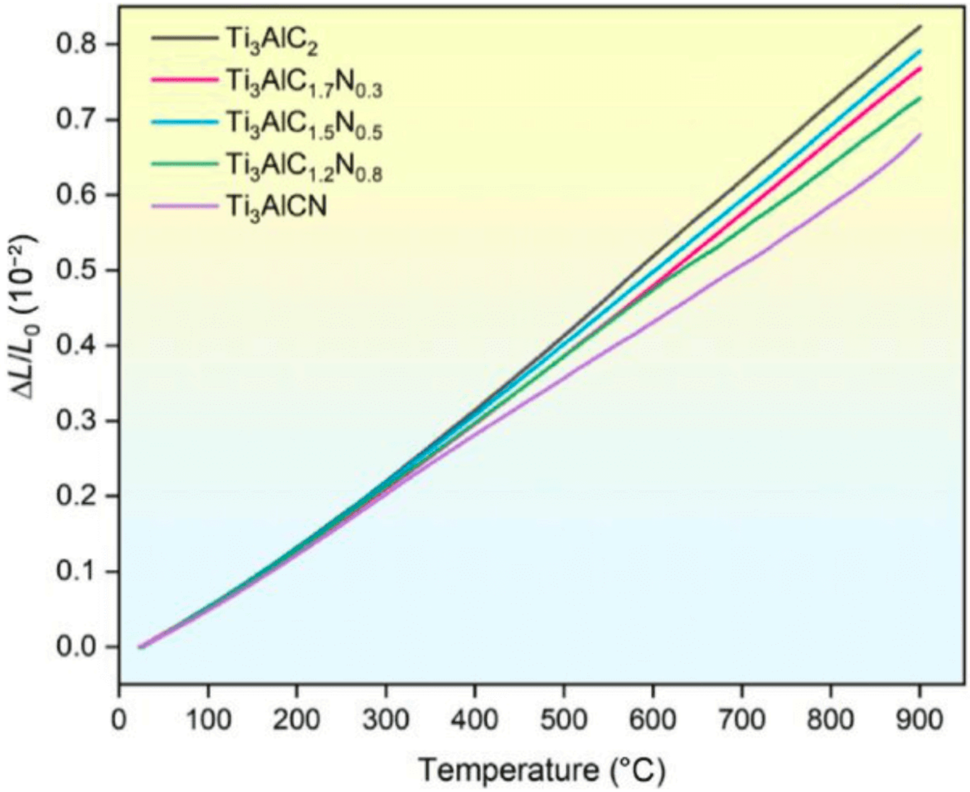

Figure 16. The thermal expansion behavior of $Ti_3AlC_{2-y}N_y$ over the temperature range of 25–900 °C. Reproduced with permission from Ref.[396] Copyright SciOpen

Mechanical Properties

MAX phases are distinguished by their unique microstructure and chemical bonding, which contribute to exceptional mechanical properties at room temperature. They typically exhibit a high Young's modulus, flexural strength, compressive strength, and fracture toughness, although they have a lower shear and hardness modulus. The high Young's modulus and strength stem from strong covalent bonds between M and A elements, while weaker bonds between the MX and A layers lead to a reduced shear modulus. Although they have a low density (4.1-5 g/cm^3), they maintain a high specific stiffness, especially Ti_2AlC, which compares favorably to Si_3N_4 ceramics and exceeds that of Ti metal[397][398][399].

Exceptions like Ta_2AlC and Ta_4AlC_3 have higher densities (up to 13.18 g/cm^3). Generally, MAX phases exhibit moderate hardness (2–5 GPa) and a Young modulus ranging from 282 to 340 GPa, placing them between ZrO_2 and Al_2O_3 ceramics, but above most metals. Although their flexural strength may be lower than that of some ceramics, they show excellent crack resistance due to high fracture toughness, similar to the interlocking microstructure of ceramics Si_3N_4)[400][401][402]. Mechanical enhancements through solid solutions or particle reinforcements can improve properties such as flexural strength and Vickers hardness. For instance, $Ti_3Al_{0.8}Si_{0.2}Sn_{0.2}C_2$) exhibits increased flexural strength, while ZrC and ZrO_2 improve the stiffness and hardness of fractures in composites Ti_3AlC_2. Substituting Ti with V or Cr can also increase the bulk modulus. The layered structure of MAX phases supports unique mechanical responses, such as nonlinear elastic kinking behavior and complex deformation mechanisms such as crack deflection and kink band formation, which are critical to their mechanical performance[389][403][403][404][405][406].

Fig.17(a) shows the flexural stress vs. displacement curves at high temperatures for large-scale Ti_2AlC bulk produced by the SHS / PHI process reveal the brittle fracture behavior from RT to 900 °C, shifting to plastic deformation beyond 950 ° C. The brittle-plastic transition temperature (BPTT) is identified between 900 and 950 ° C, with a reduced slope suggesting a decrease in Young's modulus. Fig.17(b) illustrates the temperature-dependent flexural strength and fracture displacement, comparing the results with samples of lower density. Above 950 ° C, the flexural strength decreases dramatically with increased fracture displacement, while a higher relative density improves both properties without affecting the BPTT[389].

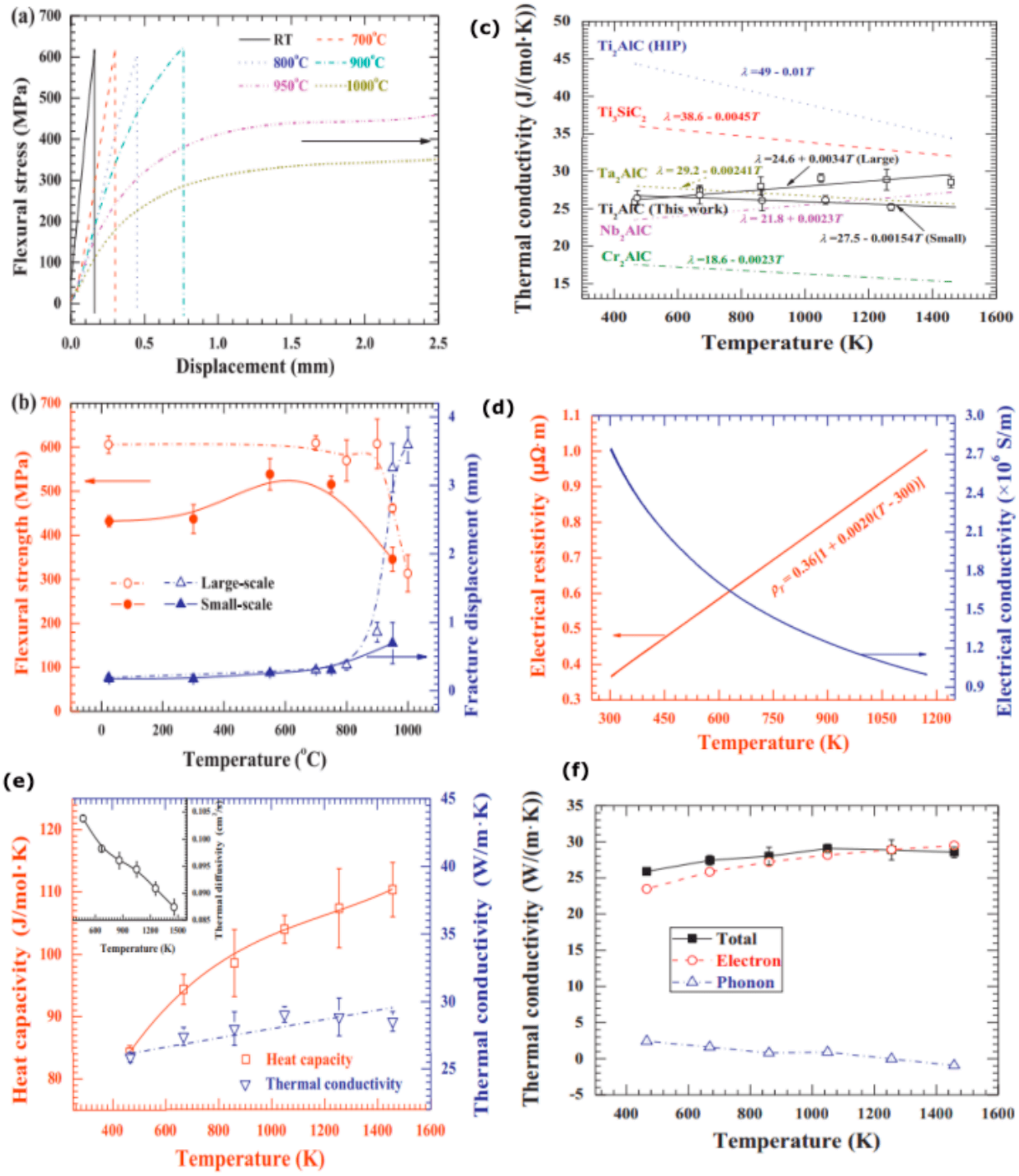

Figure 17. (a) Flexural stress–displacement curves and (b) corresponding flexural strength across the temperature range from RT to 1000 °C, (c) Thermal conductivity as a function of temperature for large-scale Ti_2AlC synthesized via the SHS/PHIP process, for Ti_2AlC, Cr_2AlC, Ta_2AlC, Nb_2AlC, and Ti_3SiC_2. (d) Temperature dependence of electrical conductivity and resistivity for large-scale Ti_2AlC produced via the SHS/PHIP process. (e) Temperature dependence of thermal conductivity, heat capacity, and thermal diffusivity for large-scale Ti_2AlC synthesized via the SHS/PHIP process, (f) Variation of electron, phonon, and total

thermal conductivities with temperature. Reproduced from Ref.[389] with permission from Copyright(2013) Elsevier

Magnetic Properties

Understanding the magnetic properties helps to obtain them in applications such as spintronics, magnetic sensors, magnetic refrigeration, biomedical applications, data transfer, etc. The magnetic ground state has been theoretically predicted for a large number of MAX phases and also experimentally observed[407][408]. However, studies on magnetic MAX phases predominantly focus on the substitution of manganese and chromium-based compounds. Such as $(V, \mathrm{Mn})_3\mathrm{GaC}_2$, $\mathrm{Cr}_2\mathrm{AlC}$, $\mathrm{Cr}_2\mathrm{GeC}$, and $(\mathrm{Cr}, \mathrm{Mn})_2\mathrm{AlC}$, as well as $\mathrm{Cr}_2\mathrm{GeC}$ and $(\mathrm{Cr}, \mathrm{Mn})_2\mathrm{GaC}$ and $(\mathrm{Mo}, \mathrm{Mn})_2\mathrm{GaC}$[408]. Recent developments made by Tao et al. in magnetic MAX phases include the ordered structures in the plane of $(M_{2/3}\mathrm{Sc}_{1/3})_2\mathrm{AlC}$ (where $M = \mathrm{Cr}, \mathrm{Mn}$)[339] and $(\mathrm{Mo}_{2/3}\mathrm{RE}_{1/3})_2\mathrm{AC}$[332][340] where (Rare-Earth)RE comprising Ce, Pr, Nd, Sm, Gd, Tb, Dy, Ho, Er, Tm, and Lu. The theoretical prediction of promising ferromagnetic properties shown by $\mathrm{F}e_3\mathrm{A}l\mathrm{C}_2$ will also enhance the exploration of work on the magnetic MAX phase. These will add more candidates for the spintronics application.

Fig.18 represents the magnetic response measured with a vibrating sample magnetometer at three different temperatures, reaching a maximum temperature of 300 K. The upper left inset shows the magnetization in and out of the plane M in low applied fields at 50 K, where the coercive field in the plane was determined to be 28$\pm$5 mT. A small remanence is observed in the in-plane direction. The bottom right inset displays the temperature dependence of the saturation moment m_s, with a fit to the functional form $1 - T$, and the remanent moment m_r in units of the Bohr magneton per Mn atom[407].

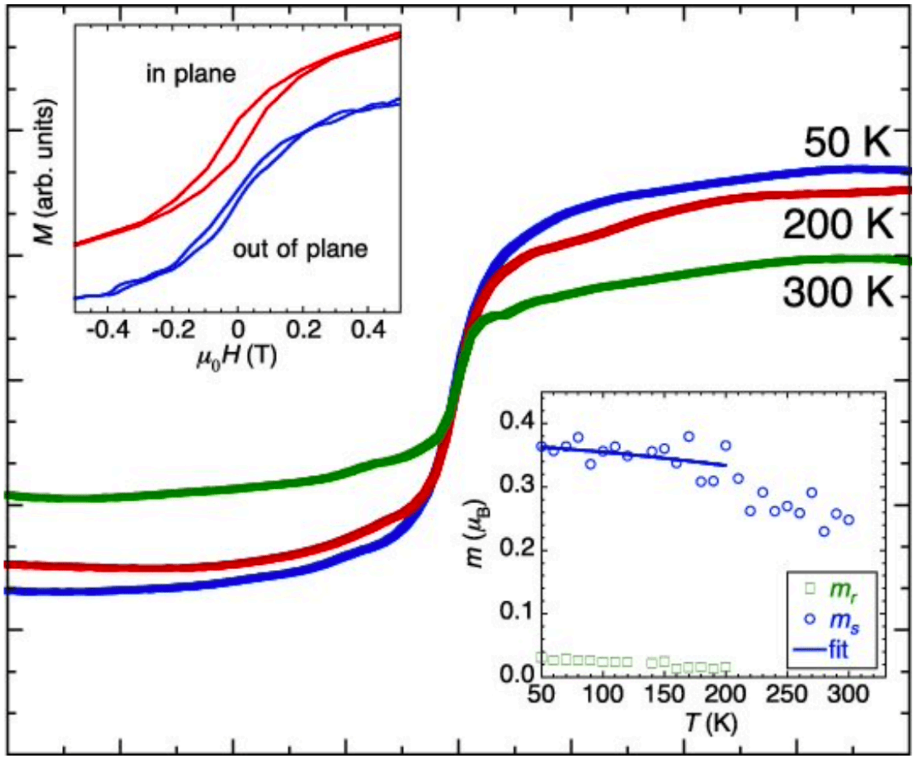

Figure 18. The magnetic response was recorded with a vibrating sample magnetometer at three distinct temperatures. Reprinted with permission from[407]. © Copyright (2023) American Physical Society

Optical Properties

MAX phases display notable anisotropic optical characteristics in the infrared and visible light regions, with distinct spectral variations observed for different polarization directions. However, this anisotropy reduces at higher energy levels, where the spectra for both polarizations converge and become almost indistinguishable across various compositions. These optical properties are largely influenced by the electronic structure of the materials, with the density of states (DOS) providing insights into the origins of spectral peaks.

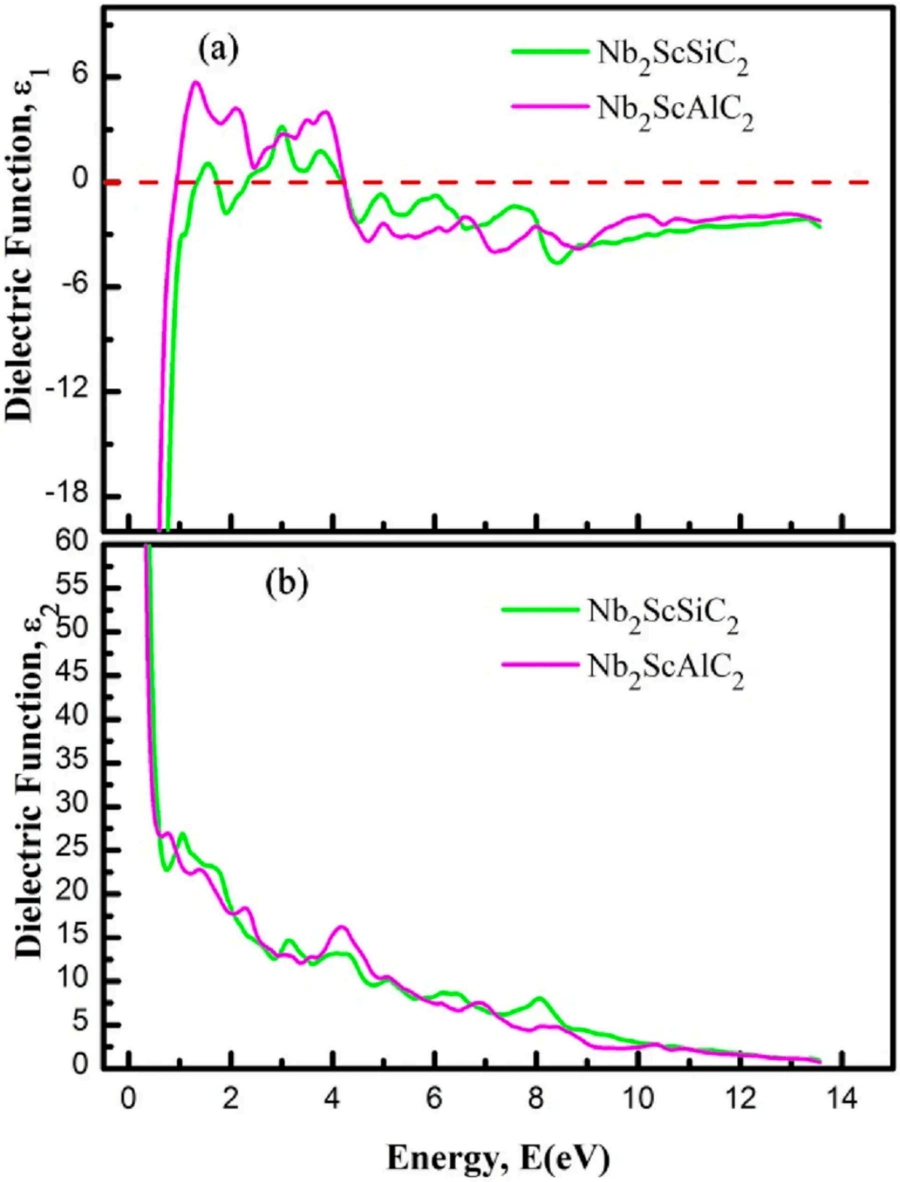

Figure 19. (a) Real part (ε_1) and (b) imaginary part (ε_2) of the dielectric function for Nb_2ScAC_2 (A = Al, Si) compounds. .Reprinted with permission from[409]. © Copyright (2023) Springer Nature

In Fig.19 the larger imaginary dielectric constant signifies greater light absorption at specific wavelengths. In contrast, the real part of the dielectric constant reflects the polarization properties of the material. It relates to the speed of light within the material, where a higher value denotes a reduced light propagation speed. One of the prominent applications of MAX phases is their effectiveness as coatings to minimize solar heating. Reflectivity analysis of Nb_2ScAC_2 (A = Al, Si)[409] compounds shows a reflectivity that exceeds 44%, meeting the threshold for solar heat reduction[410][411]. This establishes their potential as efficient thermal management materials. Furthermore, the refractive index values —$n(0) = 5.91$ for Nb_2ScAlC_2 and $n(0) = 6.64$ for Nb_2ScSiC_2—underscore their capacity to control the phase velocity of incident light, which is crucial for the precise development of electronic and photonic devices. MAX phases offer outstanding optical properties combined with flexibility for diverse applications, including solar energy control[412], advanced optical systems[413], and electronic device engineering. Their anisotropic nature and high refractive indices make them particularly well-suited for specialized thermal and optical functionalities.

A. Properties of MXene

MXene is a two-dimensional material derived from metal carbides and nitrides that is notable for its exceptional properties and the wide range of possible compositions. This compositional versatility opens up more room for potential applications, making MXene a highly promising material in fields such as energy storage, catalysis, spintronics, and electronics.

Electronic Properties

Depending on the nature of the M, X and T groups, the electronic properties of MXene vary from metallic to semiconductor[261][414]. Functionalization groups also play a vital role in the definition of electronic structures[261][415][416] as shown in Fig.20. Due to significant spin-orbit coupling predicts the existence of 2D topological insulator as shown in Fig.23 and Fig.24 predicted from DFT calculation. In Fig.23, band structures for $Mo_2TiC_2O_2$, $Mo_2ZrC_2O_2$, and $Mo_2HfC_2O_2$ are calculated with and without spin-orbit coupling (SOC). Considering SOC will introduce a band gap at the Γ point, which shows the topological insulating behavior. Fig.24 illustrates the local density of states (LDOS) as a function of energy and momentum for $Mo_2HfC_2O_2$ at the zigzag edge, with the Fermi level positioned at zero. The edge states bridge the bulk valence and conduction bands, meeting exclusively at the M point. Several other terminated MXenes, represented as M’$_x$M”$_y$Xene oxides (for $x = 2$ and $y = 1, 2$), have been theoretically found to exhibit stability along with topological insulating properties. These findings suggest that such MXenes could serve as a platform for future research in topological materials[417]. Furthermore, electronic conductivity in MXene systems has been demonstrated to be anisotropic[418][419]. In Fig.23(a) The states near the Fermi level are attributed to M -d orbitals, which contribute to electrical conductivity in MXene systems, and most terminated MXenes show metallicity compared to that of a semiconductor[415][420].

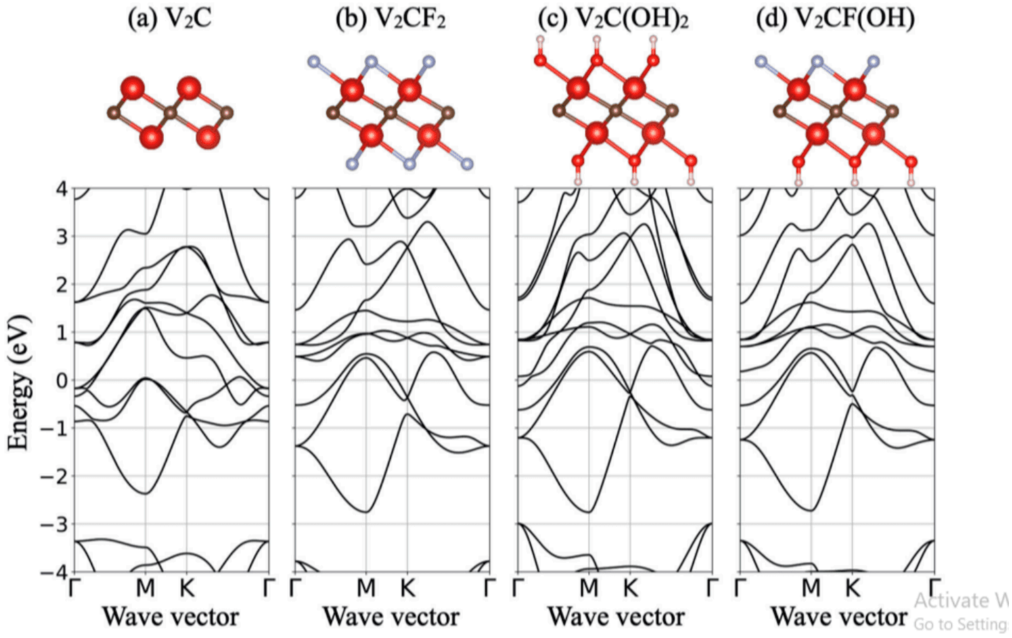

Figure 20. Electronic band diagrams of (a) V_2C, (b) V_2CF_2, (c) $V_2C(OH)_2$, and (d) $V_2CF(OH)$ in their high-symmetry states, where the Fermi level is aligned to zero energy. Reprinted with permission from Ref.[421]. © Copyright (2018) American Physical Society

Thermal Properties

Theoretical investigation by Zha *et al.*[422] found that the thermal expansion coefficient, electronic band gap, and charge carrier mobility of the systems M_2CO_2 (M = Ti, Zr, Hf) exhibit a highly anisotropic nature. Using the BoltzTraP2 code, the electronic contribution to total thermal conductivity was calculated Ref.[423][424]. Similarly, the contribution of the lattice was determined using the temperature-dependent effective potential (TDEP) code[425][426][426].

It has been observed that both the in-plane thermal conductivity, $K_{\|}$, and the out-of-plane thermal conductivity, $K_{\perp}$, show a slight decrease as the temperature increases. An anisotropy ratio greater than 2 was predicted for the entire temperature range. This anisotropy comes from both electronic and lattice contributions, with the lattice contribution being the most dominant Ref.[419].

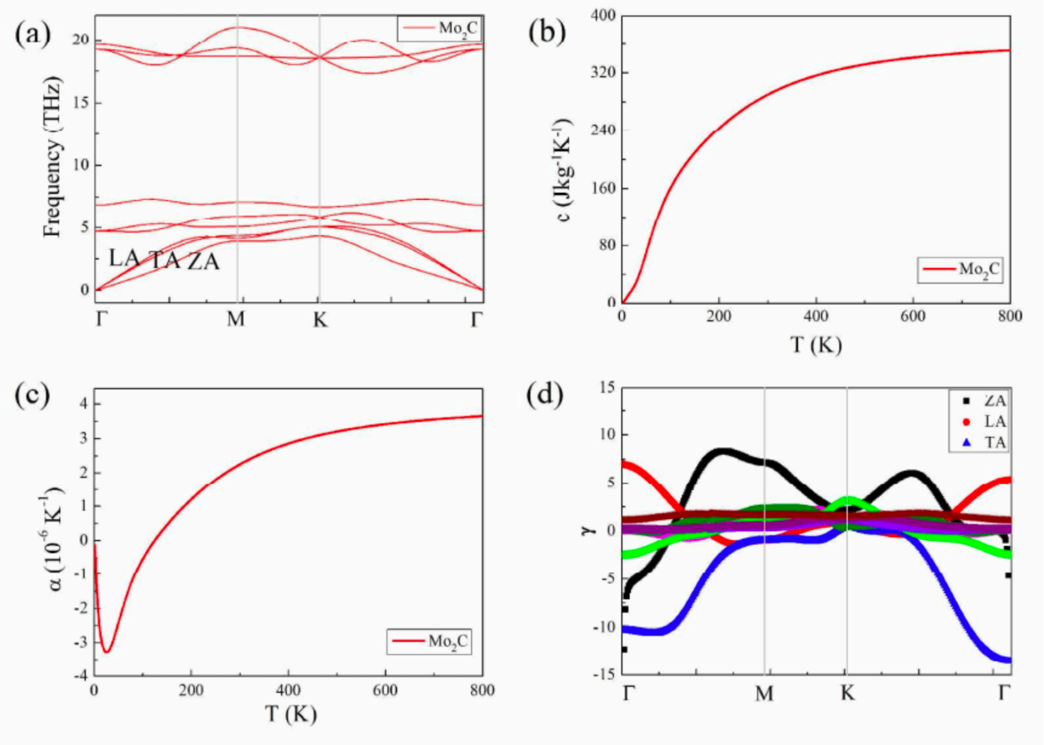

Figure 21. (a) Phonon dispersion across the full Brillouin zone (BZ); (b) temperature dependence of specific heat; (c) thermal expansion coefficient variation with temperature; (d) Grüneisen parameter distribution throughout the BZ. Reprinted with permission from Ref.[427] © Copyright (2016) American Chemical Society

The dispersion of phonons throughout the Brillouin Zone (BZ), shown in Fig.21(a), was used to examine the specific heat and thermal expansion coefficient of Mo$_2$C MXene. As depicted in Figures 21(b) and 21(c), the specific heat increases with temperature, reaching 290 J/kg·K at room temperature and 351 J / kg K at 800 K. Mo$_2$C MXene exhibits a unique thermal expansion behavior compared to functionalization MXenes and bulk materials; it contracts at low temperatures, with a negative thermal expansion coefficient of $-3.27 \times 10^{-6}\ \mathrm{K}^{-1}$ at 25 K, then expands at higher temperatures, reaching $3.65 \times 10^{-6}\ \mathrm{K}^{-1}$ at 800 K. Fig.21(d) shows that acoustic modes dominate the thermal behavior of Mo$_2$C MXene, the ZA mode contributing to both thermal contraction and expansion. The TA mode mainly causes contraction, while the LA mode drives expansion. Due to the low thermal expansion coefficient of Mo$_2$C MXene, a thermal mismatch with pure molybdenum occurs, enabling the clean Mo$_2$C MXene to be obtained by rapid cooling. This low thermal expansion also benefits practical applications by improving the temperature stability[427].

Mechanical Properties

The elastic behavior of Cr_2AlC single crystals was studied through first-principles calculations and nanoindentation tests, producing $c_{11} = 347$ GPa and $c_{33} = 332$ GPa, with experimental values, using the Oliver and Pharr method, of 317 ± 10 GPa and 320 ± 9 GPa, which confirms close agreement[428][429][430].

Kurtoglu et al. found that the elastic constant of MXene is twice larger than the corresponding MAX phase[431] and also found that nitrides are more stiff than carbides[432][433]. The measured Young modulus of 330 ± 30 GPa is lower than that of graphene (1000 ± 100 GPa) and h-BN (870 ± 70 GPa). However, this value represents the highest Young's modulus recorded for a solution-processed 2D material, exceeding that of MoS_2 at 270 ± 100 GPa and graphene oxide at 210 ± 20 GPa[434]. However, experiments revealed improvements in various mechanical properties, including tensile strength, elastic modulus, thermal and electrical conductivities, as well as electrochemical capacitance[14][435][436][437][438][439].

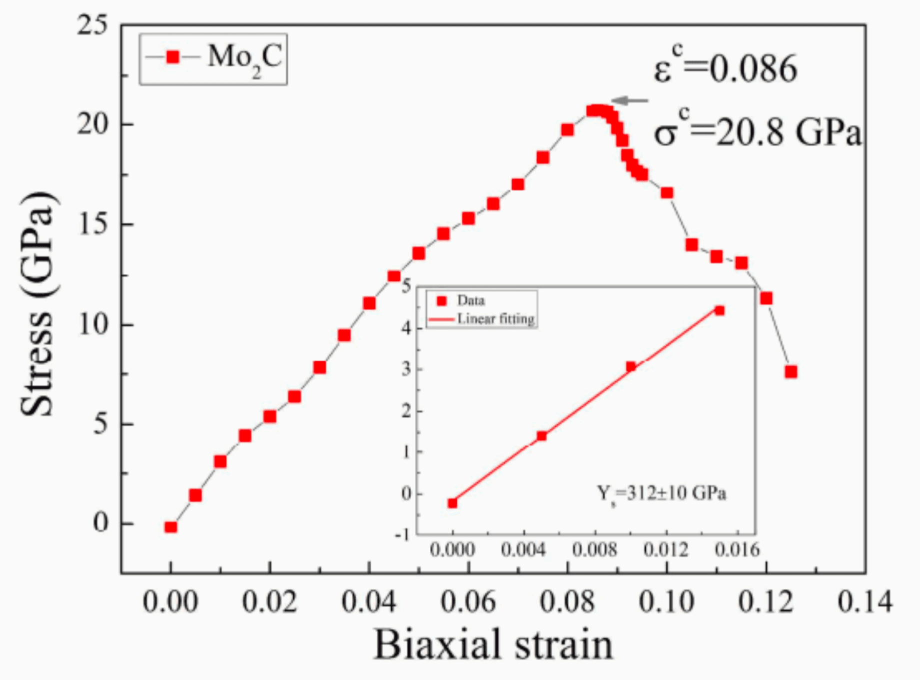

Figure 22. The stress-strain relationship for Mo_2C MXene under biaxial strain. The inset displays the linear regression of the initial curve, used to determine the biaxial elastic modulus. Reprinted from Ref.[427]. © Copyright (2016) American Chemical Society

Fig.22 illustrates the stress-strain relationship for Mo_2C MXene, showing a biaxial elastic modulus of $Y_{2D} = 312 \pm 10$ GPa, slightly exceeding that of monolayer MoS_2. Beyond a critical strain of 0.086, the material undergoes creep deformation, with an ideal strength of 20.8 GPa, close to that of monolayer MoS_2 (23.8 GPa), highlighting its robust elasticity and strength.

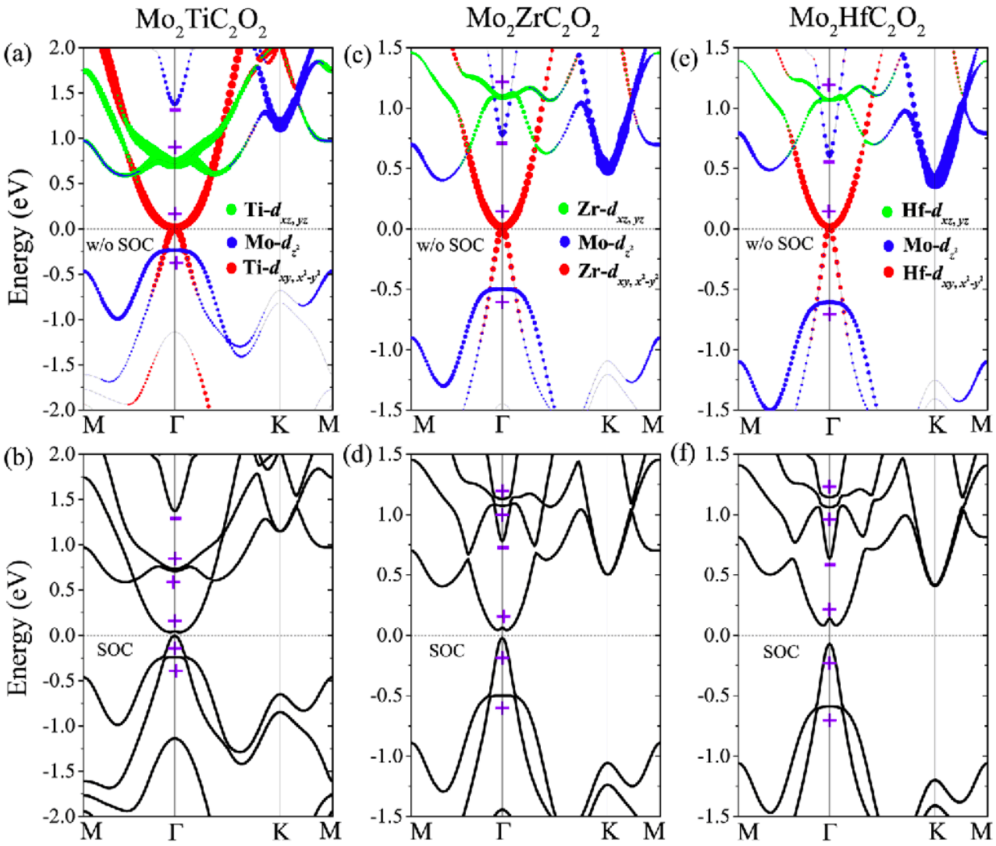

Figure 23. Calculated GGA band structures for $Mo_2TiC_2O_2$ (a, b), $Mo_2ZrC_2O_2$ (c, d), and $Mo_2HfC_2O_2$ (e, f) with and without spin-orbit coupling (SOC). Including SOC introduces a gap at the Γ point. Reprinted with permission from Ref.[440]. © Copyright (2016) American Chemical Society

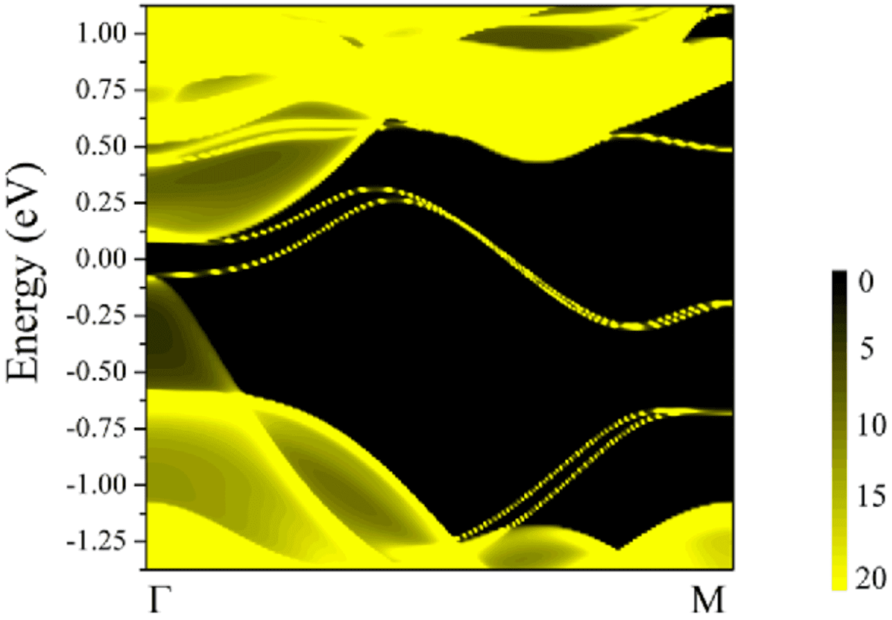

Figure 24. Energy and momentum-dependent local density of states (LDOS) for $Mo_2HfC_2O_2$ at the zigzag edge, with the Fermi level set to zero. Edge states connect the bulk valence and conduction bands, intersecting only at the M point. Reprinted with permission from Ref.[440]. © Copyright (2016) American Chemical Society

Magnetic Properties

Unfortunately, the majority of MXenes discovered so far, both theoretically and experimentally, have been found to be nonmagnetic. Exceptions include a few specific compounds, such as $(Cr_2Ti)AlC_2$, Ti_2NF_2, $Ti_2N(OH)_2$, Ti_2NO_2, V_2NF_2, $V_2N(OH)_2$, V_2NO_2, Cr_2NO_2, Mn_2C, Mn_2CF_2, $Mn_2C(OH)_2$, Mn_2CO_2, Mn_2N, Mn_2NF_2, $Mn_2N(OH)_2$, Mn_2NO_2, Cr_2C, Cr_2CF_2, and $Cr_2C(OH)_2$[441][442][443]. Upon functionalization, some MXenes have been predicted to retain a magnetic moment[444].

doi.org/10.32388/A3QP41

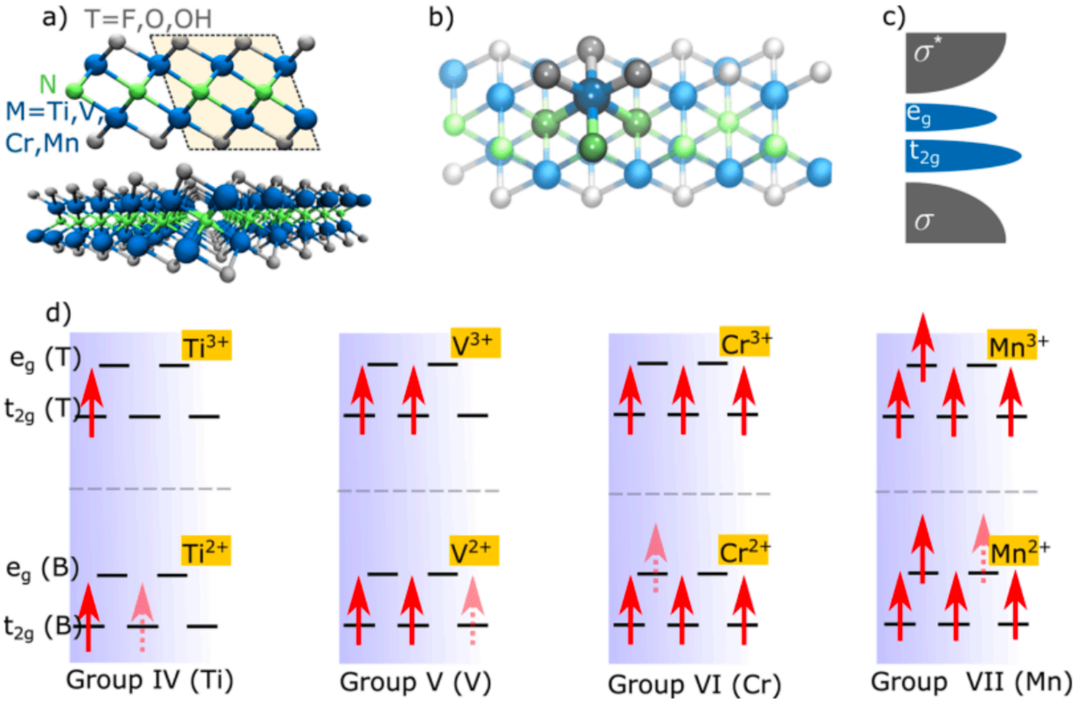

Figure 25. Illustration of the localized magnetic moments in M_2NT_2 MXenes for various transition-metal groups. (a) Side view of the MXene crystal structure with the unit cell highlighted. (b) Top view of a monolayer MXene displaying octahedral coordination. (c) Simplified density of states considered in the model. (d) Electron arrangement localized on transition-metal centers for groups IV to VII of the periodic table, where dotted spins represent equal probability of occupation in either the top (T) or bottom (B) layer states. Reprinted wih permisssion from Ref.[445]. © Copyright (2017) American Chemical Society

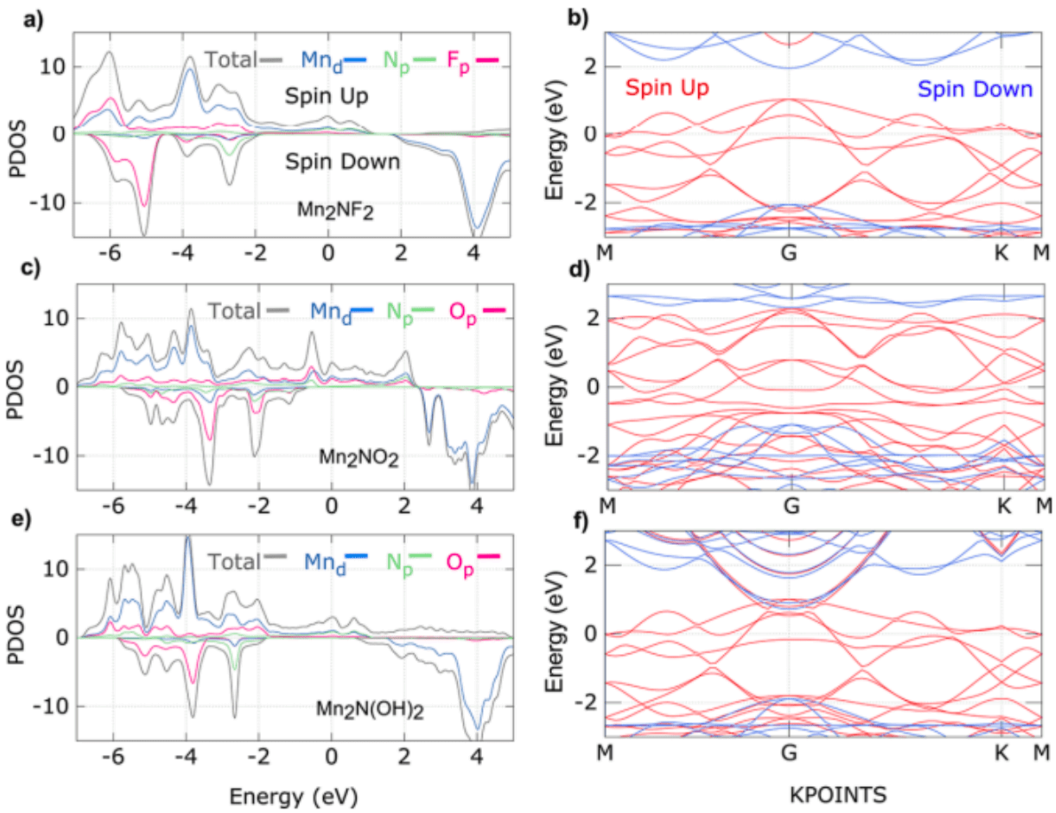

Figure 26. Electronic band structure and density of states (DOS) for Mn_2NT MXenes. Site-projected DOS for (a) Mn_2NF_2, (c) Mn_2NO_2, and (e) $Mn_2N(OH)_2$. Band structure plots for (b) Mn_2NF_2, (d) Mn_2NO_2, and (f) $Mn_2N(OH)_2$. Reprinted from Ref.[445]. © Copyright (2017) American Chemical Society

Ferromagnetic (FM) ground states are critical for 2D magnetic materials, and five nitride MXenes (Mn_2NF_2, Mn_2NO_2, $Mn_2N(OH)_2$, Ti_2NO_2, and Cr_2NO_2) was studied[445] and demonstrated robust FM behavior . For Mn_2NF_2, the FM phase is more stable than the nonmagnetic phase by 7.1 eV, with a magnetic moment of $\sim$9.0 μ_B per formula unit, primarily from localized spin density near transition-metal atoms. Unlike Mn_2C MXenes, which exhibit antiferromagnetic (AFM) states for specific terminations, nitride MXenes maintain FM states across all terminations due to an additional electron from nitrogen, stabilizing FM spin configurations.

The magnetic moments of different MXenes can also be estimated using a simplified model, mainly for M_2NT_2 MXenes with $3d$ transition metals, but this approach can be extended to include $4d$ and $5d$ elements. However, for heavier elements, increased delocalization of electrons may lead to nonmagnetic states, although larger atomic radii and reduced hybridization could still enable magnetism. From the theoretical study, using density functional theory (DFT), the results shown in Fig.25 and Fig.26[445] confirm the predictions of the model, with minor deviations arising from electron delocalization in 2D crystals. These findings highlight the tunability of MXene magnetism via transition-metal selection and surface terminations, making them versatile candidates for magnetic applications.

From Fig.26, the electronic band structure and DOS for $\mathrm{Mn_2NT}$ MXenes show robust half-metallicity with metallic conduction for the majority spins and a wide (> 3 eV) semiconducting gap for minority spins, validated across all surface terminations.

Optical Properties

MXenes exhibit remarkable optical properties, making them ideal for use in photovoltaics, photocatalysis, transparent electrodes, and optically conducting devices. These materials absorb light in a wide spectrum, including the UV-visible (300–500 nm) and near-infrared (700–800 nm) regions Ref. [446], with films as thin as 10 nm showing transmittance to 91%. Their optical properties can be tuned by adjusting the film thickness or adding compounds such as tetramethylammonium, which enhances transparency, or urea, hydrazine, and dimethyl sulfoxide (DMSO), which reduce it. MXenes also possess a tunable bandgap (up to $\sim$2 eV) and surface terminations ($-O$, $-OH$, $-F$), making them highly versatile for advanced optoelectronic applications[367][447][448][449].

Additionally, MXenes exhibit strong light absorption as a result of their high-density electronic states, and their localized surface plasmon resonance (LSPR) in the near- and mid-infrared ranges enables use in sensors, photodetectors, and solar energy harvesting. These materials also show high photothermal conversion efficiency, non-linear optical behaviors such as saturable absorption, and harmonic generation, positioning them for photothermal therapy, ultrafast lasers, and optical limiters. Despite challenges such as oxidation stability and scalable synthesis, MXenes hold great potential in photonics, optoelectronics, and energy devices.

$\mathrm{Ti_3C_2T}_x$ also demonstrates nonlinear optical properties[447], including saturable absorption (SA), where light transmission increases nonlinearly with intensity. With a nonlinear absorption coefficient of $-10^{-21}\ \mathrm{m^2V^{-2}}$, $\mathrm{Ti_3C_2T}_x$ is promising for optical switching applications[449][450][451]. This behavior is attributed to plasmon-induced absorption when the laser wavelength matches the plasmon resonance frequency. $\mathrm{Ti_3C_2T}_x$ shows nonlinear absorption across 800–1800 nm, with one-photon absorption at low intensities and multi-photon absorption at higher intensities, making it suitable for ultra-fast laser applications such as mode-locked lasers.

Moreover, $Ti_3C_2T_x$ is applicable in telecommunication (1550-1620 nm C band) and demonstrates superior resilience under high laser energy compared to other 2D materials. Furthermore, when combined with C_{60}, it forms optical diodes for signal filtering, and it can produce random lasing when dispersed in rhodamine 101 solution[452].

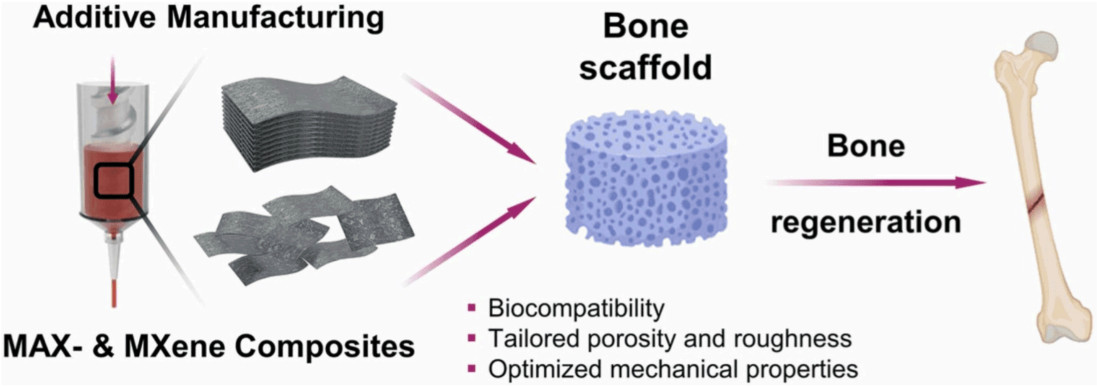

Figure 27. Reprinted with permission from[66]. © Copyright (2023) Elsevier

V. Application

Application of MAX Phase and MXene

MAX phases and MXene have shown significant potential in various applications, as some of them are listed in TableI with different synthesis, properties, and application methods, attributed to their versatile chemical compositions.

Some of the applications of MAX Phase

- **High-Temperature Structural Materials**: MAX phases exhibit excellent thermal stability,Ti_2AlC has been rigorously tested at high temperatures and exhibits remarkable stability even at extreme temperatures up to 1350 °C[453][454][455][456], oxidation resistance[38][39][40][41], and creep resistance[457][458], making them suitable for high-temperature applications in jet engines, gas turbines, and nuclear reactors[42][102][182][183][459][460].

- **Electrical and Thermal Conductors**: Their metallic nature ensures good electrical and thermal conductivity, making them ideal for use in electrical contacts[184][461] and heat sinks[186].
- **Wear-Resistant Coatings**: MAX phases combine hardness with damage tolerance, providing excellent wear and corrosion resistance[38][39][40][41][462] for coatings on cutting tools, molds, and industrial machinery[463].
- **Biomedical Applications**: Biocompatible MAX phases like Ti_3SiC_2 are explored for use in medical implants[187][188][464], prosthetics[189][465], and surgical tools due to their non-toxicity and good mechanical properties[64][65][66].
- **Energy Storage and Conversion**: MAX phases are studied for use in supercapacitors[191], batteries[68], and fuel cells due to their electrical conductivity and stability under extreme conditions.
- **Radiation Shielding**: MAX phases, particularly those based on carbides, are explored for radiation resistance in nuclear applications[102][459], such as fuel claddings and containment systems.
- **Tribological Applications**: Their self-lubricating properties make MAX phases ideal for sliding components and seals in the aerospace and automotive industries[190][273][466].
- **Catalysis and Chemical Stability**: MAX phases exhibit chemical stability in harsh environments, making them suitable for catalytic supports and components in chemical processing[62][63][64][64][67].
- **Environmental Applications**: Due to their resistance to thermal shock and oxidation[38][39][40][41][192][193], MAX phases are used in filters and components exposed to high-temperature exhaust gases.
- **Magnetic and Spintronic Applications**:
  Emerging studies suggest potential for certain MAX phases (or their derivatives like MXenes) in spintronic devices and magnetic materials[196][408][467].
- **Photocatalysis**: It can serve as precursors to photocatalytic materials for hydrogen production via water splitting and pollutant degradation due to their tunable electronic properties and layered structure[105][160][468].
- **Superconductors**: MAX phases exhibit superconducting behavior under specific conditions, attributed to their unique layered crystal structure and excellent electrical conductivity[469][470].

Some of the applications of MXene

- **Energy Storage Devices**: MXenes are extensively used in supercapacitors[15][119][130][131][132], lithium-ion batteries[471][472][473], sodium-ion batteries[474][475], and other energy storage devices due to their high conductivity and tunable surface chemistry.

- **Electromagnetic Interference (EMI) Shielding**: The exceptional electrical conductivity[118][119][120][121] and the layered structure of MXenes make them highly effective for EMI shielding applications in electronics[12][476][477].
- **Water Purification and Desalination**: MXenes, with their high adsorption capacity and hydrophilic surfaces[125][126], are used to remove heavy metals, dyes and salts from water[152][153][161][162].
- **Catalysis**: MXenes act as efficient catalysts or catalyst supports in various chemical reactions, including the hydrogen evolution reaction (HER), the oxygen evolution reaction (OER) and the reduction of carbon dioxide[148][149][150][151]. It has effective use in photocatalysis[159][160]
- **Biomedical Applications**: MXenes are explored for drug delivery, biosensors[478][479][480], photothermal therapy[163][481][482], and antimicrobial coatings[483][484] due to their biocompatibility and large surface area[156].
- **Sensors and Actuators**: Their high conductivity and ability to interact with various molecules make MXenes suitable for gas sensors[485][486], strain sensors[487][488], and biosensors[478][479][480].
- **Wearable Electronics**: MXenes are used in flexible and stretchable electronics for applications such as smart textiles[489][490], wearable health monitors[491][492] and electronic skin[493]s.
- **Thermal Management**: It has high thermal conductivity, making it an effective material for heat dissipation in electronics and other thermal management applications[494][495].
- **Electronics and Optoelectronics**: MXenes are being studied for use in transistors, memory devices, photodetectors, and other advanced electronic and optoelectronic devices[142][143][144][496][497][498].
- **Spintronics and Magnetism**: Some MXenes exhibit magnetic properties[145][146] and are being explored for potential applications in spintronics and magnetic storage devices[1][467][499].
- **CO2 Capture**: Functionalized MXenes exhibit excellent CO2 adsorption capabilities due to their chemical tunability and large surface area, making them ideal for carbon capture technologies[165][166][166][500][501].
- **Superconductors**: MXenes hold promise for superconducting technologies[502][503][504], using their exceptional metallic conductivity and unique two-dimensional layered architecture under certain conditions.

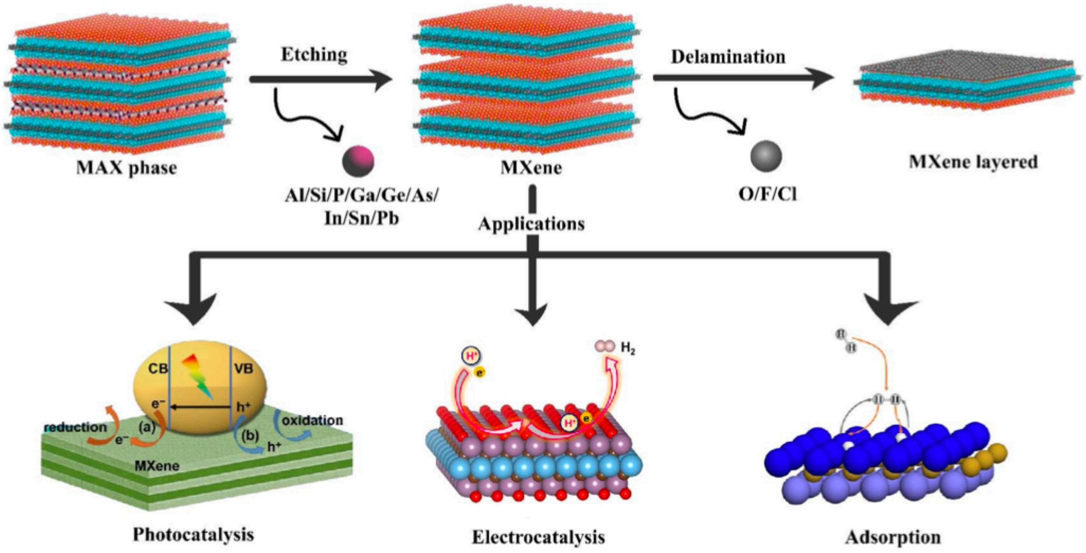

Figure 28. Reprinted with permission from Ref.[468]. © Copyright (2024) Elsevier

VI. Conclusion

In summary, MAX phases and their 2D derivative MXenes have emerged as groundbreaking energy-efficient materials appealing candidates for next-generation energy-efficient technological applications. This review addresses current status, challenges, and provides general solutions for large-scale production, improving the properties of MAX/MXenes, and highlighting their transformative potential across a wide range of industries. This paper also provides a comprehensive report on several novel and cost-effective techniques to synthesize the MAX phase and exfoliate 2D materials (MXene) from bulk. MAX phases, with their unique combination of the metal-nonmetal layered hexagonal structure, possess distinctive properties such as high electrical conductivity, high thermal conductivity, and mechanical strength which make them promising in high-temperature applications in aerospace, automotive, and energy industries. They also show impressive potential for application in extreme conditions due to their high resistance, high thermal stability, and high corrosion resistance, positioning them as ideal candidates for demanding environments where materials must perform reliably for extended periods. However, the integration of bulk properties into modern technological devices is challenging, which require high speed, high storage, low-power consumption, portability, etc. In order to fulfill the demand of modern technology, it is necessary to scale down to the 2D nano-size compatibility, addressing all its merits. So, this review expands the traditional understanding of the 2D properties (MXene), which was previously limited to the bulk (MAX phase). Although the 2D nanosheet of MXene is derived from MAX phases, the horizons for these materials have been further broadened. The ability of MXenes to tune their functionalities under various conditions such as strain engineering, applied electric field, surface functionalization (-OH, -F, or -O groups), etc., makes them a key material for specific applications. Modulation of the surface terminations of MXenes has opened up new possibilities for their use in sensors, catalysis, and environmental remediation such as water purification and CO_2 capture. MXenes are promising for the advancement of performance in energy storage and conversion, particularly in lithium-ion and sodium-ion batteries, supercapacitors, photocatalysts, and other energy-storage/harvesting systems, which could significantly add to the list of renewable energy technologies. The versatility of MXenes lies in their excellent conductivity, mechanical flexibility, and ease of functionalization, ideal for use in flexible electronics, sensors, and wearable devices. As the demand for smaller, more flexible and multifunctional electronic devices increases, the ability of MXenes to be integrated into such technologies could play a key role in the development of next-generation smart devices, health monitoring systems, and wearable technologies. Despite the promising potential of MAX phases and MXenes, challenges related to their synthesis, scalability, and long-term stability in various environments are still associated.

Through our rigorous literature survey, we have noticed that MXenes are rarely explored in the field of spin technology despite having all merits such as tunable electronic and magnetic properties, high electrical conductivity, and ability to interact with magnetic fields. The integration of MXenes into spintronic devices, such as spin valves, magnetic tunnel junctions, and spin injectors, could lead to the development of faster, more efficient, and energy-efficient devices, which are crucial for the future of information processing and storage. Understanding the emergence of macroscopic behavior of MXenes by controlling the electron spin at a fundamental level is likely to unlock new possibilities and accelerate the development of novel spintronic devices. In our next project, we aim to understand the fundamental of spin-dynamics in MXenes employing first-principles density functional theory (DFT) calculations and explore their magnetic properties, spin-polarized transport, etc. The project will also address the development of efficient methods for energy-saving spintronics technologies that pave the way for advanced information processing systems.

Statements and Declarations

Acknowledgments

DPR acknowledges Anusandhan National Research Foundation (ANRF), Govt. of India, through Sanction Order No.:CRG/2023/000310, & dated:10 October, 2024.

Author contributions

- **C. B. Subba:** First author, Formal analysis, Visualization, Validation, Calculating results, Writing-original draft, writing-review & editing.
- **D. P. Rai:** Project management, Supervision, Resources, Software, Formal analysis, Visualization, Validation, writing-review & editing.
- **Mukhriddin E. Tursnov:** Formal analysis, writing-review & editing.
- **Avazbek T. Dekhonov:** Formal analysis, Visualization, Validation, writing-review & editing.
- **Z. Pachuau**:Formal analysis, Visualization, Validation, writing-review & editing.

Data Availability Statement

Data available in the article.

References

1. a, b*Dihingia KD, Saikia S, Yedukondalu N, Saha S, Sastry GN (2022). "2D-double transition metal MXenes for spintronics applications: Surface functionalization induced ferromagnetic half-metallic complexes". Journal of Materials Chemistry C. 10(47):17886–17898.*
2. ^*Parajuli D, Samatha K. "Topological properties of MXenes". In: MXenes and their composites. Elsevier 2022. pp. 171–199.*
3. ^*Khan K, Tareen AK, Iqbal M, Hussain I, Mahmood A, et al. (2023). "Recent advances in MXenes: A future of nanotechnologies". Journal of Materials Chemistry A.*
4. a, b, c*Xu C, Wang L, Liu Z, Chen L, Guo J, et al. (2015). "Large-area high-quality 2D ultrathin Mo2C superconducting crystals". Nature materials. 14(11):1135–1141.*
5. ^*Anasori B, Lukatskaya MR, Gogotsi Y. "2D metal carbides and nitrides (MXenes) for energy storage". In: MXenes. Jenny Stanford Publishing 2023. pp. 677–722.*

6. ^Ali MR, Bacchu MS, Al-Mamun MR, Hossain MI, Khaleque A, et al. (2024). "Recent advanced in MXene research toward biosensor development". Critical Reviews in Analytical Chemistry. 54(6):1381–1398.
7. ^Jandas PJ, Prabakaran K, Luo J, Fu C, Fu YQ, et al. (2021). "Ti3C2Tx MXene-au nanoparticles doped polyimide thin film as a transducing bioreceptor for real-time acoustic detection of carcinoembryonic antigen". Sensors and Actuators A: Physical. 331:112998.
8. ^Rhouati A, Berkani M, Vasseghian Y, Golzadeh N. (2022). "MXene-based electrochemical sensors for detection of environmental pollutants: A comprehensive review". Chemosphere. 291:132921.
9. ^Lorencova L, Bertok T, Filip J, Jerigova M, Velic D, et al. (2018). "Highly stable Ti3C2Tx (MXene)/pt nanoparticles-modified glassy carbon electrode for H2O2 and small molecules sensing applications". Sensors and Actuators B: Chemical. 263:360–368.
10. ^Liu H, Duan C, Yang C, Shen W, Wang F, et al. (2015). "A novel nitrite biosensor based on the direct electrochemistry of hemoglobin immobilized on MXene-Ti3C2". Sensors and Actuators B: Chemical. 218:60–66.
11. ^Peng Q, Guo J, Zhang Q, Xiang J, Liu B, et al. (2014). "Unique lead adsorption behavior of activated hydroxyl group in two-dimensional titanium carbide". Journal of the American Chemical Society. 136(11):4113–4116.
12. a, b, cShahzad F, Alhabeb M, Hatter CB, Anasori B, Hong SM, et al. (2016). "Electromagnetic interference shielding with 2D transition metal carbides (MXenes)". Science. 353(6304):1137–1140.
13. ^Han M, Yin X, Wu H, Hou Z, Song C, et al. (2016). "Ti3C2 MXenes with modified surface for high-performance electromagnetic absorption and shielding in the x-band". ACS applied materials & interfaces. 8(32):21011–21019.
14. a, bLing Z, Ren CE, Zhao MQ, Yang J, Giammarco JM, et al. (2014). "Flexible and conductive MXene films and nanocomposites with high capacitance". Proceedings of the National Academy of Sciences. 111(47):16676–16681.
15. a, b, c, d, eLukatskaya MR, Mashtalir O, Ren CE, Dall'Agnese Y, Rozier P, et al. (2013). "Cation intercalation and high volumetric capacitance of two-dimensional titanium carbide". Science. 341(6153):1502–1505.
16. a, b, cBarsoum MW, Farber L, Levin I, Procopio A, El-Raghy T, et al. (1999). "High-resolution transmission electron microscopy of Ti4AlN3, or Ti3Al2N2 revisited". Journal of the American Ceramic Society. 82(9):2545–2547.
17. ^Choudhary E, Manjunath V, Kalubarme R, Jangir R, Devan RS. (2024). "Molten salt-shielded solid-state synthesis (MS 5) reaction-driven> 99% pure ti 3 AlC 2 MAX phase: Effect of MAX phase purity on the interlayer separation of MXenes and na-ion storage". Nanoscale. 16(37):17599–17615.

18. a, b, c, d, eLu J, Thore A, Meshkian R, Tao Q, Hultman L, et al. (2017). "Theoretical and experimental exploration of a novel in-plane chemically ordered (Cr2/3M1/3) 2AlC i-MAX phase with m= sc and y". Crystal Growth & Design. 17(11):5704–5711.
19. a, b, c, d, e, f, g, hLapauw T, Halim J, Lu J, Cabioc'h T, Hultman L, et al. (2016). "Synthesis of the novel Zr3AlC2 MAX phase". Journal of the European Ceramic Society. 36(3):943–947.
20. a, b, cJulian-Jankowiak A, Sallot P. (2018). "Microstructure and mechanical properties of Nb4AlC3 MAX phase synthesized by reactive hot pressing". Ceramics International. 44(14):16314–16324.
21. a, bHossein-Zadeh M, Mirzaee O, Mohammadian-Semnani H. (2019). "An investigation into the microstructure and mechanical properties of V4AlC3 MAX phase prepared by spark plasma sintering". Ceramics International. 45(6):7446–7457.
22. a, bShichalin OO, Ivanov NP, Seroshtan AI, Nadaraia KV, Simonenko TL, et al. (2024). "Spark plasma sintering of Ti2AlC/TiC MAX-phase based composite ceramic materials and study of their electrochemical characteristics". Ceramics International.
23. a, b, c, d, e, fBarsoum MW, El-Raghy T. (1996). "Synthesis and characterization of a remarkable ceramic: Ti3SiC2". Journal of the American Ceramic Society. 79(7):1953–1956.
24. a, b, c, d, eChen L, Dahlqvist M, Lapauw T, Tunca B, Wang F, et al. (2018). "Theoretical prediction and synthesis of (Cr2/3Zr1/3) 2AlC i-MAX phase". Inorganic Chemistry. 57(11):6237–6244.
25. a, b, c, d, e, fLapauw T, Tunca B, Cabioc'h T, Vleugels J, Lambrinou K. (2017). "Reactive spark plasma sintering of Ti3SnC2, Zr3SnC2 and Hf3SnC2 using fe, co or ni additives". Journal of the European Ceramic Society. 37(15):4539–4545.
26. a, b, cFu L, Xia W. (2021). "MAX phases as nanolaminate materials: Chemical composition, microstructure, synthesis, properties, and applications". Advanced Engineering Materials. 23(4):2001191.
27. a, bHamm CM, Schäfer T, Zhang H, Birkel CS. (2016). "Non-conventional synthesis of the 413 MAX phase V4AlC3". Zeitschrift für anorganische und allgemeine Chemie. 642(23):1397–1401.
28. a, bKubitza N, Xie R, Tarasov I, Shen C, Zhang H, et al. (2023). "Microwave-assisted synthesis of the new solid-solution (V1–x cr x) 2GaC (0≤ x≤ 1), a pauli paramagnet almost matching the stoner criterion for x= 0.80". Chemistry of Materials. 35(11):4427–4434.
29. a, bLuo W, Liu Y, Wang C, Zhao D, Yuan X, et al. (2021). "Molten salt assisted synthesis and electromagnetic wave absorption properties of (v 1- x- y ti x cr y) 2 AlC solid solutions". Journal of Materials Chemistry C. 9(24):7697–7705.

30. a, b, c *Eklund P, Dahlqvist M, Tengstrand O, Hultman L, Lu J, et al. (2012). "Discovery of the ternary nanolaminated compound nb_2GeC by a systematic theoretical-experimental approach". Physical review letters. 109(3):035502.*

31. a, b *Schneider JM, Sigumonrong DP, Music D, Walter C, Emmerlich J, et al. (2007). "Elastic properties of Cr2AlC thin films probed by nanoindentation and ab initio molecular dynamics". Scripta Materialia. 57(12):1137–1140.*

32. a, b *Rosen J, Persson PO, Ionescu M, Kondyurin A, McKenzie DR, et al. (2008). "Oxygen incorporation in Ti2AlC thin films". Applied Physics Letters. 92(6).*

33. a, b, c, d, e, f *Palmquist J-P, Li S, Persson POÅ, Emmerlich J, Wilhelmsson O, et al. (2004). "Mn+1AXn phases in the ti-si-c system studied by thin-film synthesis and ab initio calculations". Physical Review B—Condensed Matter and Materials Physics. 70(16):165401.*

34. a, b *Jacques S, Di-Murro H, Berthet M-P, Vincent H. (2005). "Pulsed reactive chemical vapor deposition in the c-ti-si system from H2/TiCl4/SiCl4". Thin Solid Films. 478(1-2):13–20.*

35. a, b *Fakih H, Jacques S, Berthet M-P, Bosselet F, Dezellus O, et al. (2006). "The growth of Ti3SiC2 coatings onto SiC by reactive chemical vapor deposition using H2 and TiCl4". Surface and Coatings Technology. 201(6):3748–3755.*

36. a, b *Frodelius J, Sonestedt M, Björklund S, Palmquist J-P, Stiller K, et al. (2008). "Ti2AlC coatings deposited by high velocity oxy-fuel spraying". Surface and Coatings Technology. 202(24):5976–5981.*

37. a, b *Maier BR, Garcia-Diaz BL, Hauch B, Olson LC, Sindelar RL, et al. (2015). "Cold spray deposition of Ti2AlC coatings for improved nuclear fuel cladding". Journal of Nuclear Materials. 466:712–717.*

38. a, b, c, d *Lambrinou K, Charalampopoulou E, Van der Donck T, Delville R, Schryvers D. (2017). "Dissolution corrosion of 316L austenitic stainless steels in contact with static liquid lead-bismuth eutectic (LBE) at 500° C". Journal of Nuclear Materials. 490:9–27.*

39. a, b, c, d *Heinzel A, Weisenburger A, Müller G. (2016). "Long-term corrosion tests of Ti3SiC2 and Ti2AlC in oxygen containing LBE at temperatures up to 700 C". Journal of Nuclear Materials. 482:114–123.*

40. a, b, c, d *Tunca B, Lapauw T, Callaert C, Hadermann J, Delville R, et al. (2020). "Compatibility of Zr2AlC MAX phase-based ceramics with oxygen-poor, static liquid lead–bismuth eutectic". Corrosion Science. 171:108704.*

41. a, b, c, d, e, f, g *Zhang Q, Wen B, Luo J, Zhou Y, San X, et al. (2023). "Synthesis of new lead-containing MAX phases of Zr3PbC2 and Hf3PbC2". Journal of the American Ceramic Society. 106(11):6390–6397.*

42. a, b *Sloof WG, Pei R, McDonald SA, Fife JL, Shen L, et al. (2016). "Repeated crack healing in MAX-phase ceramics revealed by 4D in situ synchrotron x-ray tomographic microscopy". Scientific Reports. 6(1):23040.*
43. a, b *Yu W, Vallet M, Levraut B, Gauthier-Brunet V, Dubois S. (2020). "Oxidation mechanisms in bulk Ti2AlC: Influence of the grain size". Journal of the European Ceramic Society. 40(5):1820–1828.*
44. ^ *Li S, Xiao L, Song G, Wu X, Sloof WG, et al. (2013). "Oxidation and crack healing behavior of a fine-grained Cr2AlC ceramic". Journal of the American Ceramic Society. 96(3):892–899.*
45. ^ *Farle A-S, Kwakernaak C, van der Zwaag S, Sloof WG. (2015). "A conceptual study into the potential of Mn+1AXn-phase ceramics for self-healing of crack damage". Journal of the European Ceramic Society. 35(1):37–45.*
46. ^ *Yao B, Li S, Zhang W, Yu W, Zhou Y, et al. (2022). "Self-healing behavior of Ti2AlC at a low oxygen partial pressure". Journal of Advanced Ceramics. 11(11):1687–1695.*
47. ^ *Li S, Zhang L, Yu W, Zhou Y. (2017). "Precipitation induced crack healing in a Ti2SnC ceramic in vacuum". Ceramics International. 43(9):6963–6966.*
48. ^ *Li M, Wang K, Wang J, Long D, Liang Y, et al. (2018). "Preparation of TiC/Ti2AlC coating on carbon fiber and investigation of the oxidation resistance properties". Journal of the American Ceramic Society. 101(11):5269–5280.*
49. ^ *Drouelle E, Gauthier-Brunet V, Cormier J, Villechaise P, Sallot P, et al. (2020). "Microstructure-oxidation resistance relationship in Ti3AlC2 MAX phase". Journal of Alloys and Compounds. 826:154062.*
50. ^ *Azina C, Mráz S, Greczynski G, Hans M, Primetzhofer D, et al. (2020). "Oxidation behaviour of V2AlC MAX phase coatings". Journal of the European Ceramic Society. 40(13):4436–4444.*
51. ^ *Horlait D, Grasso S, Al Nasiri N, Burr PA, Lee WE. (2016). "Synthesis and oxidation testing of MAX phase composites in the Cr–Ti–Al–C quaternary system". Journal of the American Ceramic Society. 99(2):682–690.*
52. ^ *Drouelle E, Brunet V, Cormier J, Villechaise P, Sallot P, et al. (2020). "Oxidation resistance of Ti3AlC2 and Ti3Al0.8Sn0.2C2 MAX phases: A comparison". Journal of the American Ceramic Society. 103(2):1270–1280.*
53. ^ *Tallman DJ, Anasori B, Barsoum MW. (2013). "A critical review of the oxidation of Ti2AlC, Ti3AlC2 and Cr2AlC in air". Materials Research Letters. 1(3):115–125.*
54. ^ *Bei G, Pedimonte B-J, Fey T, Greil P. (2013). "Oxidation behavior of MAX phase Ti2Al(1-x)SnxC solid solution". Journal of the American Ceramic Society. 96(5):1359–1362.*
55. ^ *Wang J, Liu S, Ren D, Shao T, Eklund P, et al. (2018). "Microstructural evolution of epitaxial Ti3AlC2 film on sapphire under ion irradiation and nanoindentation-induced deformation". Journal of Nuclear Materials. 509:181–187.*

56. ^Whittle KR, Blackford MG, Aughterson RD, Moricca S, Lumpkin GR, et al. (2010). "Radiation tolerance of Mn+1AXn phases, Ti3AlC2 and Ti3SiC2". Acta Materialia. 58(13):4362–4368.

57. ^Bowden D, Ward J, Middleburgh S, de Moraes Shubeita S, Zapata-Solvas E, et al. (2020). "The stability of irradiation-induced defects in Zr3AlC2, Nb4AlC3 and (Zr0.5, Ti0.5)3AlC2 MAX phase-based ceramics". Acta Materialia. 183:24–35.

58. ^Deng T, Sun J, Tai P, Wang Y, Zhang L, et al. (2020). "Ti3AlC2, a candidate structural material for innovative nuclear energy system: The microstructure phase transformation and defect evolution induced by energetic heavy-ion irradiation". Acta Materialia. 189:188–203.

59. ^Nappé J-C, Grosseau P, Audubert F, Guilhot B, Beauvy M, et al. (2009). "Damages induced by heavy ions in titanium silicon carbide: Effects of nuclear and electronic interactions at room temperature". Journal of Nuclear Materials. 385(2):304–307.

60. ^Ward J, Bowden D, Stewart D, Barsoum MW, Frankel P, et al. (2019). "Influence of proton-irradiation temperature on the damage accumulation in Ti3SiC2 and Ti3AlC2". Scripta Materialia. 165:98–102.

61. ^Carbajo J, Quintanilla A, Garcia-Costa AL, González-Julián J, Belmonte M, et al. (2021). "The influence of the catalyst on the CO formation during catalytic wet peroxide oxidation process." Catalysis today. 361:30–36.

62. a, bNg WHK, Gnanakumar ES, Batyrev E, Sharma SK, Pujari PK, et al. (2018). "The Ti3AlC2 MAX phase as an efficient catalyst for oxidative dehydrogenation of n-butane." Angewandte Chemie. 130(6):1501–1506.

63. a, bLu ZY, Yu HJ, Lu X, Song MC, Wu FY, et al. (2021). "Two-dimensional vanadium nanosheets as a remarkably effective catalyst for hydrogen storage in MgH2." Rare Metals. 40(11):3195–3204.

64. a, b, c, dWang B, Ruan W, Liu J, Zhang T, Yang H, et al. (2019). "Microstructure, mechanical properties, and preliminary biocompatibility evaluation of binary ti–zr alloys for dental application." Journal of Biomaterials Applications. 33(6):766–775.

65. a, bHench LL, Polak JM. (2002). "Third-generation biomedical materials." Science. 295(5557):1014–1017.

66. a, b, c, dAbdollahi Khabisi M, Shirini F, Shirini K, Khorsand H, Marian M, et al. (2023). "Additively manufactured MAX-and MXene-composite scaffolds for bone regeneration-recent advances and future perspectives." Colloids and Surfaces B: Biointerfaces. 225:113282.

67. a, b, cWang K, Du H, Wang Z, Gao M, Pan H, et al. (2017). "Novel MAX-phase Ti3AlC2 catalyst for improving the reversible hydrogen storage properties of MgH2." International journal of hydrogen energy. 42(7):4244–4251.

68. a, b, cZhao X, Chen Y, Feng M, Xu C, Du J, et al. (2024). "Synthesis, calculations and energy storage applications of high-entropy MXene." Journal of Alloys and Compounds. :174586.

69. ^Şenocak A, Sanko V, Tümay SO, Orooji Y, Demirbas E, et al. (2022). "Ultrasensitive electrochemical sensor for detection of rutin antioxidant by layered Ti3Al0.5Cu0.5C2 MAX phase." Food and Chemical Toxicology. 164:113016.

70. ^Mahmoudi Z, Tabaian SH, Rezaie HR, Mahboubi F, Ghazali MJ. (2020). "Synthesis of Ti2AlC & Ti3AlC2 MAX phases by arc-PVD using ti–al target in C2H2/ar gas mixture and subsequent annealing." Ceramics International. 46(4):4968–4975.

71. a, b, cShao H, Luo S, Descamps-Mandine A, Ge K, Lin Z, et al. (2023). "Synthesis of MAX phase nanofibers and nanoflakes and the resulting MXenes." Advanced Science. 10(1):2205509.

72. ^Derradji M, Henniche A, Wang J, Dayo AQ, Ouyang J, et al. (2018). "High performance nanocomposites from Ti3SiC2 MAX phase and phthalonitrile resin." Polymer Composites. 39(10):3705–3711.

73. ^Barsoum MW. (2000). "The MN+1AXN phases: A new class of solids: Thermodynamically stable nanolaminates." Progress in Solid State Chemistry. 28(1):201–281. doi:10.1016/S0079-6786(00)00006-6

74. ^Schuster JC, Nowotny H, Vaccaro C. (1980). "The ternary systems: CrAlC, VAlC, and TiAlC and the behavior of h-phases (M2AlC)." Journal of Solid State Chemistry. 32(2):213–219. doi:10.1016/0022-4596(80)90569-1

75. a, bJeitschko W, Nowotny H. (1967). "Die kristallstruktur von ti_3SiC_2—ein neuer komplexcarbid-typ." Monatshefte für Chemie-Chemical Monthly. 98:329–337.

76. ^ROHDE H, KUDIELKA H. (1960). "Strukturuntersuchungen an carbosulfiden von titan und zirkon." Zeitschrift für Kristallographie - Crystalline Materials. 114(1-6):447–456. doi:10.1524/zkri.1960.114.16.447

77. a, b, cWolfsgruber H, Nowotny H, Benesovsky F. (1967). "Die kristallstruktur von Ti3GeC2: Kurze mitteilung." Monatshefte fur Chemie und verwandte Teile anderer Wissenschaften. 98:2403–2405.

78. ^Dahlqvist M, Barsoum MW, Rosen J. (2024). "MAX phases–past, present, and future." Materials Today. 72:1–24.

79. a, b, c, dJeitschko W, Nowotny H, Benesovsky F. (1963). "Kohlenstoffhaltige ternäre verbindungen (v-ge-c, nb-ga-c, ta-ga-c, ta-ge-c, cr-ga-c und cr-ge-c)." Monatshefte für Chemie und verwandte Teile anderer Wissenschaften. 94:844–850.

80. ^Jeitschko W, Nowotny H, Benesovsky F. (1963). "Ein beitrag zum dreistoff: Molybdän-aluminium-kohlenstoff: Die phase mo 3 al 2 c." Monatshefte für Chemie und verwandte Teile anderer Wissenschaften. 94:247–251.

81. a, b, c, d, e, f, g, h, i, j, kJeitschko W, Nowotny H, Benesovsky F. (1963). "Carbon-containing ternary compounds (h-phase)." Monatsh Chem. 94(4):672–6.

82. a, b, c, d, e*Jeitschko W, Nowotny H, Benesovsky F. (1963). "Die h-phasen ti 2 InC, zr 2 InC, hf 2 InC und ti 2 Ge C." Monatshefte für Chemie und verwandte Teile anderer Wissenschaften. 94:1201–1205.*
83. a, b, c, d, e, f, g, h, i, j, k, l*Jeitschko W, Nowotny H, Benesovsky F. (1964). "Die h-phasen: Ti 2 cdc, ti 2 gac, ti 2 ga n, ti 2 inn, zr 2 inn und nb 2 gac." Monatshefte für Chemie und verwandte Teile anderer Wissenschaften. 95: 178–179.*
84. a, b, c*Nowotny H, Jeitschko W, Benesovsky F. (1964). "Novel complex carbides and nitrides and their relation to phases of hard substances." Planseeber Pulvermetall. 12:31–43.*
85. ^*Rieger W, Nowotny H, Benesovsky F. (1965). "Phasen mit oktaedrischen bauelementen des Übergangsmeta lls." Monatshefte für Chemie und verwandte Teile anderer Wissenschaften. 96:232–241.*
86. ^*REIFFENSTEIN E, NOWOTNY H, BENESOVSKY F. (1966). "INVESTIGATION OF THE STRUCTURAL AND M AGNETIC CHEMISTRY OF COMPLEX CARBIDES." MONATSH CHEM. 97(5):1428–1436.*
87. ^*Boller H, Nowotny H. (1967). "Zum dreistoff: Vanadin-arsen-kohlenstoff." Monatshefte für Chemie und ver wandte Teile anderer Wissenschaften. 98:2127–2132.*
88. ^*Jeitschko W, Howotny H. (1967). "THE CRYSTAL STRUCTURE OF TI 3 SIC 2—a NEW COMPLEX CARBIDE." MONATSH CHEM. 98(2):329–337.*
89. ^*Beckmann O, Boller H, Nowotny H. (1968). "Neue h-phasen: Kurze mitteilung." Monatshefte für Chemie/C hemical Monthly. 99:1580–1583.*
90. ^*Beckmann O, Boller H, Nowotny H, Benesovsky F. (1969). "Some complex carbides and nitrides in the syste ms ti-{zn, cd, hg}-{c, n} and cr-ga-n." Monatshefte für Chemie/Chemical Monthly. 100:1465–1470.*
91. ^*Beckmann O, Boller H, Nowotny H. (1970). "Die kristallstrukturen von Ta2S2C und Ti4S5 (Ti0,81S)". Monat shefte für Chemie/Chemical Monthly. 101(4):945–955.*
92. a, b, c, d*Nowotny H. (1971). "Strukturchemie einiger verbindungen der übergangsmetalle mit den elementen c, si, ge, sn". Progress in Solid State Chemistry. 5:27–70.*
93. a, b, c*Pietzka MA, Schuster JC. (1994). "Summary of constitutional data on the aluminum-carbon-titanium s ystem". Journal of Phase Equilibria. 15:392–400.*
94. ^*Pietzka MA, Schuster JC. (1996). "Phase equilibria in the quaternary system ti-al-c-n". Journal of the Ameri can Ceramic Society. 79(9):2321–2330.*
95. a, b, c*Barsoum MW. (2000). "The MN+ 1AXN phases: A new class of solids: Thermodynamically stable nanol aminates". Progress in Solid State Chemistry. 28(1-4):201–281.*
96. ^*Hadi MA, Monira U, Chroneos A, Naqib SH, Islam AKMA, et al. (2019). "Phase stability and physical proper ties of (Zr1-xNbx)2AlC MAX phases". Journal of Physics and Chemistry of Solids. 132:38–47.*

97. a, b, c, d*Fashandi H, Dahlqvist M, Lu J, Palisaitis J, Simak SI, et al. (2017). "Synthesis of Ti3AuC2, Ti3Au2C2 and Ti3IrC2 by noble metal substitution reaction in Ti3SiC2 for high-temperature-stable ohmic contacts to SiC". Nature Materials. 16(8):814–818.*

98. ^*Wang J, Zhou Y. (2009). "Recent progress in theoretical prediction, preparation, and characterization of layered ternary transition-metal carbides". Annual Review of Materials Research. 39(1):415–443.*

99. ^*Gandara M, Mladenović D, de Jesus Oliveira Martins M, Rakocevic L, Kruszynski de Assis JM, et al. (2024). "MAX phase (Nb4AlC3) for electrocatalysis applications". Small. :2310576.*

100. ^*Shahbaz M, Sabir N, Amin N, Zulfiqar Z, Zahid M. (2024). "Synthesis and characterization of chromium aluminum carbide MAX phases (CrxAlCx-1) for potential biomedical applications". Frontiers in Chemistry. 12:1413253.*

101. a, b*Gonzalez-Julian J. (2021). "Processing of MAX phases: From synthesis to applications". Journal of the American Ceramic Society. 104(2):659–690.*

102. a, b, c*Hoffman EN, Vinson DW, Sindelar RL, Tallman DJ, Kohse G, et al. (2012). "MAX phase carbides and nitrides: Properties for future nuclear power plant in-core applications and neutron transmutation analysis". Nuclear Engineering and Design. 244:17–24.*

103. ^*Tallman DJ. (2015). "On the potential of MAX phases for nuclear applications". Drexel University.*

104. ^*Lee WE, Giorgi E, Harrison R, Maître A, Rapaud O. (2014). "Nuclear applications for ultra-high temperature ceramics and MAX phases". Ultra-High Temperature Ceramics: Materials for Extreme Environment Applications. :391–415.*

105. a, b*Chirica IM, Mirea AG, Neațu Ș, Florea M, Barsoum MW, et al. (2021). "Applications of MAX phases and MXenes as catalysts". Journal of Materials Chemistry A. 9(35):19589–19612.*

106. ^*Dahlqvist M, Barsoum MW, Rosen J. (2024). "MAX phases – past, present, and future". Materials Today. 72:1–24. doi:10.1016/j.mattod.2023.11.010*

107. a, b, c, d, e, f, g*Liu Z, Zheng L, Sun L, Qian Y, Wang J, et al. (2014). "(Cr2/3Ti1/3)3AlC2 and (Cr5/8Ti3/8)4AlC3: New MAX-phase compounds in Ti–Cr–Al–C system". Journal of the American Ceramic Society. 97(1):67–69.*

108. a, b, c, d, e*Dahlqvist M, Lu J, Meshkian R, Tao Q, Hultman L, et al. (2017). "Prediction and synthesis of a family of atomic laminate phases with kagomé-like and in-plane chemical ordering". Science Advances. 3(7):e1700642.*

109. ^*Mockuté A, Lu J, Moon EJ, Yan M, Anasori B, et al. (2015). "Solid solubility and magnetism upon Mn incorporation in the bulk ternary carbides Cr2AlC and Cr2GaC". Materials Research Letters. 3(1):16–22.*

110. a, bDahlqvist M, Rosen J. (2022). "The rise of MAX phase alloys—large-scale theoretical screening for the prediction of chemical order and disorder". Nanoscale. 14(30):10958–10971.

111. a, b, c, d, e, f, g, h, i, j, kZhang Z, Duan X, Jia D, Zhou Y, van der Zwaag S. (2021). "On the formation mechanisms and properties of MAX phases: A review". Journal of the European Ceramic Society. 41(7):3851–3878.

112. a, bAlam MS, Chowdhury MA, Khandaker T, Hossain MS, Islam MS, et al. (2024). "Advancements in MAX phase materials: Structure, properties, and novel applications". RSC Advances. 14(37):26995–27041.

113. ^Guo M, Cao G, Pan H, Guo J, Chen C, et al. (2024). "Recent progress in synthesis of MAX phases and oxidation & corrosion mechanism: A review". Materials Research Letters. 12(11):765–796.

114. ^Naguib M, Kurtoglu M, Presser V, Lu J, Niu J, et al. (2011). "Two-dimensional nanocrystals produced by exfoliation of Ti3AlC2". Advanced Materials. 23(37):4248–4253. doi:10.1002/adma.201102306

115. ^Mashtalir O, Naguib M, Mochalin VN, Dall'Agnese Y, Heon M, et al. "Intercalation and delamination of layered carbides and carbonitrides". In: MXenes. Jenny Stanford Publishing 2023. pp. 359–377.

116. a, b, cNaguib M, Kurtoglu M, Presser V, Lu J, Niu J, et al. "Two-dimensional nanocrystals produced by exfoliation of Ti3AlC2". In: MXenes. Jenny Stanford Publishing 2023. pp. 15–29.

117. ^Shi C, Beidaghi M, Naguib M, Mashtalir O, Gogotsi Y, et al. (2014). "Structure of nanocrystalline Ti3C2 MXene using atomic pair distribution function". Physical Review Letters. 112(12):125501.

118. a, bVahidMohammadi A, Rosen J, Gogotsi Y. (2021). "The world of two-dimensional carbides and nitrides (MXenes)". Science. 372(6547):eabf1581.

119. a, b, c, d, eAli S, Marwat MA, Khan MF, Adam KM, Din ZU, et al. (2023). "Ti3SiC2-coupled NiCoMn LDH nanocomposites as positive electrode for high performance supercapacitors". Journal of Alloys and Compounds. 956:170229.

120. a, bBao Z, Bing N, Zhu X, Xie H, Yu W. (2021). "Ti3C2Tx MXene contained nanofluids with high thermal conductivity, super colloidal stability and low viscosity". Chemical Engineering Journal. 406:126390.

121. a, bAli Shayesteh Zeraati, Seyyed Alireza Mirkhani, Pengcheng Sun, Michael Naguib, Paul V. Braun, et al. (2021). Improved synthesis of ti 3 c 2 t x MXenes resulting in exceptional electrical conductivity, high synthesis yield, and enhanced capacitance. Nanoscale. 13(6):3572–3580.

122. ^Yassmin Ibrahim, Ahmed Mohamed, Ahmed M. Abdelgawad, Kamel Eid, Aboubakr M. Abdullah, et al. (2020). The recent advances in the mechanical properties of self-standing two-dimensional MXene-based nanostructures: Deep insights into the supercapacitor. Nanomaterials. 10(10):1916.

123. ^Pengfei Jia, Jingyi Lu, Ruofan He, Guangyong Jiang, Xin Jiang, et al. (2022). Octopus sucker-inspired hierarchical structure MXene@ carbon nanotubes enhancing the mechanical properties and fire safety of thermop

lastic polyurethane composites through the interfacial engineering. Chemical Engineering Journal. 450:138184.

124. ^*Qin Yang, Mingzi Li, Rong Chen, Dahang Gao, Zhen Wang, et al. (2023). Enhanced mechanical strength of metal ion-doped MXene-based double-network hydrogels for highly sensitive and durable flexible sensors. ACS Applied Materials & Interfaces. 15(44):51774–51784.*
125. a, b*Ahmad Amiri, Yijun Chen, Chew Bee Teng, Mohammad Naraghi. (2020). Porous nitrogen-doped MXene-based electrodes for capacitive deionization. Energy Storage Materials. 25:731–739.*
126. a, b*Yu Long, Ying Tao, Tongxin Shang, Haotian Yang, Zejun Sun, et al. (2022). Roles of metal ions in MXene synthesis, processing and applications: A perspective. Advanced Science. 9(12):2200296.*
127. ^*Matthew G. Quesne, C. Richard A. Catlow, Nora H. de Leeuw. (2021). How bulk and surface properties of ti 4 SiC 3, v 4 SiC 3, nb 4 SiC 3 and zr 4 SiC 3 tune reactivity: A computational study. Faraday Discussions. 230:87–99.*
128. ^*Aurélie Champagne, Jean-Christophe Charlier. (2020). Physical properties of 2D MXenes: From a theoretical perspective. Journal of Physics: Materials. 3(3):032006.*
129. ^*Hongling Li, Zhi Kai Ng, Roland Yingjie Tay, Shiyong Huang, Siu Hon Tsang, et al. (2023). Flexible graphene/MXene composite thin films for high-performance electromagnetic interference shielding and joule heating. ACS Applied Nano Materials. 6(18):16730–16739. doi:10.1021/acsanm.3c02925*
130. a, b*Yanwu Zhu, Shanthi Murali, Meryl D. Stoller, Kameswaran J. Ganesh, Weiwei Cai, et al. (2011). Carbon-based supercapacitors produced by activation of graphene. Science. 332(6037):1537–1541.*
131. a, b*Yuanlong Shao, Jianmin Li, Yaogang Li, Hongzhi Wang, Qinghong Zhang, et al. (2017). Flexible quasi-solid-state planar micro-supercapacitor based on cellular graphene films. Materials Horizons. 4(6):1145–1150.*
132. a, b*Manavalan Vijayakumar, George Elsa, Aamani Nirogi, Rajendran Navaneethan, Ammaiyappan Bharathi Sankar, et al. (2021). MXenes and their composites for hybrid capacitors and supercapacitors: A critical review. Emergent Materials. 4(3):655–672.*
133. a, b*Yedluri Anil Kumar, Chaitany Jayprakash Raorane, HH Hegazy, Tholkappiyan Ramachandran, Seong Cheol Kim, et al. (2023). 2D MXene-based supercapacitors: A promising path towards high-performance energy storage. Journal of Energy Storage. 72:108433.*
134. ^*Sonia Bansal, Pankaj Chaudhary, Bharat Bhushan Sharma, Sunaina Saini, Aman Joshi. (2024). Review of MXenes and their composites for energy storage applications. Journal of Energy Storage. 87:111420.*
135. ^*Tolendra Kshetri, Duy Thanh Tran, Huu Tuan Le, Dinh Chuong Nguyen, Hien Van Hoa, et al. (2021). Recent advances in MXene-based nanocomposites for electrochemical energy storage applications. Progress in Ma*

terials Science. 117:100733.

136. ^*Iftikhar Hussain, Charmaine Lamiel, Muhammad Sufyan Javed, Muhammad Ahmad, Sumanta Sahoo, et al. (2023). MXene-based heterostructures: Current trend and development in electrochemical energy storage devices. Progress in Energy and Combustion Science. 97:101097.*
137. ^*Tholkappiyan Ramachandran, Abdel-Hamid Ismail Mourad, Mostafa SA ElSayed. (2023). Nb2CTx-based MXenes most recent developments: From principles to new applications. Energies. 16(8):3520.*
138. ^*Ilancheliyan Samylingam, Kumaran Kadirgama, Lingenthiran Samylingam, Navid Aslfattahi, Devarajan Ramasamy, et al. (2024). Review of Ti3C2Tx MXene nanofluids: Synthesis, characterization, and applications. Engineering, Technology & Applied Science Research. 14(3):14708–14712.*
139. ^*Jaroslaw Wozniak, Mateusz Petrus, Tomasz Cygan, Artur Lachowski, Marek Kostecki, et al. (2021). Investigation of MXenes oxidation process during sps method annealing. Materials. 14(20):6011.*
140. ^*Salim Ullah, Faisal Shahzad, Bensheng Qiu, Xiaona Fang, Ayesha Ammar, et al. (2022). MXene-based aptasensors: Advances, challenges, and prospects. Progress in Materials Science. 129:100967.*
141. ^*Hui Ma, Mianqi Xue. (2021). Recent advances in the photothermal applications of two-dimensional nanomaterials: Photothermal therapy and beyond. Journal of Materials Chemistry A. 9(33):17569–17591.*
142. a, b, c, d*Michael Ghidiu, Michael Naguib, Chenyang Shi, Olha Mashtalir, LM Pan, et al. (2014). Synthesis and characterization of two-dimensional nb 4 c 3 (MXene). Chemical Communications. 50(67):9517–9520.*
143. a, b*Olha Mashtalir, Maria R. Lukatskaya, Meng-Qiang Zhao, Michel W. Barsoum, Yury Gogotsi. Amine-assisted delamination of Nb2C MXene for li-ion energy storage devices. In: MXenes.: Jenny Stanford Publishing 2023. pp. 401–414.*
144. a, b, c*Kanit Hantanasirisakul, Yury Gogotsi. (2023). Electronic and optical properties of 2D transition metal carbides and nitrides (MXenes). MXenes. :135–205.*
145. a, b*D. Parajuli, Susmitha Uppugalla, N. Murali, A. Ramakrishna, B. Suryanarayana, et al. (2023). Synthesis and characterization MXene-ferrite nanocomposites and its application for dying and shielding. Inorganic Chemistry Communications. 148:110319.*
146. a, b*Nathan C. Frey, Arkamita Bandyopadhyay, Hemant Kumar, Babak Anasori, Yury Gogotsi, et al. (2019). Surface-engineered MXenes: Electric field control of magnetism and enhanced magnetic anisotropy. ACS Nano. 13(3):2831–2839.*
147. ^*Andrew D. Dillon, Michael J. Ghidiu, Alex L. Krick, Justin Griggs, Steven J. May, et al. (2016). Highly conductive optical quality solution-processed films of 2D titanium carbide. Advanced Functional Materials. 26(23):4162–4168.*

148. a, b *Ayesha Tariq, S. Irfan Ali, Deji Akinwande, Syed Rizwan. (2018). Efficient visible-light photocatalysis of 2D-MXene nanohybrids with Gd3+-and Sn4+-codoped bismuth ferrite. ACS Omega. 3(10):13828–13836.*

149. a, b *Asif Shahzad, Kashif Rasool, Mohsin Nawaz, Waheed Miran, Jiseon Jang, et al. (2018). Heterostructural TiO2/Ti3C2Tx (MXene) for photocatalytic degradation of antiepileptic drug carbamazepine. Chemical Engineering Journal. 349:748–755.*

150. a, b *Jiangyong Diao, Minmin Hu, Zan Lian, Zhaojin Li, Hui Zhang, et al. (2018). Ti3C2T x MXene catalyzed ethylbenzene dehydrogenation: Active sites and mechanism exploration from both experimental and theoretical aspects. ACS Catalysis. 8(11):10051–10057.*

151. a, b *Liu CY, Li EY. (2018). "Termination effects of pt/v-ti n+ 1C n T2 MXene surfaces for oxygen reduction reaction catalysis." ACS applied materials & interfaces. 11(1):1638–1644.*

152. a, b *Wei Z, Zhang P, Tian W, Qin X, Zhang Y, et al. (2018). "Alkali treated Ti3C2Tx MXenes and their dye adsorption performance." Materials Chemistry and Physics. 206:270–276.*

153. a, b *Srimuk P, Halim J, Lee J, Tao Q, Rosen J, et al. (2018). "Two-dimensional molybdenum carbide (MXene) with divacancy ordering for brackish and seawater desalination via cation and anion intercalation." ACS Sustainable Chemistry & Engineering. 6(3):3739–3747.*

154. ^ *Mai YJ, Li YG, Li SL, Zhang LY, Liu CS, et al. (2019). "Self-lubricating Ti3C2 nanosheets/copper composite coatings." Journal of Alloys and Compounds. 770:1–5.*

155. ^ *Zhang H, Wang L, Chen Q, Li P, Zhou A, et al. (2016). "Preparation, mechanical and anti-friction performance of MXene/polymer composites." Materials & Design. 92:682–689.*

156. a, b *Alimohammadi F, Sharifian Gh M, Attanayake NH, Thenuwara AC, Gogotsi Y, et al. (2018). "Antimicrobial properties of 2D MnO2 and MoS2 nanomaterials vertically aligned on graphene materials and Ti3C2 MXene." Langmuir. 34(24):7192–7200.*

157. ^ *Miao H, Teng Z, Wang C, Chong H, Wang G. (2019). "Recent progress in two-dimensional antimicrobial nanomaterials." Chemistry–A European Journal. 25(4):929–944.*

158. ^ *Gogotsi Y. (2023). "MXenes: From discovery to applications of two-dimensional metal carbides and nitrides." CRC Press.*

159. a, b *Kumar S, Kumari N, Seo Y. (2023). "MXenes: Versatile 2D materials with tailored surface chemistry and diverse applications." Journal of Energy Chemistry.*

160. a, b, c, d *Reghunath BS, Davis D, Sunaja Devi KR. (2021). "Synthesis and characterization of Cr2AlC MAX phase for photocatalytic applications." Chemosphere. 283:131281.*

161. [a, b]Khan K, Tareen AK, Iqbal M, Zhang Y, Mahmood A, et al. (2024). "Recent progress and new horizons in emerging novel MXene-based materials for energy storage applications for current environmental remediation and energy crises." Electrochemical Energy Reviews. 7(1):22.

162. [a, b]Lingamdinne LP, Kulkarni R, Koduru JR, Karri RR, Somala AR, et al. (2024). "MXenes for advanced energy storage and environmental remediation applications: Synthesis, properties, and challenges." Journal of Energy Storage. 101:113806.

163. [a, b]Li N, Wang Y, Li Y, Zhang C, Fang G. (2024). "Recent advances in photothermal therapy at near-infrared-II based on 2D MXenes." Small. 20(6):2305645.

164. ^Garcia DD. (2020). "Carbide MXenes surface tension effect on CO2 capture."

165. [a, b]Li X, Zhan M, Liu Y, Tu W, Li H. (2024). "MXene synthesis and carbon capture applications: Mini-review." Chemistry–A European Journal. :e202400874.

166. [a, b, c, d]Orasugh JT, Temane LT, Ray SS. "Application of MXenes in water purification, CO2 capture and conversion." In: Two-dimensional materials for environmental applications.: Springer 2023. pp. 17–74.

167. [a, b]Morales-Salvador R, Morales-García Á, Viñes F, Illas F. (2018). "Correction: Two-dimensional nitrides as highly efficient potential candidates for CO 2 capture and activation." Physical Chemistry Chemical Physics. 20(37):24490–24493.

168. ^Gogotsi Y, Huang Q. (2021). "MXenes: Two-dimensional building blocks for future materials and devices." ACS Nano. 15(4):5775–5780. doi:10.1021/acsnano.1c03161

169. ^Padture NP, Gell M, Jordan EH. (2002). "Thermal barrier coatings for gas-turbine engine applications." Science. 296(5566):280–284.

170. ^Gonzalez-Julian J, Go T, Mack DE, Vaßen R. (2018). "Thermal cycling testing of TBCs on Cr2AlC MAX phase substrates." Surface and coatings technology. 340:17–24.

171. ^Smialek JL, Harder BJ, Garg A. (2016). "Oxidative durability of TBCs on Ti2AlC MAX phase substrates." Surface and Coatings Technology. 285:77–86.

172. ^Boatemaa L, Bosch M, Farle AS, Bei GP, van der Zwaag S, et al. (2018). "Autonomous high-temperature healing of surface cracks in Al2O3 containing Ti2AlC particles." Journal of the American Ceramic Society. 101(12):5684–5693. doi:10.1111/jace.15793

173. ^Smialek JL, Nesbitt JA, Gabb TP, Garg A, Miller RA. (2018). "Hot corrosion and low cycle fatigue of a Cr2AlC-coated superalloy." Materials Science and Engineering: A. 711:119–129.

174. ^Keskin B, Mehrabani SAN, Arefi-Oskoui S, Vatanpour V, Teber OO, et al. (2022). "Development of Ti2AlN MAX phase/cellulose acetate nanocomposite membrane for removal of dye, protein and lead ions." Carbohyd

rate Polymers. 296:119913.

175. ^*Abood TW, Shabeeb KM, Alzubaydi AB, Majdi HS, Al-Juboori RA, et al. (2023). "Effect of MAX phase Ti3ALC2 on the ultrafiltration membrane properties and performance." Membranes. 13(5):456.*
176. ^*Abood T, Shabeeb K, Alzubaydi A, Goh P, Ismail A, et al. (2024). "Effect of MXene Ti3C2 on the PVDF ultrafiltration membrane properties and performance." Eng Technol J. 42:754–67.*
177. ^*Hall K, Dey M, Matzke C, Gupta S. (2019). "Synthesis and characterization of novel polymer matrix composites reinforced with max phases (Ti3SiC2, Ti3AlC2, and Cr2AlC) or MoAlB by fused deposition modeling." International Journal of Ceramic Engineering & Science. 1(3):144–154.*
178. ^*Bai P, Wang S, Zhao B, Wang X, Ma J, et al. (2022). "Electrically conductive and corrosion resistant MAX phases with superior electromagnetic wave shielding performance." Journal of the European Ceramic Society. 42(16):7414–7420.*
179. a, b*Huang J, Wan H, Li M, Zhang Y, Zhu J, et al. (2021). "In-situ growth of MAX phase coatings on carbonised wood and their terahertz shielding properties." Journal of Advanced Ceramics. 10:1291–1298.*
180. ^*Alam MS, Chowdhury MA, Kowser MA, Islam MS, Islam MM, et al. (2024). "Advances of MAX phases: Synthesis, characterizations and challenges." Engineering Reports. 6(8):e12911.*
181. ^*Zheng Ming Sun. (2011). Progress in research and development on MAX phases: A family of layered ternary compounds. International Materials Reviews. 56(3):143–166.*
182. a, b*Boatemaa L, Bosch M, Farle AS, Bei GP, van der Zwaag S, et al. (2018). Autonomous high-temperature healing of surface cracks in Al2O3 containing Ti2AlC particles. Journal of the American Ceramic Society. 101(12):5684–5693.*
183. a, b*Pei R, McDonald SA, Shen L, van der Zwaag S, Sloof WG, et al. (2017). Crack healing behaviour of Cr2AlC MAX phase studied by x-ray tomography. Journal of the European Ceramic Society. 37(2):441–450.*
184. a, b*Grieseler R, Camargo MK, Hopfeld M, Schmidt U, Bund A, et al. (2017). Copper-MAX-phase composite coatings obtained by electro-co-deposition: A promising material for electrical contacts. Surface and Coatings Technology. 321:219–228.*
185. ^*Prikhna TA, Ostash OP, Kuprin AS, Podhurska VY, Serbenyuk TB, et al. (2021). A new MAX phases-based electroconductive coating for high-temperature oxidizing environment. Composite Structures. 277:114649.*
186. a, b*Shu S, Yang H, Tong C, Qiu F. (2016). Fabrication of TiCx-TiB2/al composites for application as a heat sink. Materials. 9(8):642.*
187. a, b*Marian M, Quiroz Esteban CD, Zambrano DF, Ramteke SM, Ramos Grez J, et al. (2024). Ti3C2Tx and Mo2TiC2Tx MXenes as additives in synovial fluids-towards an enhanced biotribological performance of 3D-pri*

nted implants. Applied Materials Today. 41:102464.

188. [a], [b]*Mishnaevsky L Jr, Levashov E, Valiev RZ, Segurado J, Sabirov I, et al. (2014). Nanostructured titanium-based materials for medical implants: Modeling and development. Materials Science and Engineering: R: Reports. 81:1–19.*
189. [a], [b]*Cai Z, Bunce N, Nunn ME, Okabe T. (2001). Porcelain adherence to dental cast CP titanium: Effects of surface modifications. Biomaterials. 22(9):979–986.*
190. [a], [b]*Yu W, Chen D, Tian L, Zhao H, Wang X. (2019). Self-lubricate and anisotropic wear behavior of AZ91D magnesium alloy reinforced with ternary Ti2AlC MAX phases. Journal of materials science & technology. 35(3):275–284.*
191. [a], [b]*Cho I, Selvaraj AR, Bak J, Kim H, Prabakar K. (2023). Mechanochemical pretreated mn+ 1AXn (MAX) phase to synthesize 2D-Ti3C2Tx MXene sheets for high-performance supercapacitors. Nanomaterials. 13(11):1741.*
192. [a], [b]*Liu J, Li S, Yao B, Zhang J, Lu X, et al. (2018). Thermal stability and thermal shock resistance of Fe2AlB2. Ceramics International. 44(13):16035–16039.*
193. [a], [b]*Chen J, Wu Z, Li B, Deng M, Yan W, et al. (2024). Influence of Cr2AlC on the thermal shock and corrosion resistance of low carbon Al2O3-c refractory. Journal of the European Ceramic Society. 44(13):7943–7952.*
194. [a], [b], [c]*Zhou J, Zha X, Zhou X, Chen F, Gao G, et al. (2017). Synthesis and electrochemical properties of two-dimensional hafnium carbide. ACS nano. 11(4):3841–3850.*
195. [a], [b]*Halim J, Kota S, Lukatskaya MR, Naguib M, Zhao MQ, et al. (2016). Synthesis and characterization of 2D molybdenum carbide (MXene). Advanced Functional Materials. 26(18):3118–3127.*
196. [a], [b]*Haq BU, Kim SH, Tahir SA, Ahmed R, Chaudhry AR, et al. (2024). V2XT2 (x: C, n; t: O, f) MXenes; potential two-dimensional materials for spintronics, optoelectronics, and photovoltaic applications. Materials Today Communications. :109370.*
197. [^]*Goossens N, Tunca B, Lapauw T, Lambrinou K, Vleugels J. MAX phases, structure, processing, and properties. In: Michael Pomeroyeditor. Encyclopedia of materials.: Netherlands: Elsevier 2021. pp. 182–199. doi:10.1016/B978-0-12-818542-1.00015-1. ISBN 9780128185421*
198. [^]*Lin ZJ, Zhuo MJ, Zhou YC, Li MS, Wang JY. (2006). Structural characterization of a new layered-ternary Ta4AlC3 ceramic. Journal of materials research. 21(10):2587–2592.*
199. [a], [b], [c], [d], [e], [f]*Husmann S, Budak Ö, Shim H, Liang K, Aslan M, et al. (2020). Ionic liquid-based synthesis of MXene. Chemical Communications. 56(75):11082–11085.*

200. ^Qureshi MW, Ali MA, Ma X, Tang G, Javed MU, et al. (2022). Verification of stability and unraveling the electronic and physical properties of bulk and (001)-surfaces of newly synthesized Ti2ZnX (x= c, n) MAX phases. Surfaces and Interfaces. 31:102032.

201. a, b, cDing H, Li Y, Lu J, Luo K, Chen K, et al. (2019). Synthesis of MAX phases Nb2CuC and Ti2 (Al0. 1Cu0. 9) n by a-site replacement reaction in molten salts. Materials Research Letters. 7(12):510–516.

202. ^Thore A, Dahlqvist M, Alling B, RosÈn J. (2014). First-principles calculations of the electronic, vibrational, and elastic properties of the magnetic laminate Mn2GaC. Journal of Applied Physics. 116(10).

203. a, b, cLai CC, Fashandi H, Lu J, Palisaitis J, Persson PO, et al. (2017). Phase formation of nanolaminated mo 2 AuC and mo 2 (au 1- x ga x) 2 c by a substitutional reaction within au-capped mo 2 GaC and mo 2 ga 2 c thin films. Nanoscale. 9(45):17681–17687.

204. a, bKashiwaya S, Lai CC, Lu J, Petruhins A, Rosen J, et al. (2020). Formation of Ti2AuN from au-covered Ti2AlN thin films: A general strategy to thermally induce intercalation of noble metals into MAX phases. Crystal Growth & Design. 20(6):4077–4081.

205. ^Yeh CL, Yang WJ. (2013). Formation of MAX solid solutions (ti, v) 2AlC and (cr, v) 2AlC with Al2O3 addition by SHS involving aluminothermic reduction. Ceramics International. 39(7):7537–7544.

206. ^Yeh CL, Yang WJ. (2015). Effects of ti and TiO2 on combustion synthesis of (ti, v) 2AlC/Al2O3 solid solution composites. Materials and Manufacturing Processes. 30(3):292–297.

207. ^Li Y, Lu J, Li M, Chang K, Zha X, et al. (2020). Multielemental single–atom-thick a layers in nanolaminated V2 (sn, a) c (a= fe, co, ni, mn) for tailoring magnetic properties. Proceedings of the National Academy of Sciences. 117(2):820–825.

208. ^Bai L, Yin H, Zhang X. (2016). Energy storage performance of v n+ 1 c n monolayer as electrode material studied by first-principles calculations. RSC advances. 6(60):54999–55006.

209. ^Mizuno Y, Sato K, Mrinalini M, Suzuki TS, Sakka Y. (2013). Fabrication of textured Ti3AlC2 by spark plasma sintering and their anisotropic mechanical properties. Journal of the Ceramic Society of Japan. 121(1412):366–369.

210. ^Hadi MA, Ahmed I, Ali MA, Hossain MM, Nasir MT, et al. (2022). A comparative DFT exploration on m-and a-site double transition metal MAX phase, Ti3ZnC2. Open Ceramics. 12:100308.

211. ^Naguib M, Bentzel GW, Shah J, Halim J, Caspi EN, et al. (2014). "New solid solution MAX phases: (Ti0.5, V0.5)3AlC2, (Nb0.5, V0.5)2AlC, (Nb0.5, V0.5)4AlC3 and (Nb0.8, Zr0.2)2AlC". Materials Research Letters. 2(4):233–240.

212. ^Zhou Y, Meng F, Zhang J. (2008). "New MAX-phase compounds in the v–cr–al–c system". Journal of the American Ceramic Society. 91(4):1357–1360.
213. ^Rawn CJ, Barsoum MW, El-Raghy T, Procipio A, Hoffmann CM, et al. (2000). "Structure of Ti4AlN3—a layered mn+1AXn nitride". Materials Research Bulletin. 35(11):1785–1796.
214. ^Li C, Wang B, Li Y, Wang R. (2009). "First-principles study of electronic structure, mechanical and optical properties of V4AlC3". Journal of Physics D: Applied Physics. 42(6):065407.
215. a, bHu C, Li F, Zhang J, Wang J, Wang J, et al. (2007). "Nb4AlC3: A new compound belonging to the MAX phases". Scripta Materialia. 57(10):893–896.
216. ^Griseri M, Tunca B, Lapauw T, Huang S, Popescu L, et al. (2019). "Synthesis, properties and thermal decomposition of the Ta4AlC3 MAX phase". Journal of the European Ceramic Society. 39(10):2973–2981.
217. ^Feng X, Zeng C, Sui F, Liu J, Wu K, et al. (2024). "Synthesis and characterization of a new out-of-plane ordered double-transition-metal MAX phase, Mo2VAlC2, and its two-dimensional derivate Mo2VC2Tx MXene". Materials Science and Engineering: B. 305:117403.
218. a, bDeysher G, Shuck CE, Hantanasirisakul K, Frey NC, Foucher AC, et al. (2019). "Synthesis of Mo4VAlC4 MAX phase and two-dimensional Mo4VC4 MXene with five atomic layers of transition metals". ACS Nano. 14(1):204–217.
219. ^Zheng L, Wang J, Lu X, Li F, Wang J, et al. (2010). "(Ti0.5Nb0.5)5AlC4: A new-layered compound belonging to MAX phases". Journal of the American Ceramic Society. 93(10):3068–3071.
220. ^Urbankowski P, Anasori B, Hantanasirisakul K, Yang L, Zhang L, et al. (2017). "2D molybdenum and vanadium nitrides synthesized by ammoniation of 2D transition metal carbides (MXenes)". Nanoscale. 9(45):17722–17730.
221. a, b, cHan M, Maleski K, Shuck CE, Yang Y, Glazar JT, et al. (2020). "Tailoring electronic and optical properties of MXenes through forming solid solutions". Journal of the American Chemical Society. 142(45):19110–19118.
222. a, b, cNaguib M, Halim J, Lu J, Cook KM, Hultman L, et al. (2013). "New two-dimensional niobium and vanadium carbides as promising materials for li-ion batteries". Journal of the American Chemical Society. 135(43):15966–15969.
223. ^Meshkian R, Näslund LÅ, Halim J, Lu J, Barsoum MW, et al. (2015). "Synthesis of two-dimensional molybdenum carbide, Mo2C, from the gallium based atomic laminate Mo2Ga2C". Scripta Materialia. 108:147–150.
224. a, b, cPersson I, El Ghazaly A, Tao Q, Halim J, Kota S, et al. (2018). "Tailoring structure, composition, and energy storage properties of MXenes from selective etching of in-plane, chemically ordered MAX phases". Small.

14(17):1703676.

225. ^a, b^ *Soundiraraju B, George BK. (2017). "Two-dimensional titanium nitride (Ti2N) MXene: Synthesis, characterization, and potential application as surface-enhanced raman scattering substrate". ACS Nano. 11(9):8892–8900.*
226. ^a, b, c^ *Naguib M, Mashtalir O, Carle J, Presser V, Lu J, et al. (2012). "Two-dimensional transition metal carbides". ACS Nano. 6(2):1322–1331.*
227. ^a, b, c, d, e^ *Meshkian R, Dahlqvist M, Lu J, Wickman B, Halim J, et al. (2018). "W-based atomic laminates and their 2D derivative W1.33C MXene with vacancy ordering". Advanced Materials. 30(21):1706409.*
228. ^^ *Halim J, Palisaitis J, Lu J, Thörnberg J, Moon EJ, et al. (2018). "Synthesis of two-dimensional Nb1.33C (MXene) with randomly distributed vacancies by etching of the quaternary solid solution (Nb2/3Sc1/3)2AlC MAX phase". ACS Applied Nano Materials. 1(6):2455–2460.*
229. ^^ *Zhou J, Zha X, Chen FY, Ye Q, Eklund P, et al. (2016). "A two-dimensional zirconium carbide by selective etching of Al3C3 from nanolaminated Zr3Al3C5". Angewandte Chemie International Edition. 55(16):5008–5013.*
230. ^a, b^ *Tran MH, Schäfer T, Shahraei A, Dürrschnabel M, Molina-Luna L, et al. (2018). "Adding a new member to the MXene family: Synthesis, structure, and electrocatalytic activity for the hydrogen evolution reaction of V4C3Tx". ACS Applied Energy Materials. 1(8):3908–3914.*
231. ^^ *Urbankowski P, Anasori B, Makaryan T, Er D, Kota S, et al. (2016). "Synthesis of two-dimensional titanium nitride ti4n3 (MXene)". Nanoscale. 8(22):11385–11391.*
232. ^^ *Pinto D, Anasori B, Avireddy H, Shuck CE, Hantanasirisakul K, et al. (2020). "Synthesis and electrochemical properties of 2D molybdenum vanadium carbides–solid solution MXenes". Journal of Materials Chemistry A. 8(18):8957–8968.*
233. ^a, b, c^ *Anasori B, Xie Y, Beidaghi M, Lu J, Hosler BC, et al. (2015). "Two-dimensional, ordered, double transition metals carbides (MXenes)". ACS Nano. 9(10):9507–9516.*
234. ^a, b, c, d^ *Meshkian R, Tao Q, Dahlqvist M, Lu J, Hultman L, et al. (2017). "Theoretical stability and materials synthesis of a chemically ordered MAX phase, Mo2ScAlC2, and its two-dimensional derivate Mo2ScC2 MXene". Acta Materialia. 125:476–480.*
235. ^^ *Zheng L, Zhou Y, Feng Z. (2013). "Preparation, structural featrures, properties and prospective of MAX phases". Aerosp Mater Technol. 43(6):1–23.*
236. ^^ *Schuster JC, Nowotny H, Vaccaro C. (1980). "The ternary systems: CrAlC, VAlC, and TiAlC and the behavior of h-phases (M2AlC)". Journal of Solid State Chemistry. 32(2):213–219.*

237. a, b Du Z, Wu C, Chen Y, Cao Z, Hu R, et al. (2021). "High-entropy atomic layers of transition-metal carbides (MXenes)". Advanced Materials. 33(39):2101473.
238. a, b Chen L, Li Y, Liang K, Chen K, Li M, et al. (2023). "Two-dimensional MXenes derived from medium/high-entropy MAX phases M2GaC (m= ti/v/nb/ta/mo) and their electrochemical performance". Small Methods. 7(8):2300054.
239. ^ Bao W, Wang XG, Ding H, Lu P, Zhu C, et al. (2020). "High-entropy M2AlC-MC (m= ti, zr, hf, nb, ta) composite: Synthesis and microstructures". Scripta Materialia. 183:33–38.
240. ^ Chen K, Chen Y, Zhang J, Song Y, Zhou X, et al. (2021). "Medium-entropy (ti, zr, hf)2SC MAX phase". Ceramics International. 47(6):7582–7587.
241. ^ Lu Chen, Youbing Li, Biao Zhao, Shanshan Liu, Huibin Zhang, et al. (2023). "Multiprincipal element M2FeC (m= ti, v, nb, ta, zr) MAX phases with synergistic effect of dielectric and magnetic loss." Advanced Science. 10(10):2206877.
242. ^ Guangqi He, Yi Zhang, Pei Yao, Xingchao Li, Ke Ma, et al. (2023). "A novel medium-entropy (TiVNb) 2AlC MAX phase: Fabrication, microstructure, and properties." Journal of Materials Science & Technology. 137:91–99.
243. ^ Chao Liu, Yue-yang Yang, Zhi-fang Zhou, Ce-wen Nan, Yuan-hua Lin. (2022). "(Ti0. 2V0. 2Cr0. 2Nb0. 2Ta0. 2) 2AlC–(Ti0. 2V0. 2Cr0. 2Nb0. 2Ta0. 2) c high-entropy ceramics with low thermal conductivity." Journal of the American Ceramic Society. 105(4):2764–2771.
244. ^ Linjing Qiao, Jianqiang Bi, Guandong Liang, Chen Liu, Zhuangzhuang Yin, et al. (2023). "Synthesis and electromagnetic wave absorption performances of a novel (Mo0. 25Cr0. 25Ti0. 25V0. 25) 3AlC2 high-entropy MAX phase." Journal of Materials Science & Technology. 137:112–122.
245. a, b Bensu Tunca, Shuigen Huang, Nick Goossens, Konstantina Lambrinou, Jozef Vleugels. (2022). "Chemically complex double solid solution MAX phase-based ceramics in the (ti, zr, hf, v, nb)-(al, sn)-c system." Materials Research Letters. 10(2):52–61.
246. ^ Wansen Ma, Meng Wang, Qingjie Yi, Dejun Huang, Jie Dang, et al. (2022). "A new Ti2V0. 9Cr0. 1C2Tx MXene with ultrahigh gravimetric capacitance." Nano Energy. 96:107129.
247. ^ Srinivasa Kartik Nemani, Bowen Zhang, Brian C. Wyatt, Zachary D. Hood, Sukriti Manna, et al. (2021). "High-entropy 2D carbide mxenes: TiVNbMoC3 and TiVCrMoC3." ACS nano. 15(8):12815–12825.
248. ^ Wansen Ma, Zeming Qiu, Meng Wang, Chaowen Tan, Liwen Hu, et al. (2023). "A novel high-entropy MXene Ti1. 1V1. 2Cr0. 8Nb1. 0Mo0. 9C4Tx for high-performance supercapacitor." Scripta Materialia. 235:115596.

249. a, b*Jie Zhou, Quanzheng Tao, Bilal Ahmed, Justinas Palisaitis, Ingemar Persson, et al. (2022). "High-entropy laminate metal carbide (MAX phase) and its two-dimensional derivative MXene." Chemistry of Materials. 34(5):2098–2106.*

250. a, b*Babak Anasori, Joseph Halim, Jun Lu, Cooper A. Voigt, Lars Hultman, et al. (2015). "Mo2TiAlC2: A new ordered layered ternary carbide." Scripta Materialia. 101:5–7.*

251. a, b, c, d*Babak Anasori, Martin Dahlqvist, Joseph Halim, Eun Ju Moon, Jun Lu, et al. (2015). "Experimental and theoretical characterization of ordered MAX phases Mo2TiAlC2 and Mo2Ti2AlC3." Journal of Applied Physics. 118(9).*

252. a, b*Jimmy Thörnberg, Joseph Halim, Jun Lu, Rahele Meshkian, Justinas Palisaitis, et al. (2019). "Synthesis of (v 2/3 sc 1/3) 2 AlC i-MAX phase and v 2- x c MXene scrolls." Nanoscale. 11(31):14720–14726.*

253. a, b, c*Martin Dahlqvist, Andrejs Petruhins, Jun Lu, Lars Hultman, Johanna Rosen. (2018). "Origin of chemically ordered atomic laminates (i-MAX): Expanding the elemental space by a theoretical/experimental approach." ACS nano. 12(8):7761–7770.*

254. ^*Zetan Liu, Jingkun Xu, Xiaoqing Xi, Weijia Luo, Ji Zhou. (2023). "Molten salt dynamic sealing synthesis of MAX phases (Ti3AlC2, Ti3SiC2 et al.) powder in air." Ceramics International. 49(1):168–178.*

255. a, b*Michael Naguib, Murat Kurtoglu, Volker Presser, Jun Lu, Junjie Niu, et al. (2011). "Two-dimensional nanocrystals produced by exfoliation of Ti3AlC2." Advanced materials (Deerfield Beach, Fla). 23:4248–53. doi:10.1002/adma.201102306*

256. ^*Chunfeng Hu, Haibin Zhang, Fangzhi Li, Qing Huang, Yiwang Bao. (2013). "New phases' discovery in MAX family." International Journal of Refractory Metals and Hard Materials. 36:300–312.*

257. ^*Martin Magnuson, Maurizio Mattesini. (2017). "Chemical bonding and electronic-structure in MAX phases as viewed by x-ray spectroscopy and density functional theory." Thin Solid Films. 621:108–130. doi:10.1016/j.tsf.2016.11.005*

258. ^*Andrejs Petruhins. (2018). "Synthesis and characterization of magnetic nanolaminated carbides." Linköping University Electronic Press.*

259. ^*Michael Naguib, Vadym N. Mochalin, Michel W. Barsoum, Yury Gogotsi. (2014). "25th anniversary article: MXenes: A new family of two-dimensional materials." Advanced materials. 26(7):992–1005.*

260. ^*Aurélie Champagne, Lu Shi, Thierry Ouisse, Benoît Hackens, Jean-Christophe Charlier. (2018). "Electronic and vibrational properties of { ext{V}}_{2} ext{C}-based MXenes: From experiments to first-principles modeling." Phys Rev B. 97:115439. doi:10.1103/PhysRevB.97.115439*

261. a, b, c Mohammad Khazaei, Masao Arai, Taizo Sasaki, Chan-Yeup Chung, Natarajan S. Venkataramanan, et al. (2013). "Novel electronic and magnetic properties of two-dimensional transition metal carbides and nitrides." Advanced Functional Materials. 23(17):2185–2192.

262. ^ Brian C. Wyatt, Srinivasa Kartik Nemani, Krishay Desai, Harpreet Kaur, Bowen Zhang, et al. (2021). "High-temperature stability and phase transformations of titanium carbide (Ti3C2T x) MXene." Journal of Physics: Condensed Matter. 33(22):224002.

263. ^ Peer Bärmann, Lukas Haneke, Jens Matthies Wrogemann, Martin Winter, Olivier Guillon, et al. (2021). "Scalable synthesis of MAX phase precursors toward titanium-based MXenes for lithium-ion batteries." ACS applied materials & interfaces. 13(22):26074–26083.

264. ^ Srinivasa Kartik Nemani, Bowen Zhang, Brian C. Wyatt, Zachary D. Hood, Sukriti Manna, et al. (2021). "High-entropy 2D carbide MXenes: TiVNbMoC3 and TiVCrMoC3." ACS Nano. 15(8):12815–12825. doi:10.1021/acsnano.1c02775

265. a, b Paulius Malinovskis, Justinas Palisaitis, Per O. Å. Persson, Erik Lewin, Ulf Jansson. (2016). "Synthesis and characterization of MoB2-x thin films grown by nonreactive DC magnetron sputtering." Journal of Vacuum Science & Technology A. 34(3):031511. doi:10.1116/1.4948234

266. ^ Kathleen Maleski, Mohamed Alhabeb. (2019). "Top-down MXene synthesis (selective etching)." 2D metal carbides and nitrides (MXenes) structure, properties and applications. :69–87.

267. a, b, c, d, e Youbing Li, Shuairu Zhu, Erxiao Wu, Haoming Ding, Jun Lu, et al. (2023). "Nanolaminated ternary transition metal carbide (MAX phase)-derived core–shell structure electrocatalysts for hydrogen evolution and oxygen evolution reactions in alkaline electrolytes." The Journal of Physical Chemistry Letters. 14(2):481–488.

268. ^ CC Lai, H. Fashandi, J. Lu, J. Palisaitis, PO Persson. (2017). Å., hultman, l., eklund, p., & rosen, j.(2017). Nanoscale. 9:17681.

269. ^ Youbing Li, Mian Li, Jun Lu, Baokai Ma, Zhipan Wang, et al. (2019). "Single-atom-thick active layers realized in nanolaminated Ti3(AlxCu1–x)C2 and its artificial enzyme behavior." ACS Nano. 13(8):9198–9205. doi:10.1021/acsnano.9b03530

270. ^ Rawaid Ali, Peng Song, Muhammad Khan, Shabir Ali, Majid Rasool Kamli, et al. (2023). "Tribological and oxidation resistance performance of Ti2AlC MAX-phase generated by reactive spark plasma sintering." Journal of Materials Research and Technology. 26:8309–8326. doi:10.1016/j.jmrt.2023.09.110

271. ^ NC Ghosh, SP Harimkar. (2012). "Consolidation and synthesis of MAX phases by spark plasma sintering (SPS): A review". Advances in science and technology of Mn+ 1AXn phases. :47–80.

272. ^*Mohammad Yunus, Rakesh Kumar, Bikas C. Maji, Madangopal Krishnan. (2022). "An optimized method for synthesizing phase-pure Ti3AlC2 MAX-phase through spark plasma sintering". Journal of the European Ceramic Society. 42(2):354–363.*

273. a, b*Carl Magnus, Joanne Sharp, William M. Rainforth. (2020). "The lubricating properties of spark plasma sintered (SPS) Ti3SiC2 MAX phase compound and composite". Tribology Transactions. 63(1):38–51.*

274. ^*Christopher Salvo, Ernesto Chicardi, Rosalía Poyato, Cristina García-Garrido, José Antonio Jiménez, et al. (2021). "Synthesis and characterization of a nearly single bulk Ti2AlN max phase obtained from ti/AlN powder mixture through spark plasma sintering". Materials. 14(9):2217.*

275. a, b*Olivier Guillon, Jesus Gonzalez-Julian, Benjamin Dargatz, Tobias Kessel, Gabi Schierning, et al. (2014). "Field-assisted sintering technology/spark plasma sintering: Mechanisms, materials, and technology developments". Advanced Engineering Materials. 16(7):830–849.*

276. ^*Wulong Liu, Changjun Qiu, Jie Zhou, Zhihui Ding, Xiaobing Zhou, et al. (2015). "Fabrication of Ti2AlN ceramics with orientation growth behavior by the microwave sintering method". Journal of the European Ceramic Society. 35(5):1385–1391.*

277. ^*Jerzy Lis, Roman Pampuch, Tomasz Rudnik, Zbigniew Węgrzyn. (1997). "Reaction sintering phenomena of self-propagating high-temperature synthesis-derived ceramic powders in the ti⊠ si⊠ c system". Solid State Ionics. 101:59–64.*

278. ^*CL Yeh, YG Shen. (2009). "Effects of TiC and Al4C3 addition on combustion synthesis of Ti2AlC". Journal of Alloys and Compounds. 470(1-2):424–428.*

279. ^*A. Hendaoui, M. Andasmas, A. Amara, A. Benaldjia, P. Langlois, et al. (2008). "SHS of high-purity MAX compounds in the ti-al-c system". International Journal of Self-Propagating High-Temperature Synthesis. 17:129–135.*

280. ^*Aiguo Zhou, Chang-An Wang, Zhenbin Ge, Lifeng Wu, et al. (2001). "Preparation of Ti3AlC2 and Ti2AlC by self-propagating high-temperature synthesis". Journal of materials science letters. 20(21):1971–1973.*

281. ^*Michał Łopaciński, Jan Puszynski, Jerzy Lis. (2001). "Synthesis of ternary titanium aluminum carbides using self-propagating high-temperature synthesis technique". Journal of the American Ceramic Society. 84(12):3051–3053.*

282. ^*Per Eklund, Manfred Beckers, Ulf Jansson, Hans Högberg, Lars Hultman. (2010). "The mn+ 1AXn phases: Materials science and thin-film processing". Thin Solid Films. 518(8):1851–1878.*

283. ^*C. Walter, D. P. Sigumonrong, T. El-Raghy, J. M. Schneider. (2006). "Towards large area deposition of Cr2AlC on steel". Thin Solid Films. 515(2):389–393. doi:10.1016/j.tsf.2005.12.219.*

284. a, b, c*Lin Feng, Meiqian Lv, Qian Qian, Ruixiang Luo, Bo Huang. (2023). "The synthesis of high purity Ti3AlC2 MAX phase via molten salt method". Advanced Powder Technology. 34(1):103920. doi:10.1016/j.apt.2022.103920.*
285. ^*Anmin Liu, Qiyue Yang, Xuefeng Ren, Fanning Meng, Liguo Gao, et al. (2020). "Energy-and cost-efficient NaCl-assisted synthesis of MAX-phase Ti3AlC2 at lower temperature". Ceramics International. 46(5):6934–6939.*
286. a, b*Keke Guan, Wen Lei, Honghong Wang, Xuefeng Liu, Jin Luo, et al. (2022). "Efficient synthesis of Ti3AlC2 powders with high purity by microwave-assisted molten salt method". Ceramics International. 48(11):16357–16363.*
287. ^*Apurv Dash, Robert Vaßen, Olivier Guillon, Jesus Gonzalez-Julian. (2019). "Molten salt shielded synthesis of oxidation prone materials in air". Nature materials. 18(5):465–470.*
288. a, b*Apurv Dash, Yoo Jung Sohn, Robert Vaßen, Olivier Guillon, Jesus Gonzalez-Julian. (2019). "Synthesis of Ti3SiC2 MAX phase powder by a molten salt shielded synthesis (MS3) method in air". Journal of the European Ceramic Society. 39(13):3651–3659.*
289. ^*Xiaoqiang Li, Xi Xie, Jesus Gonzalez-Julian, Jürgen Malzbender, Rui Yang. (2020). "Mechanical and oxidation behavior of textured Ti2AlC and Ti3AlC2 MAX phase materials". Journal of the European Ceramic Society. 40(15):5258–5271. doi:10.1016/j.jeurceramsoc.2020.07.043.*
290. a, b*Wubian Tian, Peiling Wang, Guojun Zhang, Yanmei Kan, Yongxiang Li, et al. (2006). "Synthesis and thermal and electrical properties of bulk Cr2AlC". Scripta Materialia. 54(5):841–846.*
291. a, b*L. Chlubny, J. Lis, K. Chabior, P. Chachlowska, C. Kapusta. (2015). "Processing and properties of MAX phases–based materials using SHS technique". Archives of Metallurgy and Materials. 60.*
292. ^*M. A. Eryomina, S. F. Lomayeva, S. L. Demakov. (2021). "Synthesis of composite based on Ti2AlC with added nanographite via wet ball milling followed by spark plasma sintering". Materials Chemistry and Physics. 273:125114. doi:10.1016/j.matchemphys.2021.125114.*
293. ^*W. Jeitschko, H. Nowotny, F. Benesovsky. (1963). "Ti 2 AlN, eine stickstoffhaltige h-phase". Monatshefte für Chemie und verwandte Teile anderer Wissenschaften. 94:1198–1200.*
294. a, b*Zhijun Lin, Mujin Zhuo, Yanchun Zhou, Meishuan Li, Jingyang Wang. (2006). "Microstructures and theoretical bulk modulus of layered ternary tantalum aluminum carbides". Journal of the American Ceramic Society. 89(12):3765–3769.*
295. ^*Johannes Etzkorn, Martin Ade, Harald Hillebrecht. (2007). "Ta3AlC2 and Ta4AlC3- single-crystal investigations of two new ternary carbides of tantalum synthesized by the molten metal technique". Inorganic che*

mistry. 46(4):1410–1418.

296. ^*Bouchaib Manoun, SK Saxena, T. El-Raghy, MW Barsoum. (2006). "High-pressure x-ray diffraction study of Ta4AlC3". Applied physics letters. 88(20).*
297. ^*Nina J. Lane, Michael Naguib, Jun Lu, Lars Hultman, Michel W. Barsoum. (2012). "Structure of a new bulk Ti5Al2C3 MAX phase produced by the topotactic transformation of Ti2AlC". Journal of the European Ceramic Society. 32(12):3485–3491.*
298. ^*H. Boller, H. Nowotny. (1968). "Die kristallstruktur von v 2 PC und v 5 p 3 n: Kurze mitteilung". Monatshefte für Chemie-Chemical Monthly. 99:672–675.*
299. a, b*H. Nowotny, H. Boller, O. Beckmann. (1970). "Alloy phases crystallizing with structures which occur with non-metallic compounds". Journal of Solid State Chemistry. 2(3):462–471.*
300. a, b*HELGA ROHDE, HEINZ KUDIELKA. (1960). "Strukturuntersuchungen an carbosulfiden von titan und zirkon". Zeitschrift für Kristallographie-Crystalline Materials. 114(1-6):447–456.*
301. a, b*Rackl T, Johrendt D. (2020). "The MAX phase borides Zr2SB and Hf2SB." Solid State Sciences. 106:106316.*
302. ^*Rackl T, Eisenburger L, Niklaus R, Johrendt D. (2019). "Syntheses and physical properties of the MAX phase boride nb2SB and the solid solutions n b2SBxc1-x (x= 0–1)." Physical Review Materials. 3(5):054001.*
303. a, b, c*Li Y, Liang J, Ding H, Lu J, Mu X, et al. (2021). "Near-room temperature ferromagnetic behavior of single-atom-thick 2D iron in nanolaminated ternary MAX phases." Applied Physics Reviews. 8(3).*
304. ^*Liu X, Li Y, Ding H, Chen L, Du S, et al. (2023). "Topotactic transition of Ti4AlN3 MAX phase in lewis acid molten salt." Journal of Materiomics. 9(6):1032–1038.*
305. ^*Ingason AS, Petruhins A, Dahlqvist M, Magnus F, Mockute A, et al. (2014). "A nanolaminated magnetic phase: Mn2GaC." Materials Research Letters. 2(2):89–93.*
306. ^*Beckmann O, Boller H, Nowotny H, Benesovsky F. (1969). "Einige komplexcarbide und-nitride in den systemen ti-{zn, cd, hg}-{c, n} und cr-ga-n." Monatshefte für Chemie/Chemical Monthly. 100(5):1465–1470.*
307. a, b, c*Cuskelly DT, Richards ER, Kisi EH, Keast VJ. (2015). "Ti3GaC2 and Ti3InC2: First bulk synthesis, DFT stability calculations and structural systematics." Journal of Solid State Chemistry. 230:418–425.*
308. ^*Hu C, Lai C-C, Tao Q, Lu J, Halim J, et al. (2015). "Mo2ga2c: A new ternary nanolaminated carbide." Chemical Communications. 51(30):6560–6563.*
309. ^*Lai C-C, Meshkian R, Dahlqvist M, Lu J, Näslund L-Å, et al. (2015). "Structural and chemical determination of the new nanolaminated carbide Mo2Ga2C from first principles and materials analysis." Acta Materialia. 99:157–164.*

310. [a, b] *Li S, Yang Z, Khaledialidusti R, Lin S, Yu J, et al. (2023). "High-throughput study and machine learning on MAX and MAB phases: New materials and fingerprints of superior lattice thermal conductivities." Acta Materialia. 254:119001.*
311. [a, b, c] *Wilhelmsson O, Palmquist J-P, Nyberg T, Jansson U. (2004). "Deposition of Ti2AlC and Ti3AlC2 epitaxial films by magnetron sputtering." Applied physics letters. 85(6):1066–1068.*
312. ^ *Boller H, Nowotny H. (1966). "Röntgenographische untersuchungen im system: Vanadin-arsen-kohlenstoff." Monatshefte für Chemie und verwandte Teile anderer Wissenschaften. 97:1053–1058.*
313. ^ *Chen K, Bai X, Mu X, Yan P, Qiu N, et al. (2021). "MAX phase Zr2SeC and its thermal conduction behavior." Journal of the European Ceramic Society. 41(8):4447–4451.*
314. ^ *Wang X, Chen K, Wu E, Zhang Y, Ding H, et al. (2022). "Synthesis and thermal expansion of chalcogenide MAX phase Hf2SeC." Journal of the European Ceramic Society. 42(5):2084–2088.*
315. [a, b] *Zhang Q, Zhou Y, San X, Li W, Bao Y, et al. (2022). "Zr2SeB and Hf2SeB: Two new MAB phase compounds with the Cr2AlC-type MAX phase (211 phase) crystal structures." Journal of Advanced Ceramics. 11(11):1764–1776.*
316. [a, b, c, d, e, f, g] *Ding H, Li Y, Li M, Chen K, Liang K, et al. (2023). "Chemical scissor–mediated structural editing of layered transition metal carbides." Science. 379(6637):1130–1135.*
317. ^ *Li Y, Qin Y, CHEN K, CHEN L, Zhang X, et al. (2021). "Molten salt synthesis of nanolaminated Sc2SnC MAX phase." 无机材料学报. 36(7).*
318. ^ *Xu Q, Zhou Y, Zhang H, Jiang A, Tao Q, et al. (2020). "Theoretical prediction, synthesis, and crystal structure determination of new MAX phase compound v2SnC." Journal of Advanced Ceramics. 9:481–492.*
319. ^ *Kuchida S, Muranaka T, Kawashima K, Inoue K, Yoshikawa M, et al. (2013). "Superconductivity in Lu2SnC." Physica C: superconductivity. 494:77–79.*
320. [a, b] *Barsoum MW, El-Raghy T. (2001). "The MAX phases: Unique new carbide and nitride materials: Ternary ceramics turn out to be surprisingly soft and machinable, yet also heat-tolerant, strong and lightweight." American scientist. 89(4):334–343.*
321. ^ *Dubois S, Cabioc'h T, Chartier P, Gauthier V, Jaouen M. (2007). "A new ternary nanolaminate carbide: Ti3SnC2." Journal of the American Ceramic Society. 90(8):2642–2644.*
322. ^ *Zhang J, Liu B, Wang JY, Zhou YC. (2009). "Low-temperature instability of Ti2SnC: A combined transmission electron microscopy, differential scanning calorimetry, and x-ray diffraction investigations." Journal of Materials Research. 24(1):39–49.*

323. a, b, c*Boller H. (1973). "Mixed pnictides with ordered TiP-type (ti2SC-type)." Monatshefte für Chemie/Chemical Monthly. 104:166–171.*

324. ^*Zhang Q, Zhou Y, San X, Wan D, Bao Y, et al. (2023). "Thermal explosion synthesis of first te-containing layered ternary Hf2TeB MAX phase." Journal of the European Ceramic Society. 43(1):173–176.*

325. ^*Fashandi H, Lai C-C, Dahlqvist M, Lu J, Rosén J, et al. (2017). "Ti2au2c and ti3au2c2 formed by solid state reaction of gold with ti2AlC and ti3AlC2." Chemical Communications. 53(69):9554–9557.*

326. ^*Shi Y, Kashiwaya S, Helmer P, Lu J, Andersson M, et al. (2023). "Synthesis of Cr2AuC via thermal substitution reaction in au-covered Cr2GaC and Cr2GeC thin films." Results in Materials. 18:100403.*

327. a, b, c, d*Jeitschko W, Nowotny HT, Benesovsky F. (1964). "Carbides of formula T2MC." Journal of the Less Common Metals. 7(2):133–138.*

328. a, b*Wen B, Liu Y, Cao L, San X, Zhou Y, et al. (2025). "Synthesis of two new o-MAX phases Mo2VAlC2 and Mo2V2AlC3 and their derivatives o-MXene Mo2VC2Tx and Mo2V2C3Tx." Journal of the European Ceramic Society. 45(2):116964.*

329. a, b, c, d*Caspi EN, Chartier P, Porcher F, Damay F, Cabioc'h T. (2015). "Ordering of (cr, v) layers in nanolamellar (Cr0.5V0.5)n+1AlCn compounds." Materials Research Letters. 3(2):100–106.*

330. ^*Wyatt BC, Thakur A, Nykiel K, Hood ZD, Adhikari SP, et al. (2023). "Design of atomic ordering in Mo2Nb2C3Tx MXenes for hydrogen evolution electrocatalysis." Nano Letters. 23(3):931–938.*

331. a, b, c, d, e, f, g*Chen Z, Chong H, Sun S, Yang J, Yao G, et al. (2022). "Synthesis and characterizations of solid-solution i-MAX phase (W1/3Mo1/3R1/3)2AlC (r= gd, tb, dy, ho, er and y) and derivated i-MXene with improved electrochemical properties". Scripta Materialia. 213:114596.*

332. a, b, c, d, e, f, g, h, i, j, k, l, m, n, o, p, q, r, s, t, u, v*Tao Q, Lu J, Dahlqvist M, Mockute A, Calder S, et al. (2019). "Atomically layered and ordered rare-earth i-MAX phases: A new class of magnetic quaternary compounds". Chemistry of Materials. 31(7):2476–2485.*

333. a, b, c, d, e, f, g*Yang J, Liu R, Jia N, Wu K, Fu X, et al. (2021). "Novel w-based in-plane chemically ordered (W2/3R1/3)2AlC (r= gd, tb, dy, ho, er, tm and lu) MAX phases and their 2D W1.33C MXene derivatives". Carbon. 183:76–83.*

334. a, b*Tao Q, Dahlqvist M, Lu J, Kota S, Meshkian R, et al. (2017). "Two-dimensional Mo1.33C MXene with divacancy ordering prepared from parent 3D laminate with in-plane chemical ordering". Nature Communications. 8(1):14949.*

335. ^*Niu Y, Fu S, Zhang K, Dai B, Zhang H, et al. (2020). "Synthesis, microstructure, and properties of high purity mo2TiAlC2 ceramics fabricated by spark plasma sintering". Journal of Advanced Ceramics. 9:759–768.*

336. a, b, c Bagheri S, Lipatov A, Vorobeva NS, Sinitskii A. (2023). "Interlayer incorporation of a-elements into MXenes via selective etching of a' from mn+1A'1–xa"xcn MAX phases". ACS Nano. 17(19):18747–18757.

337. a, b, c, d, e, f, g Sun S, Ma Z, Chen Z, Liu P, Song Y, et al. (2023). "The crystallographic structure and properties of novel quaternary nanolaminated rare-earth-cr-based i-MAX phases". Acta Materialia. 242:118479.

338. ^ Li Y, Li M, Lu J, Ma B, Wang Z, et al. (2019). "Single-atom-thick active layers realized in nanolaminated Ti3(alxCu1–x)C2 and its artificial enzyme behavior". ACS Nano. 13(8):9198–9205.

339. a, b, c Petruhins A, Dahlqvist M, Lu J, Hultman L, Rosen J. (2019). "Theoretical prediction and experimental verification of the chemically ordered atomic-laminate i-MAX phases (Cr2/3Sc1/3)2GaC and (Mn2/3Sc1/3)2GaC". Crystal Growth & Design. 20(1):55–61.

340. a, b, c, d, e, f, g, h, i Petruhins A, Lu J, Hultman L, Rosen J. (2019). "Synthesis of atomically layered and chemically ordered rare-earth (RE) i-MAX phases;(Mo2/3RE1/3)2GaC with RE= gd, tb, dy, ho, er, tm, yb, and lu". Materials Research Letters. 7(11):446–452.

341. ^ Bai D, Wang Q, Deng B, Li Y, Huang A, et al. (2025). "Liquid metal assistant self-propagating high-temperature synthesis of s-containing high-entropy MAX-phase materials". Journal of Materials Science & Technology. 209:1–8.

342. ^ Du C-F, Xue Y, Wang C, Zeng Q, Wang J, et al. (2023). "Synthesis of a high-entropy (TiVCrMo)3AlC2 MAX and its tribological properties in a wide temperature range". Journal of the European Ceramic Society. 43(11):4684–4695.

343. ^ Du Z, Wu C, Chen Y, Zhu Q, Cui Y, et al. (2022). "High-entropy carbonitride MAX phases and their derivative MXenes". Advanced Energy Materials. 12(6):2103228.

344. ^ Zou H, Zhang W, Zhang J, Ren L, Wang W, et al. (2024). "Synthesis of a novel textured high entropy M4AlC3 (m= ti, v, mo, nb, ta) composites with improved mechanical properties via spark plasma sintering". Journal of the European Ceramic Society. 44(12):6889–6900.

345. ^ Alam MS, Chowdhury MA, Kowser MA, Islam MS, Islam MM, et al. (2024). "Advances of MAX phases: Synthesis, characterizations and challenges". Engineering Reports. 6(8):e12911. doi:10.1002/eng2.12911

346. ^ Chen L, Dahlqvist M, Lapauw T, Tunca B, Wang F, et al. (2018). "Theoretical prediction and synthesis of (Cr2/3Zr1/3)2AlC i-MAX phase". Inorganic Chemistry. 57(11):6237–6244. doi:10.1021/acs.inorgchem.8b00021

347. ^ Li L, Zhou A, Xu L, Li Z, Wang L. (2013). "Synthesis of high pure Ti3AlC2 and Ti2AlC powders from TiH2 powders as ti source by tube furnace". Journal of Wuhan University of Technology-Mater Sci Ed. 28(5):882–887.

348. ^Tunca B, Lapauw T, Karakulina OM, Batuk M, Cabioc'h T, et al. (2017). "Synthesis of MAX phases in the zr-ti-al-c system". Inorganic Chemistry. 56(6):3489–3498.
349. ^Barsoum M. (2013). "MAX phases: Properties of machinable ternary carbides and nitrides". MAX Phases: Properties of Machinable Ternary Carbides and Nitrides. Wiley. doi:10.1002/9783527654581. ISBN 9783527330119
350. ^Khazaei M, Ranjbar A, Esfarjani K, Bogdanovski D, Dronskowski R, et al. (2018). "Insights into exfoliation possibility of MAX phases to MXenes". Physical Chemistry Chemical Physics. 20(13):8579–8592.
351. ^Dronskowski R, Blöchl PE. (1993). "Crystal orbital hamilton populations (COHP): Energy-resolved visualization of chemical bonding in solids based on density-functional calculations". The Journal of Physical Chemistry. 97(33):8617–8624.
352. ^Deringer VL. (2011). "Tchougréeff AL and dronskowski r". J Phys Chem A. 2011:115.
353. ^Maintz S, Deringer VL, Tchougréeff AL, Dronskowski R. "LOBSTER: A tool to extract chemical bonding from plane-wave based DFT". Wiley Online Library 2016.
354. ^Ghidiu M, Lukatskaya MR, Zhao M-Q, Gogotsi Y, Barsoum MW. "Conductive two-dimensional titanium carbide 'clay'with high volumetric capacitance". In: MXenes.: Jenny Stanford Publishing 2023. pp. 379–399.
355. a, bLiu F, Zhou A, Chen J, Jia J, Zhou W, et al. (2017). "Preparation of Ti3C2 and Ti2C MXenes by fluoride salts etching and methane adsorptive properties". Applied Surface Science. 416:781–789.
356. ^Alhabeb M, Maleski K, Anasori B, Lelyukh P, Clark L, et al. (2017). "Guidelines for synthesis and processing of two-dimensional titanium carbide (Ti3C2Tx MXene)". Chemistry of Materials. 29(18):7633–7644.
357. ^Qiao J-B, Gong Y, Liu H, Shi J-A, Gu L, et al. (2018). "Two-dimensional spinodal interface in one-step grown graphene-molybdenum carbide heterostructures". Physical Review Materials. 2(5):054002.
358. ^Zhao H, Cai K, Ma Z, Cheng Z, Jia T, et al. (2018). "Synthesis of molybdenum carbide superconducting compounds by microwave-plasma chemical vapor deposition". Journal of Applied Physics. 123(5).
359. ^Deng R, Zhang H, Zhang Y, Chen Z, Sui Y, et al. (2017). "Graphene/Mo2C heterostructure directly grown by chemical vapor deposition". Chinese Physics B. 26(6):067901.
360. ^Gogotsi Y. (2015). "Transition metal carbides go 2D". Nature Materials. 14(11):1079–1080.
361. ^Geng D, Zhao X, Li L, Song P, Tian B, et al. (2016). "Controlled growth of ultrathin Mo2C superconducting crystals on liquid cu surface". 2D Materials. 4(1):011012.
362. ^Jia J, Xiong T, Zhao L, Wang F, Liu H, et al. (2017). "Ultrathin n-doped Mo2C nanosheets with exposed active sites as efficient electrocatalyst for hydrogen evolution reactions". ACS Nano. 11(12):12509–12518.

363. ^*Xiao X, Yu H, Jin H, Wu M, Fang Y, et al. (2017). "Salt-templated synthesis of 2D metallic MoN and other nitrides". ACS Nano. 11(2):2180–2186.*

364. ^*Joshi S, Wang Q, Puntambekar A, Chakrapani V. (2017). "Facile synthesis of large area two-dimensional layers of transition-metal nitride and their use as insertion electrodes". ACS Energy Letters. 2(6):1257–1262.*

365. ^*Zhang Z, Zhang F, Wang H, Chan CH, Lu W, et al. (2017). "Substrate orientation-induced epitaxial growth of face centered cubic mo2c superconductive thin film". Journal of Materials Chemistry C. 5(41):10822–10827.*

366. ^*Zhang F, Zhang Z, Wang H, Chan CH, Chan NY, et al. (2017). "Plasma-enhanced pulsed-laser deposition of single-crystalline m o2c ultrathin superconducting films". Physical Review Materials. 1(3):034002.*

367. a, b, c, d*Rahman M, Al Mamun MS. (2024). "Future prospects of MXenes: Synthesis, functionalization, properties, and application in field effect transistors". Nanoscale Advances. 6(2):367–385.*

368. ^*Naguib M, Gogotsi Y, Barsoum MW. (2015). "Mxenes: A new family of two-dimensional materials and its application as electrodes for li and na-ion batteries". In: Electrochemical society meeting abstracts 227.: The Electrochemical Society, Inc. pp. 849–849.*

369. ^*Yang J, Naguib M, Ghidiu M, Pan LM, Gu J, et al. (2016). "Two-dimensional nb-based M4C3 solid solutions (MXenes)". Journal of the American Ceramic Society. 99(2):660–666.*

370. a, b, c*Wu J, Guan Y, Li K, Xie Q, Wang Z, et al. (2021). "2D porous Nb4N5@ Nb2C heterojunctions for high-performance li-ion batteries". 2D Materials. 9(1):015029.*

371. a, b*Huang J, Lu X, Sun T, Yu D, Xu Z, et al. (2023). "Boosting high-voltage dynamics towards high-energy-density lithium-ion capacitors". Energy & Environmental Materials. 6(4):e12505.*

372. ^*Peng C, Wei P, Chen X, Zhang Y, Zhu F, et al. (2018). "A hydrothermal etching route to synthesis of 2D MXene (Ti3C2, Nb2C): Enhanced exfoliation and improved adsorption performance". Ceramics International. 44(15):18886–18893.*

373. ^*Cai C, Wang R, Liu S, Yan X, Zhang L, et al. (2020). "Synthesis of self-assembled phytic acid-MXene nanocomposites via a facile hydrothermal approach with elevated dye adsorption capacities". Colloids and Surfaces A: Physicochemical and Engineering Aspects. 589:124468.*

374. ^*Guo Y, Jin S, Wang L, He P, Hu Q, et al. (2020). "Synthesis of two-dimensional carbide Mo2CTx MXene by hydrothermal etching with fluorides and its thermal stability". Ceramics International. 46(11):19550–19556.*

375. ^*Singh B, Bahadur R, Neekhra S, Gandhi M, Srivastava R. (2021). "Hydrothermal-assisted synthesis and stability of multifunctional MXene nanobipyramids: Structural, chemical, and optical evolution". ACS Applied Materials & Interfaces. 13(2):3011–3023.*

376. ^Ashraf I, Ahmad S, Nazir F, Dastan D, Shi Z, et al. (2022). "Hydrothermal synthesis and water splitting application of d-Ti3C2 MXene/V2O5 hybrid nanostructures as an efficient bifunctional catalyst". International Journal of Hydrogen Energy. 47(64):27383–27396.
377. ^Kuang D, Wang L, Guo X, She Y, Du B, et al. (2021). "Facile hydrothermal synthesis of Ti3C2Tx-TiO2 nanocomposites for gaseous volatile organic compounds detection at room temperature". Journal of Hazardous Materials. 416:126171.
378. ^Xue N, Li X, Zhang M, Han L, Liu Y, et al. (2020). "Chemical-combined ball-milling synthesis of fluorine-free porous MXene for high-performance lithium ion batteries". ACS Applied Energy Materials. 3(10):10234–10241.
379. ^Zhang T, Jiang X, Li G, Yao Q, Lee JY. (2018). "A red-phosphorous-assisted ball-milling synthesis of few-layered Ti3C2Tx (MXene) nanodot composite". ChemNanoMat. 4(1):56–60.
380. ^Tian S, Cheng G, Tang Z, Sha F, Xuan Z, et al. (2020). "Fabrication of two-dimensional Ti3C2Tx MXenes by ball milling pretreatment and mild etchant and their microstructure". Ceramics International. 46(18):28949–28954.
381. ^Yang L, Zheng W, Zhang P, Chen J, Tian WB, et al. (2018). "MXene/CNTs films prepared by electrophoretic deposition for supercapacitor electrodes". Journal of Electroanalytical Chemistry. 830:1–6.
382. ^Xu S, Wei G, Li J, Ji Y, Klyui N, et al. (2017). "Binder-free Ti3C2Tx MXene electrode film for supercapacitor produced by electrophoretic deposition method". Chemical Engineering Journal. 317:1026–1036.
383. ^Collini P, Kota S, Dillon AD, Barsoum MW, Fafarman AT. (2017). "Electrophoretic deposition of two-dimensional titanium carbide (MXene) thick films". Journal of The Electrochemical Society. 164(9):D573.
384. ^Collini P. Deposizione elettroforetica di film di MXENE per applicazioni funzionali.(electrophoretic deposition of MXene films for functional applications).
385. ^Ali I, Ud Din MF, Gu ZG. (2022). "MXenes thin films: From fabrication to their applications". Molecules. 27(15):4925.
386. ^Namvari M, Chakrabarti BK. (2024). "Electrophoretic deposition of MXenes and their composites: Toward a scalable approach". Advances in Colloid and Interface Science. :103208.
387. a, bBarsoum MW. Introduction. In: MAX phases.: John Wiley & Sons, Ltd 2013. p. All. doi:10.1002/9783527654581.ch1. ISBN 9783527654581
388. a, bWang XH, Zhou YC. (2010). "Layered machinable and electrically conductive Ti2AlC and Ti3AlC2 ceramics: A review". Journal of Materials Science & Technology. 26(5):385–416.

389. a, b, c, d, e *Bai Y, He X, Wang R, Sun Y, Zhu C, et al. (2013). "High temperature physical and mechanical properties of large-scale Ti2AlC bulk synthesized by self-propagating high temperature combustion synthesis with pseudo hot isostatic pressing". Journal of the European Ceramic Society. 33(13-14):2435–2445.*

390. a, b *Das P, Jahan N, Ali MA. (2023). "DFT insights into nb-based 211 MAX phase carbides: Nb2AC (a= ga, ge, tl, zn, p, in, and cd)". RSC Advances. 13(8):5538–5556.*

391. ^ *Appl Bouhemadou. (2009). Calculated structural, electronic and elastic properties of m 2 GeC (m= ti, v, cr, zr, nb, mo, hf, ta and w). Applied Physics A. 96:959–967.*

392. ^ *Chunfeng Hu, Fangzhi Li, Lingfeng He, Mingyue Liu, Jie Zhang, et al. (2008). In situ reaction synthesis, electrical and thermal, and mechanical properties of Nb4AlC3. Journal of the American Ceramic Society. 91(7):2258–2263.*

393. ^ *Chunfeng Hu, Zhijun Lin, Lingfeng He, Yiwang Bao, Jingyang Wang, et al. (2007). Physical and mechanical properties of bulk Ta4AlC3 ceramic prepared by an in situ reaction synthesis/hot-pressing method. Journal of the American Ceramic Society. 90(8):2542–2548.*

394. ^ *YW Bao, XH Wang, HB Zhang, YC Zhou. (2005). Thermal shock behavior of Ti3AlC2 from between 200° c and 1300° c. Journal of the European Ceramic Society. 25(14):3367–3374.*

395. ^ *Yuelei Bai, Xiaodong He, Chuncheng Zhu, Guiqing Chen. (2012). Microstructures, electrical, thermal, and mechanical properties of bulk ti 2 AlC synthesized by self-propagating high-temperature combustion synthesis with pseudo hot isostatic pressing. Journal of the American Ceramic Society. 95(1):358–364.*

396. ^ *Weiwei Zhang, Shibo Li, Shukai Fan, Xuejin Zhang, Xiachen Fan, et al. (2024). Ti 3 AlC 2- y n y carbonitride MAX phase solid solutions with tunable mechanical, thermal, and electrical properties. Journal of Advanced Ceramics. 13(9):1473–1481.*

397. ^ *Michel W. Barsoum. (2013). MAX phases: Properties of machinable ternary carbides and nitrides. John Wiley & Sons.*

398. ^ *SE Lofland, JD Hettinger, K. Harrell, P. Finkel, S. Gupta, et al. (2004). Elastic and electronic properties of select m 2 AX phases. Applied Physics Letters. 84(4):508–510.*

399. ^ *JD Hettinger, SE Lofland, P. Finkel, T. Meehan, J. Palma, et al. (2005). Electrical transport, thermal transport, and elastic properties of m 2 al c (m= ti, cr, nb, and v). Physical Review B—Condensed Matter and Materials Physics. 72(11):115120.*

400. ^ *Le Fu, Håkan Engqvist, Wei Xia. (2018). Spark plasma sintering of biodegradable Si3N4 bioceramic with sr, mg and si as sintering additives for spinal fusion. Journal of the European Ceramic Society. 38(4):2110–2119.*

401. ^ *Corrado Piconi, G. Maccauro. (1999). Zirconia as a ceramic biomaterial. Biomaterials. 20(1):1–25.*

402. ^Christiane Lago Ojaimi, Julieta Adriana Ferreira, Fabio Andre dos Santos, Adilson Luiz Chinelatto, Eliria Maria de Jesus Agnolon Pallone, et al. (2018). Mechanical characterisation and hydrothermal degradation of Al2O3-15 vol% ZrO2 nanocomposites consolidated by two-step sintering. Ceramics International. 44(14):16128–16136.

403. a, bGuobing Ying, Xiaodong He, Mingwei Li, Wenbo Han, Fei He, et al. (2011). Synthesis and mechanical properties of high-purity Cr2AlC ceramic. Materials Science and Engineering: A. 528(6):2635–2640.

404. ^G-P Bei, G. Laplanche, V. Gauthier-Brunet, J. Bonneville, S. Dubois. (2013). Compressive behavior of ti 3 AlC 2 and ti 3 al 0.8 sn 0.2 c 2 MAX phases at room temperature. Journal of the American Ceramic Society. 96(2):567–576.

405. ^Zhimei Sun, Rajeev Ahuja, Sa Li, Jochen M. Schneider. (2003). Structure and bulk modulus of m 2 AlC (m= ti, v, and cr). Applied Physics Letters. 83(5):899–901.

406. ^Wei Zhang, Nahum Travitzky, Chunfeng Hu, Yanchun Zhou, Peter Greil. (2009). Reactive hot pressing and properties of Nb2AlC. Journal of the American Ceramic Society. 92(10):2396–2399.

407. a, b, cArni Sigurdur Ingason, Aurelija Mockute, Martin Dahlqvist, Fridrik Magnus, S. Olafsson, et al. (2013). Magnetic self-organized atomic laminate from first principles and thin film synthesis. Physical Review Letters. 110(19):195502.

408. a, b, cArni Sigurdur Ingason, Martin Dahlqvist, Rose. (2016). Magnetic MAX phases from theory and experiments; a review. Journal of Physics: Condensed Matter. 28(43):433003.

409. a, bAhmed Azzouz-Rached, Mohammed Bendjemai, Mudasser Husain, Ali Bentouaf, Hamza Rekab-Djabri, et al. (2023). Numerical simulation studies of the new quaternary MAX phase as future engineering applications: The case study of the Nb2ScAC2 (a= al, si) compounds. Scientific Reports. 13(1):22953.

410. ^MA Ali, MM Hossain, MM Uddin, AKMA Islam, D. Jana, et al. (2021). DFT insights into new b-containing 212 MAX phases: Hf2AB2 (a= in, sn). Journal of Alloys and Compounds. 860:158408.

411. ^S. Li, Rajeev Ahuja, MW Barsoum, Puru Jena, Börje Johansson. (2008). Optical properties of Ti3SiC2 and Ti4AlN3. Applied Physics Letters. 92(22).

412. ^A. Chowdhury, MA Ali, MM Hossain, MM Uddin, SH Naqib, et al. (2018). Predicted MAX phase Sc2InC: Dynamical stability, vibrational and optical properties. physica status solidi (b). 255(3):1700235.

413. ^AKM Naim Ishtiaq, Md Nasir Uddin, Noor Afsary, Md Koushik Alam, Shariful Islam, et al. (2024). First-principles study of electronic, mechanical, and optical properties of M3GaB2 (m= ti, hf) MAX phases. Heliyon. 10(13).

414. ^Mohammad Khazaei, Avanish Mishra, Natarajan S. Venkataramanan, Abhishek K. Singh, Seiji Yunoki. (2019). Recent advances in MXenes: From fundamentals to applications. Current Opinion in Solid State and Materials Science. 23(3):164–178.

415. a, bChen Si, Jian Zhou, Zhimei Sun. (2015). Half-metallic ferromagnetism and surface functionalization-induced metal–insulator transition in graphene-like two-dimensional Cr2C crystals. ACS Applied Materials & Interfaces. 7(31):17510–17515.

416. ^Mohammad Khazaei, Vei Wang, Cem Sevik, Ahmad Ranjbar, Masao Arai, et al. (2018). Electronic structures of iMAX phases and their two-dimensional derivatives: A family of piezoelectric materials. Physical Review Materials. 2(7):074002.

417. ^Deependra Parajuli, K. Samatha. Chapter 5 - topological properties of MXenes. In: Kishor Kumar Sadasivuni, Kalim Deshmukh, S. K. Khadheer Pasha, Tomáš Kovářříkeditors. Mxenes and their composites.: Elsevier 2022. pp. 171–199. (Micro and nano technologies). doi:10.1016/B978-0-12-823361-0.00015-0. ISBN 978-0-12-823361-0

418. ^T. Ouisse, Lu Shi, BA Piot, Benoît Hackens, V. Mauchamp, et al. (2015). Magnetotransport properties of nearly-free electrons in two-dimensional hexagonal metals and application to the m n+ 1 AX n phases. Physical Review B. 92(4):045133.

419. a, bAurélie Champagne, J-L Battaglia, T. Ouisse, Francesco Ricci, A. Kusiak, et al. (2020). Heat capacity and anisotropic thermal conductivity in Cr2AlC single crystals at high temperature. The Journal of Physical Chemistry C. 124(43):24017–24028.

420. ^Mohammad Khazaei, Masao Arai, Taizo Sasaki, Chan-Yeup Chung, Natarajan S. Venkataramanan, et al. (2013). Novel electronic and magnetic properties of two-dimensional transition metal carbides and nitrides. Advanced Functional Materials. 23(17):2185–2192. doi:10.1002/adfm.201202502

421. ^Champagne A, Shi L, Ouisse T, Hackens B, Charlier JC. (2018). "Electronic and vibrational properties of v2c-based MXenes: From experiments to first-principles modeling." Physical Review B. 97(11):115439.

422. ^Zha XH, Huang Q, He J, He H, Zhai J, et al. (2016). "The thermal and electrical properties of the promising semiconductor MXene Hf2CO2." Scientific Reports. 6(1):27971.

423. ^Madsen GK, Singh DJ. (2006). "BoltzTraP. A code for calculating band-structure dependent quantities." Computer Physics Communications. 175(1):67–71.

424. ^Madsen GK, Carrete J, Verstraete MJ. (2018). "BoltzTraP2, a program for interpolating band structures and calculating semi-classical transport coefficients." Computer Physics Communications. 231:140–145.

425. ^Hellman O, Abrikosov IA, Simak SI. (2011). "Lattice dynamics of anharmonic solids from first principles." Physical Review B—Condensed Matter and Materials Physics. 84(18):180301.

426. a, bHellman O, Steneteg P, Abrikosov IA, Simak SI. (2013). "Temperature dependent effective potential method for accurate free energy calculations of solids." Physical Review B—Condensed Matter and Materials Physics. 87(10):104111.

427. a, b, cZha XH, Yin J, Zhou Y, Huang Q, Luo K, et al. (2016). "Intrinsic structural, electrical, thermal, and mechanical properties of the promising conductor Mo2C MXene." The Journal of Physical Chemistry C. 120(28):15082–15088.

428. ^Oliver WC, Pharr GM. (1992). "An improved technique for determining hardness and elastic modulus using load and displacement sensing indentation experiments." Journal of Materials Research. 7(6):1564–1583.

429. ^Albayrak IC, Basu S, Sakulich A, Yeheskel O, Barsoum MW. (2010). "Elastic and mechanical properties of polycrystalline transparent yttria as determined by indentation techniques." Journal of the American Ceramic Society. 93(7):2028–2034.

430. ^Badr HO, Champagne A, Ouisse T, Charlier JC, Barsoum MW. (2020). "Elastic properties and hardness values of v2AlC and cr2AlC single crystals." Physical Review Materials. 4(8):083605.

431. ^Kurtoglu M, Naguib M, Gogotsi Y, Barsoum MW. (2012). "First principles study of two-dimensional early transition metal carbides." MRS Communications. 2:133–137.

432. ^Yorulmaz U, Özden A, Perkgöz NK, Ay F, Sevik C. (2016). "Vibrational and mechanical properties of single layer MXene structures: A first-principles investigation." Nanotechnology. 27(33):335702.

433. ^Lei JC, Zhang X, Zhou Z. (2015). "Recent advances in MXene: Preparation, properties, and applications." Frontiers of Physics. 10:276–286.

434. ^Lipatov A, Lu H, Alhabeb M, Anasori B, Gruverman A, et al. (2018). "Elastic properties of 2D Ti3C2Tx MXene monolayers and bilayers." Science Advances. 4(6):eaat0491.

435. ^Mazhar S, Qarni AA, Haq YU, Haq ZU, Murtaza I. (2020). "Promising PVC/MXene based flexible thin film nanocomposites with excellent dielectric, thermal and mechanical properties." Ceramics International. 46(8):12593–12605.

436. ^Boota M, Anasori B, Voigt C, Zhao MQ, Barsoum MW, et al. (2016). "Pseudocapacitive electrodes produced by oxidant-free polymerization of pyrrole between the layers of 2D titanium carbide (MXene)." Advanced Materials. 28(7):1517–1522.

437. ^Zhang L, Zhang S, Wang C, Zhou Q, Zhang H, et al. (2021). "Highly sensitive capacitive flexible pressure sensor based on a high-permittivity MXene nanocomposite and 3D network electrode for wearable electronic

s." ACS Sensors. 6(7):2630–2641.

438. ^*Zhao MQ, Ren CE, Ling Z, Lukatskaya MR, Zhang C, et al. (2014). "Flexible MXene/carbon nanotube composite paper with high volumetric capacitance." Advanced Materials. 27(2).*
439. ^*Wu X, Huang B, Lv R, Wang Q, Wang Y. (2019). "Highly flexible and low capacitance loss supercapacitor electrode based on hybridizing decentralized conjugated polymer chains with MXene." Chemical Engineering Journal. 378:122246.*
440. a, b*Si C, Jin KH, Zhou J, Sun Z, Liu F. (2016). "Large-gap quantum spin hall state in MXenes: D-band topological order in a triangular lattice." Nano Letters. 16(10):6584–6591. Available from: https://api.semanticscholar.org/CorpusID:27205*
441. ^*Kumar H, Frey NC, Dong L, Anasori B, Gogotsi Y, et al. (2017). "Tunable magnetism and transport properties in nitride MXenes." ACS Nano. 11(8):7648–7655. doi:10.1021/acsnano.7b02578*
442. ^*Wang G. (2016). "Theoretical prediction of the intrinsic half-metallicity in surface-oxygen-passivated Cr2N MXene." The Journal of Physical Chemistry C. 120(33):18850–18857. doi:10.1021/acs.jpcc.6b05224*
443. ^*He J, Lyu P, Nachtigall P. (2016). "New two-dimensional mn-based MXenes with room-temperature ferromagnetism and half-metallicity." J Mater Chem C. 4:11143–11149. doi:10.1039/C6TC03917K*
444. ^*He J, Lyu P, Sun LZ, Morales García Á, Nachtigall P. (2016). "High temperature spin-polarized semiconductivity with zero magnetization in two-dimensional janus MXenes." J Mater Chem C. 4:6500–6509. doi:10.1039/C6TC01287F*
445. a, b, c, d*Kumar H, Frey NC, Dong L, Anasori B, Gogotsi Y, et al. (2017). "Tunable magnetism and transport properties in nitride MXenes." ACS Nano. 11(8):7648–7655.*
446. ^*Gao X, Jia Z, Wang B, Wu X, Sun T, et al. (2021). "Synthesis of NiCo-LDH/MXene hybrids with abundant heterojunction surfaces as a lightweight electromagnetic wave absorber." Chemical Engineering Journal. 419:130019.*
447. a, b*Jiang X, Liu S, Liang W, Luo S, He Z, et al. (2018). "Broadband nonlinear photonics in few-layer MXene Ti3C2Tx (t= f, o, or OH)." Laser & Photonics Reviews. 12(2):1700229.*
448. ^*Di Vito A, Pecchia A, Auf der Maur M, Di Carlo A. (2020). "Nonlinear work function tuning of lead-halide perovskites by MXenes with mixed terminations." Advanced Functional Materials. 30(47):1909028.*
449. a, b*Jhon YI, Koo J, Anasori B, Seo M, Lee JH, et al. (2017). "Metallic MXene saturable absorber for femtosecond mode-locked lasers." Advanced Materials. 29(40):1702496.*
450. ^*Wang Z, Meng X, Chaudhuri K, Alhabeb M, Kim YL, et al. (2017). "Active metamaterials based on monolayer titanium carbide MXene for random lasing." In: CLEO: QELS_fundamental science.: Optica Publishing Gro*

up pp. FTu4G–7.

451. *^Dong Y, Chertopalov S, Maleski K, Anasori B, Hu L, et al. (2018). "Saturable absorption in 2D Ti3C2 MXene thin films for passive photonic diodes." Advanced Materials. 30(10):1705714.*
452. *^Mauchamp V, Bugnet M, Bellido EP, Botton GA, Moreau P, et al. (2014). "Enhanced and tunable surface plasmons in two-dimensional ti3c2 stacks: Electronic structure versus boundary effects." Physical Review B. 89(23):235428.*
453. *^Sundberg M, Malmqvist G, Magnusson A, El-Raghy T. (2004). "Alumina forming high temperature silicides and carbides." Ceramics International. 30(7):1899–1904.*
454. *^Gonzalez-Julian J, Onrubia S, Bram M, Broeckmann C, Vassen R, et al. (2018). "High-temperature oxidation and compressive strength of Cr2AlC MAX phase foams with controlled porosity." Journal of the American Ceramic Society. 101(2):542–552.*
455. *^Kondakov AA, Karpov AV, Grachev VV, Sytschev AE. (2020). "Temperature dependence of electrical resistivity of the TiN/TiAl3/ti2AlN composite material." Russian Journal of Non-Ferrous Metals. 61:216–220.*
456. *^Rajak DK, Pagar DD, Kumar R, Pruncu CI. (2019). "Recent progress of reinforcement materials: A comprehensive overview of composite materials." Journal of Materials Research and Technology. 8(6):6354–6374.*
457. *^Dash A, Malzbender J, Rasinski M, Guillon O, Gonzalez-Julian J. (2022). "Effect of texture and grain size on the compressive creep of Ti3SiC2 MAX phase ceramics." Materialia. 21:101295.*
458. *^Drouelle E, Joulain A, Cormier J, Gauthier-Brunet V, Villechaise P, et al. (2017). "Deformation mechanisms during high temperature tensile creep of Ti3AlC2 MAX phase." Journal of Alloys and Compounds. 693:622–630.*
459. *^a, b Tunes MA, Imtyazuddin M, Kainz C, Pogatscher S, Vishnyakov VM. (2021). "Deviating from the pure MAX phase concept: Radiation-tolerant nanostructured dual-phase Cr2AlC." Science Advances. 7(13):eabf6771.*
460. *^Cui B, Lee WE, Cui B, Lee WE. (2013). "High-temperature oxidation behaviour of MAX phase ceramics." Refractories Worldforum. 5(1):105–112.*
461. *^Davydov DM, Amosov AP, Latukhin EI. (2015). "Synthesis of MAX-phase of titanium silicon carbide (Ti3SiC2) as a promising electric contact material by SHS pressing method." Applied Mechanics and Materials. 792:596–601.*
462. *^Guo Y, Xie X, Liu Z, Zhuo L, Zhang J, et al. (2024). "Wear-resistant ag-MAX phase 3D interpenetrating-phase composites: Processing, structure, and properties." Nano Research. 17(2):806–819.*
463. *^Sokol M, Natu V, Kota S, Barsoum MW. (2019). "On the chemical diversity of the MAX phases." Trends in Chemistry. 1(2):210–223.*

464. ^*Scheibe B, Wychowaniec JK, Scheibe M, Peplińska B, Jarek M, et al. (2019). "Cytotoxicity assessment of ti–al–c based MAX phases and Ti3C2Tx MXenes on human fibroblasts and cervical cancer cells." ACS Biomaterials Science & Engineering. 5(12):6557–6569.*
465. ^*Yokoyama K, Ichikawa T, Murakami H, Miyamoto Y, Asaoka K. (2002). "Fracture mechanisms of retrieved titanium screw thread in dental implant." Biomaterials. 23(12):2459–2465.*
466. ^*Magnus C. (2023). "Sliding wear of MAX phase composites Ti3SiC2–TiC and Ti3AlC2–Ti2AlC at 400° c and the influence of counterface material (steel, Al2O3, and Si3N4) on wear behaviour." Wear. 516:204588.*
467. a, b*Choudhuri I, Bhauriyal P, Pathak B. (2019). "Recent advances in graphene-like 2D materials for spintronics applications." Chemistry of Materials. 31(20):8260–8285.*
468. a, b*Serafin J, Dziejarski B, Achieng GO, Vendrell X, Chaitoglou S, et al. (2024). "Comprehensive analysis of MAX phase and MXene materials for advanced photocatalysis, electrocatalysis and adsorption in hydrogen evolution and storage." Journal of Industrial and Engineering Chemistry.*
469. ^*Hadi MA. "First-principles study of superconducting MAX phases." University of Rajshahi 2015.*
470. ^*Keivanloo M, Sandoghchi M, Mohammadizadeh MR, Khazaei M. (2024). "Study on superconductivity in nb2SC and nb2AsC MAX phases at various pressures." Scientific Reports. 14(1):17516.*
471. ^*Yorulmaz U, Demiroğlu İ, Çakir D, Gülseren O, Sevik C. (2020). "A systematical ab-initio review of promising 2D MXene monolayers towards li-ion battery applications." Journal of Physics: Energy. 2(3):032006.*
472. ^*Yin T, Li Y, Wang R, Al-Hartomy OA, Al-Ghamdi A, et al. (2021). "Synthesis of Ti3C2Fx MXene with controllable fluorination by electrochemical etching for lithium-ion batteries applications." Ceramics International. 47(20):28642–28649.*
473. ^*Li X, Wang C, Cao Y, Wang G. (2018). "Functional MXene materials: Progress of their applications." Chemistry–An Asian Journal. 13(19):2742–2757.*
474. ^*Aslam MK, AlGarni TS, Javed MS, Shah SSA, Hussain S, et al. (2021). "2D MXene materials for sodium ion batteries: A review on energy storage." Journal of Energy Storage. 37:102478.*
475. ^*Lei YJ, Yan ZC, Lai WH, Chou SL, Wang YX, et al. (2020). "Tailoring MXene-based materials for sodium-ion storage: Synthesis, mechanisms, and applications." Electrochemical Energy Reviews. 3:766–792.*
476. ^*Verma R, Thakur P, Chauhan A, Jasrotia R, Thakur A. (2023). "A review on MXene and its' composites for electromagnetic interference (EMI) shielding applications." Carbon. 208:170–190.*
477. ^*Iqbal A, Sambyal P, Koo CM. (2020). "2D MXenes for electromagnetic shielding: A review." Advanced Functional Materials. 30(47):2000883.*

478. ^a,^b*Wu X, Ma P, Sun Y, Du F, Song D, et al. (2021). "Application of MXene in electrochemical sensors: A review." Electroanalysis. 33(8):1827–1851.*

479. ^a,^b*Xu B, Zhi C, Shi P. (2020). "Latest advances in MXene biosensors." Journal of Physics: Materials. 3(3):031001.*

480. ^a,^b*Thenmozhi R, Maruthasalamoorthy S, Nirmala R, Navamathavan R. (2021). "MXene based transducer for biosensor applications." Journal of The Electrochemical Society. 168(11):117507.*

481. ^*Huang Z, Cui X, Li S, Wei J, Li P, et al. (2020). "Two-dimensional MXene-based materials for photothermal therapy". Nanophotonics. 9(8):2233–2249.*

482. ^*Xu D, Li Z, Li L, Wang J. (2020). "Insights into the photothermal conversion of 2D MXene nanomaterials: Synthesis, mechanism, and applications". Advanced Functional Materials. 30(47):2000712.*

483. ^*Seidi F, Shamsabadi AA, Firouzjaei MD, Elliott M, Saeb MR, et al. (2023). "MXenes antibacterial properties and applications: A review and perspective". Small. 19(14):2206716.*

484. ^*Rasool K, Helal M, Ali A, Ren CE, Gogotsi Y, et al. (2016). "Antibacterial activity of Ti3C2Tx MXene". ACS Nano. 10(3):3674–3684.*

485. ^*Bhardwaj R, Hazra A. (2021). "MXene-based gas sensors". Journal of Materials Chemistry C. 9(44):15735–15754.*

486. ^*Reddy MSB, Aich S. (2024). "Recent progress in surface and heterointerface engineering of 2D MXenes for gas sensing applications". Coordination Chemistry Reviews. 500:215542.*

487. ^*Li H, Du Z. (2019). "Preparation of a highly sensitive and stretchable strain sensor of MXene/silver nanocomposite-based yarn and wearable applications". ACS Applied Materials & Interfaces. 11(49):45930–45938.*

488. ^*Wang H, Zhou R, Li D, Zhang L, Ren G, et al. (2021). "High-performance foam-shaped strain sensor based on carbon nanotubes and Ti3C2Tx MXene for the monitoring of human activities". ACS Nano. 15(6):9690–9700.*

489. ^*Ahmed A, Hossain MM, Adak B, Mukhopadhyay S. (2020). "Recent advances in 2D MXene integrated smart-textile interfaces for multifunctional applications". Chemistry of Materials. 32(24):10296–10320.*

490. ^*Meena JS, Choi SB, Jung SB, Kim JW. (2022). "Recent progress of Ti3C2Tx-based MXenes for fabrication of multifunctional smart textiles". Applied Materials Today. 29:101612.*

491. ^*Yang L, Wang H, Yuan W, Li Y, Gao P, et al. (2021). "Wearable pressure sensors based on MXene/tissue papers for wireless human health monitoring". ACS Applied Materials & Interfaces. 13(50):60531–60543.*

492. ^*Grabowski K, Srivatsa S, Vashisth A, Mishnaevsky L Jr, Uhl T. (2022). "Recent advances in MXene-based sensors for structural health monitoring applications: A review". Measurement. 189:110575.*

493. ^Iravani S, Rabiee N, Makvandi P. (2024). "Advancements in MXene-based composites for electronic skins". Journal of Materials Chemistry B.

494. ^Wang J, Shen M, Liu Z, Wang W. (2022). "MXene materials for advanced thermal management and therma l energy utilization". Nano Energy. 97:107177.

495. ^Zhang Z, Zhang N, Li J, Chen L, Cao X. (2024). "MXene-based flexible composite phase change material for battery thermal management application". Applied Thermal Engineering. :124898.

496. ^Ali S, Raza A, Afzal AM, Iqbal MW, Hussain M, et al. (2022). "Recent advances in 2D-MXene based nanoco mposites for optoelectronics". Advanced Materials Interfaces. 9(31):2200556.

497. ^Montazeri K, Currie M, Barsoum MW, Nabet B. (2022). "Ultra-high speed, high-sensitivity spin-cast MXen e-semiconductor-MXene photodetectors". Advanced Functional Materials. 32(51):2206942.

498. ^Kim H, Wang Z, Alshareef HN. (2019). "MXetronics: Electronic and photonic applications of MXenes". Nano Energy. 60:179–197.

499. ^Amrillah T, Hermawan A, Cristian YB, Oktafiani A, Dewi DMM, et al. (2023). "Potential of MXenes as a nov el material for spintronic devices: A review". Physical Chemistry Chemical Physics. 25(28):18584–18608.

500. ^Chen Y, Liu C, Guo S, Mu T, Wei L, et al. (2022). "CO2 capture and conversion to value-added products prom oted by MXene-based materials". Green Energy & Environment. 7(3):394–410.

501. ^Aliyu M, Yusuf BO, Abdullahi AS, Bakare AI, Umar M, et al. (2024). "Ti2C-MXene/activated carbon nanoco mposite for efficient CO2 capture: Insights into thermodynamics properties". Separation and Purification Te chnology. 340:126737.

502. ^Kamysbayev V, Filatov AS, Hu H, Rui X, Lagunas F, et al. (2020). "Covalent surface modifications and super conductivity of two-dimensional metal carbide MXenes". Science. 369(6506):979–983.

503. ^Yang Y, Ting CS. (2020). "Electronic structures and electron–phonon superconductivity of Nb2C-based MX enes". Journal of Physics D: Applied Physics. 53(48):485301.

504. ^Sevik C, Bekaert J, Milošević MV. (2023). "Superconductivity in functionalized niobium-carbide MXenes". N anoscale. 15(19):8792–8799.

Declarations

Funding: No specific funding was received for this work.

Potential competing interests: No potential competing interests to declare.